DOT/FAA/AR-07/50

Air Traffic Organization
Operations Planning
Office of Aviation Research
and Development
Washington, DC 20591

Development and Validation of Crack Growth Models and Life Enhancement Methods for Rotorcraft Damage Tolerance

November 2007

Final Report

This document is available to the U.S. public through the National Technical Information Service (NTIS), Springfield, Virginia 22161.

U.S. Department of Transportation
Federal Aviation Administration

NOTICE

This document is disseminated under the sponsorship of the U.S. Department of Transportation in the interest of information exchange. The United States Government assumes no liability for the contents or use thereof. The United States Government does not endorse products or manufacturers. Trade or manufacturer's names appear herein solely because they are considered essential to the objective of this report. This document does not constitute FAA certification policy. Consult your local FAA aircraft certification office as to its use.

This report is available at the Federal Aviation Administration William J. Hughes Technical Center's Full-Text Technical Reports page: actlibrary.tc.faa.gov in Adobe Acrobat portable document format (PDF).

Technical Report Documentation Page

1. Report No.	2. Government Accession No.	3. Recipient's Catalog No.
DOT/FAA/AR-07/50		

4. Title and Subtitle	5. Report Date
DEVELOPMENT AND VALIDATION OF CRACK GROWTH MODELS AND LIFE ENHANCEMENT METHODS FOR ROTORCRAFT DAMAGE TOLERANCE	November 2007
	6. Performing Organization Code
7. Author(s) S. R. Daniewicz and J. C. Newman	8. Performing Organization Report No.
9. Performing Organization Name and Address Mississippi State University P.O. Box 6156 Mississippi State, MS 39762	10. Work Unit No. (TRAIS)
	11. Contract or Grant No. DTFA03-02-C-00043
12. Sponsoring Agency Name and Address U.S. Department of Transportation Federal Aviation Administration Air Traffic Organization Operations Planning Office of Aviation Research and Development Washington, DC 20591	13. Type of Report and Period Covered Final Report
	14. Sponsoring Agency Code ASW-112

15. Supplementary Notes

The Federal Aviation Administration Airport and Aircraft Safety R&D Division COTR was Dy Le.

16. Abstract

Fatigue crack growth from a hole with a pre-existing compressive residual stress is simulated using two-dimensional elastic-plastic finite element analyses. The analyses allow a determination of the crack-opening stress as the crack propogates through the residual stress, from which the effective stress-intensity factor range (ΔK_{eff}) and the fatigue crack growth is predicted. Results from these simulations are compared with experimental data and to predictions made using a conventional superposition of the elastic stress-intensity factor. The crack closure-based methodology resulted in predictions that compared well with the experimental data, while the results using superposition were nonconservative. Predictions from the closure-based method are highly dependent on the $da/dN = f(\Delta K_{eff})$ constituitive relationship used, highlighting the need for experimental methods to reliably measure this correlation.

17. Key Words	18. Distribution Statement
Fatigue, Crack closure, Residual stress, Finite element analysis, Superposition	This document is available to the U.S. public through the National Technical Information Service (NTIS), Springfield, Virginia 22161.

19. Security Classif. (of this report)	20. Security Classif. (of this page)	21. No. of Pages	22. Price
Unclassified	Unclassified	90	

Form DOT F 1700.7 (8-72) Reproduction of completed page authorized

TABLE OF CONTENTS

	Page
EXECUTIVE SUMMARY	vii
1. INTRODUCTION	1
1.1 Purpose	1
1.2 Background	1
2. DISCUSSION	1
3. EVALUATION APPROACH	5
3.1 Laboratory Testing of Fatigue Crack Growth	5
3.1.1 Tensile Overload	5
3.1.2 Cold Expansion	8
3.2 Finite Element Analysis	9
3.2.1 Tensile Overload Simulation	10
3.2.2 Cold Expansion Simulation	10
3.2.3 Crack Growth Simulation	11
3.3 Fatigue Crack Growth Prediction Methodologies	11
3.3.1 Superposition Prediction Methodology	11
3.3.2 Finite Element Prediction Methodology	12
3.4 Results	13
3.4.1 Tensile Overload Results	13
3.4.2 Cold Expansion Results	18
3.4.3 Convergence Issues	21
4. SUMMARY	22
5. REFERENCES	23
APPENDICES	
A—Sikorsky Final Report	
B—FASTRAN Analysis of Overloaded and Cold-Worked Hole Specimens	

LIST OF FIGURES

Figure		Page
1	Fatigue Crack Growth Specimen	6
2	2024 Stress-Strain Curve	7
3	2024 Baseline Crack Growth Rate Data	7
4	7075 Stress-Strain Curve	9
5	7075 Baseline Crack Growth Rate Data	9
6	Finite Element Model Mesh	10
7	Crack Closure-Based Crack Growth Prediction Methodology	13
8	Residual-Stress Results From Finite Element Simulation of the Tensile Overload	13
9	Predicted Crack-Opening Stress Tests A2-30 and A2-31	14
10	2024 Fatigue Crack Growth: Predicted and Actual, Test A2-30	15
11	2024 Fatigue Crack Growth: Predicted and Actual, Test A2-31	15
12	2024 Center Crack Specimen Fatigue Crack Growth: Predicted and Actual	16
13	2024 Fatigue Crack Growth, Superposition Predictions With Slotted and Unslotted Residual Stress and Actual, Test A2-30	17
14	Test A2-31 Short-Crack Profile	17
15	Test A2-31 Long-Crack Profile	18
16	Residual-Stress Results From Finite Element Simulation of the Cold Expansion Process	18
17	Predicted Opening Stress for the 7075-T6 Simulations	19
18	7075 Fatigue Crack Growth for Cold-Expanded Hole: Predicted and Actual	20
19	7075 Fatigue Crack Growth for Non-Cold-Expanded Hole: Predicted and Actual	20
20	7075 Fatigue Crack Growth, Superposition Predictions With Slotted and Unslotted Residual Stress and Actual	21
21	Opening Stresses for Different Element Sizes in Test A2-30 Simulation	22

LIST OF TABLES

Table		Page
1	2024 Test Matrix	6

LIST OF SYMBOLS AND ACRONYMS

K	Stress-intensity factor
R	Stress ratio
ΔK	Stress-intensity factor range
ΔK_{eff}	Effective stress-intensity factor range
EDM	Electrical discharged machining

EXECUTIVE SUMMARY

Fatigue is the source of at least half of all mechanical failures. The fatigue problem is complex and not fully understood, but it is very important in the design of mechanical systems. Fatigue is especially of interest to the aircraft industry. Many components used in aircraft are fastened together and fastener holes are prevalent. These holes are a source of high stress concentration, and, therefore, are a potential site for fatigue cracks.

One technique used to enhance the fatigue strength of a fastener hole is to introduce a compressive residual-stress field around the hole. An applied load must overcome this residual stress before the crack can grow, thus leading to a longer fatigue life. Although it is widely recognized that compressive residual stress improves fatigue life, in many applications, the benefits of compressive residual stresses are not included in the final predicted fatigue life. In these cases, the residual stress provides added confidence against usage uncertainty, but is not quantified, leading to conservative life predictions. If the residual stress can be included accurately in the fatigue life prediction, the decreased time in part inspection and replacement can be very beneficial to the aircraft industry.

The effect of residual stress on fatigue crack propagation is of great practical significance and has been the focus of much research. This research has been reviewed in several studies. There are numerous methods of introducing residual stress into mechanical components, including shot peening, interference fit fasteners, low plasticity burnishing, laser shock peening, tensile overloading, and cold expansion. The methods investigated in this report are tensile overloading and cold expansion.

1. INTRODUCTION.

1.1 PURPOSE.

The effect of residual stress on fatigue crack propagation is of great practical significance and has been the focus of much research because it can improve the fatigue life of a component. This research has been reviewed in several studies [1, 2, 3, 4, 5, and 6]. There are numerous methods of introducing residual stress into mechanical components, including shot peening, interference fit fasteners, low plasticity burnishing, laser shock peening, tensile overloading, and cold expansion. The methods investigated here are tensile overloading and cold expansion.

1.2 BACKGROUND.

Fatigue is the source of at least half of all mechanical failures [6]. The fatigue problem is complex and not fully understood, but it is very important in the design of mechanical systems. Fatigue is especially of interest to the aircraft industry. Many components used in aircraft are fastened together and fastener holes are prevalent. These holes are a source of high stress concentration, and therefore, are a potential site for fatigue cracks.

One technique used to enhance the fatigue strength of a fastener hole is to introduce a compressive residual-stress field around the hole. An applied load must overcome this residual stress before the crack can grow, thus leading to a longer fatigue life. Although it is widely recognized that compressive residual stress improves fatigue life, in many applications, the benefits of compressive residual stresses are not included in the final predicted fatigue life [7]. In these cases, the residual stress provides added confidence against usage uncertainty, but is not quantified, leading to conservative life predictions. If the residual stress can be included accurately in the fatigue life prediction, the decreased time in part inspection and replacement can be very beneficial to the aircraft industry.

2. DISCUSSION.

There are a variety of methods of introducing residual stress into mechanical components. These methods are detailed in the following paragraphs. They include tensile overloading, split sleeve cold expansion, and superposition.

Tensile overloading occurs when a single tensile load is applied to a component exhibiting a stress gradient, causing plastic deformation and subsequent compressive residual stress. A disadvantage of this process, when applied to a hole, is that the residual stress is not uniform around the hole. The tangential residual stress changes from compressive to tensile at different locations around the hole, and this tensile residual stress can be very deleterious if the configuration of the component does not allow the loading to be in the desired direction.

Split sleeve cold expansion is a technique used frequently by the aircraft industry to improve the fatigue performance of structures. The basic split sleeve cold expansion process was developed by The Boeing Company in the late 1960s [8], and Fatigue Technology Inc. has marketed an efficient method accepted as the standard practice in the United States [9]. The process involves radially expanding a hole to create a zone of residual compressive stresses around the hole that

protects it from the effects of cyclic stresses. Using a tapered mandrel fitted with a lubricated sleeve and drawing the mandrel/sleeve combination through the hole using a hydraulic puller produces the radial expansion. The diameter of the mandrel and the sleeve is greater than the starting diameter of the hole. As the mandrel/sleeve is pulled through the hole, the material expands, allowing the mandrel to pass through the hole. The area surrounding the hole is in a subsequent state of compression that protects the hole from fatigue cracking. The function of the disposable split sleeve is to reduce mandrel pull force, ensure correct radial expansion of the hole, preclude damage to the hole, and allow one-sided processing. A finish ream is employed to diminish the effects of the damage to the hole. Unlike the tensile overloading, cold expansion leads to a uniform tangential residual stress around the hole.

Cold expansion has been investigated in numerous studies. Many analytical solutions for computation of the residual stress have been developed, but most have achieved only limited agreement with experimental results [10, 11, 12, and 13]. Researchers have suggested that the poor results are attributed to the analytical models' assumption of two-dimensional plane stress or plane strain [14 and 15]. Another problem with the analytical models is the exclusion of the reaming process.

To better simulate the cold expansion operation, finite element analyses have been employed. A finite element simulation can include all processes included in cold expansion, including the reaming step. Many two-dimensional simulations have been conducted using either plane stress or plane strain, along with two-dimensional axisymmetric simulations to account for the three-dimensional effects of the mandrel removal. Kang, et al. [15] have shown that the residual stress is significantly different at different sections through-the-thickness. Pavier, et al. [8] also used a two-dimensional axisymmetric model to simulate the cold expansion process. They concluded that residual stresses can only be estimated accurately by using a realistic simulation of cold expansion. Poussard, et al. [14] further illustrated the need for a three-dimensional simulation to account for the through-the-thickness variation of residual stress.

Another factor in the simulation of cold expansion is the unloading response of the material as the mandrel is pulled through the hole. Several studies have shown that the residual stress predicted in the region of reverse yielding is sensitive to the compressive yielding behavior [15]. Neither isotropic nor kinematic hardening models used in finite element simulations adequately account for the Bauschinger effect.

Superposition techniques are also frequently used when assessing the effects of a known residual-stress field on fatigue crack propagation. The superposition involves the computation of a stress-intensity factor $(K)_R$, which is associated with the initial pre-existing residual-stress field. This factor is then superposed upon the stress-intensity factor that results from external loading $(K)_L$ to give the total resultant stress-intensity factor for the maximum and minimum loads:

$$K_{\max} = \left(K_{\max}\right)_L + \left(K\right)_R \tag{1}$$

$$K_{\min} = (K_{\min})_L + (K)_R \tag{2}$$

The stress-intensity factor range (ΔK) and stress ratio (R) is then calculated as the following:

$$\Delta K = K_{\max} - K_{\min} \tag{3}$$

$$R = \frac{K_{\min}}{K_{\max}} \tag{4}$$

The ΔK does not change since the stress-intensity factor from the residual stress is negated, and the stress ratio holds the dependence of the stress-intensity factor from the residual stress. Fatigue crack growth is predicted using a correlation of the form

$$\frac{da}{dN} = f(\Delta K, R) \tag{5}$$

The superposition method described by equation 5 is widely used, but the dependence of R results in more rigorous calculations. To remove the stress ratio from the function and simplify the calculations for this work, the following superposition method was employed. Maximum and minimum values of the total resultant stress-intensity factor (K) are computed for the cyclic loading, and negative resultant K values are set to zero. A total resultant ΔK is then calculated. This resultant ΔK may then be used to compute the predicted fatigue crack growth rate *da/dN* in the residual-stress field using a correlation of the form

$$\frac{da}{dN} = f(\Delta K, R = 0) \tag{6}$$

The superposition technique is used extensively because of its simplicity. It has been criticized by some researchers because it considers only the initial residual-stress field that exists in the uncracked structure, with no acknowledgement of the redistribution of residual stress that occurs as the propagating fatigue crack penetrates the residual-stress field with its free or partially free surfaces [1, 16, 17, 18, 19, 20, 21, and 22]. Other researchers have argued that the redistribution of residual stress is of no consequence [2 and 23].

Bueckner [24] has demonstrated mathematically that, for linear elastic materials, stress-intensity factors resulting from a given applied loading may be computed using the stress distribution in the uncracked structure. Heaton [25] has presented a mathematically rigorous proof that generalizes Bueckner's formulation to include both thermal and residual-stress fields. The work of Bueckner and Heaton suggests that, for linear elastic materials, the redistribution of applied and residual stresses due to fatigue crack propagation is of no consequence when computing stress-intensity factors and subsequent fatigue crack growth through use of equations 2 or 3.

The conclusions arrived at by Bueckner and Heaton are applicable to linear elastic materials only. The existence of plastic deformation at the crack tip, even under small-scale yielding conditions, will produce crack-generated residual stresses at the crack tip [26 and 27] and closure along the crack surface of the propagating crack [28 and 29]. The superposition methodology is unable to account for the influence of these effects. Consequently, the use of linear elastic superposition techniques for prediction of the effects of residual stress on fatigue crack

propagation may result in crack growth predictions that correlate poorly with experimental observations [1].

As an alternative to superposition based fatigue crack growth prediction, the effective stress-intensity factor range (ΔK_{eff}) first introduced by Elber can be used [28 and 29]. The ΔK_{eff} is employed to enable consideration of crack closure in fatigue crack growth predictions. Elber considers that as a crack propagates, crack closure occurs as a result of plastically deformed material left in the path taken by the crack. This material is referred to as the plastic wake. The plastic wake enables the crack to close before minimum load is reached, and Elber reasoned that the stress-intensity factor at the crack tip does not change while the crack is closed even when the applied load is changing. The value of K when the crack is first fully opened is defined as K_o, and the reduced range of K due to closure is given by

$$\Delta K_{\text{eff}} = K_{\max} - K_o \tag{7}$$

The ΔK_{eff} has a relationship with the fatigue crack growth rate of the form

$$\frac{da}{dN} = g(\Delta K_{\text{eff}}) \tag{8}$$

Since Elber first introduced ΔK_{eff}, several methods have been developed to predict K_o in a given structure. One such method is elastic-plastic finite element analysis, which can be used to study plasticity-induced crack closure by simulating fatigue crack growth as a discrete number of incremental crack extensions. If the initial residual stress is introduced as a distribution of incompatible strain, then this type of analysis can be made to incorporate the effect of initial residual stress as well. The presence of an initial residual-stress field may cause significant differences in the crack closure behavior when compared to an analysis containing no initial residual stresses. The initial residual-stress and its redistribution as the crack propagates may also result in final crack opening away from the crack tip, potentially complicating the methodology used to predict fatigue crack growth.

A number of researchers have simulated plasticity-induced closure using finite element analyses. McClung [30] and Solanki, et al. [31] have provided critical overviews of these analyses. The basic algorithm employed by the studies is the same. An elastic-plastic model is built with a suitably refined mesh, and remote tractions are applied to simulate cyclic loading. The crack tip node is released during each cycle, advancing the crack one element length and allowing a plastic wake to form. Crack closure is predicted by monitoring the contact between crack faces. This process is repeated until the crack-opening stress values have stabilized. There are many variables to consider when using finite element to simulate closure: element type, mesh size, crack-opening level determination, crack-opening level stabilization, crack advance scheme, and constitutive model [32].

Although many studies have been performed employing finite element analyses to simulate fatigue crack growth and crack closure, few have considered a crack growing through an initial residual-stress field. Beghini and Bertini [33] employed a finite element-based technique to

study the interaction between residual-stress fields and crack closure. They found that the finite element analysis resulted in K_o values that compared fairly well with experimental values. More recently, Choi and Song [34] have also used a finite element analysis to predict crack closure in compressive residual-stress fields. They found very good agreement between the finite element predictions and experimental measurements of K_o in a tensile residual-stress field, but poorer agreement in a compressive residual-stress field.

In the research reported here, fatigue crack growth from a hole under the influence of residual stress is considered. The crack closure level is computed from a finite element simulation and a fatigue life is predicted. This method of fatigue life prediction is compared with a superposition technique and experimental data.

3. EVALUATION APPROACH.

3.1 LABORATORY TESTING OF FATIGUE CRACK GROWTH.

3.11 Tensile Overload.

Liu [35] measured fatigue crack growth from a hole using the specimen shown in figure 1. Constant-amplitude loading was used, and a residual stress was induced near the hole using a single tensile overload. The material used was a 2024-T351 aluminum alloy in the longitudinal transverse orientation with t = 6.35 mm, w = 76.2 mm, h = 304.8 mm, and $2r$ = 19.05 mm. Tensile tests were conducted by Liu to determine the stress-strain relationship for the alloy, shown in figure 2. Center-cracked specimens were also tested under constant-amplitude cyclic loading to develop baseline crack growth rate (da/dN) curves at R ratios of 0.1 and 0.7. This data is shown in figure 3 in conjunction with the da/dN—ΔK_{eff} curve taken from NASGRO [36].

Two specimens with the dimensions shown in figure 1 were tested. These specimens were subjected to one overload cycle σ = 250 MPa to introduce a residual-stress field near the hole. An elox cut was then inserted into the edge of the hole. The specimens were then subjected to constant-amplitude loading with R = 0.1. The test matrix is shown in table 1.

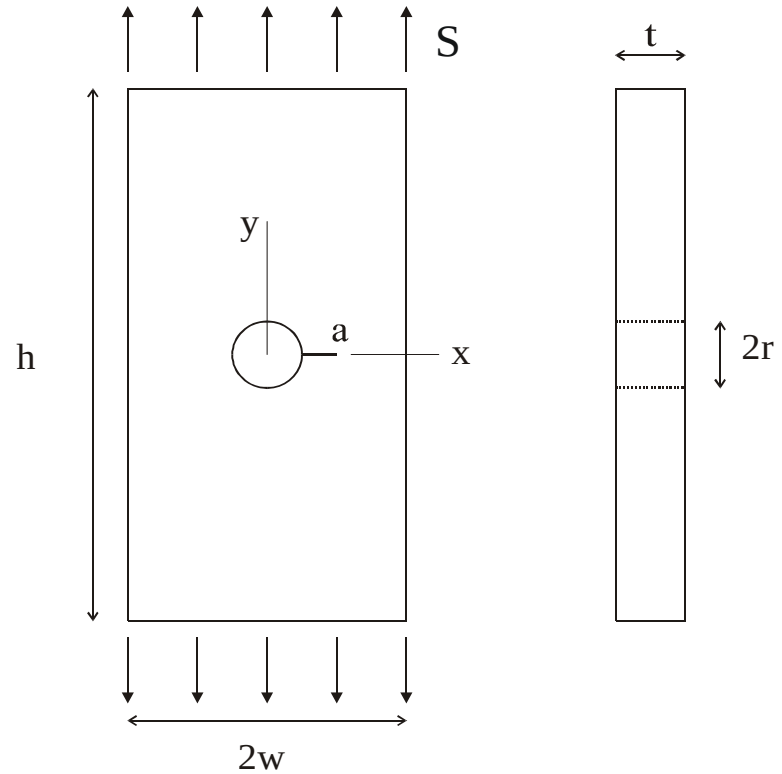

Figure 1. Fatigue Crack Growth Specimen

Table 1. 2024 Test Matrix

Test	Stress Level, S	Elox Cut Length, l_n	Elox Cut Width, w_n
A2-30	103.4 MPa	1.994 mm	0.152 mm
A2-31	124.1 MPa	1.029 mm	0.152 mm

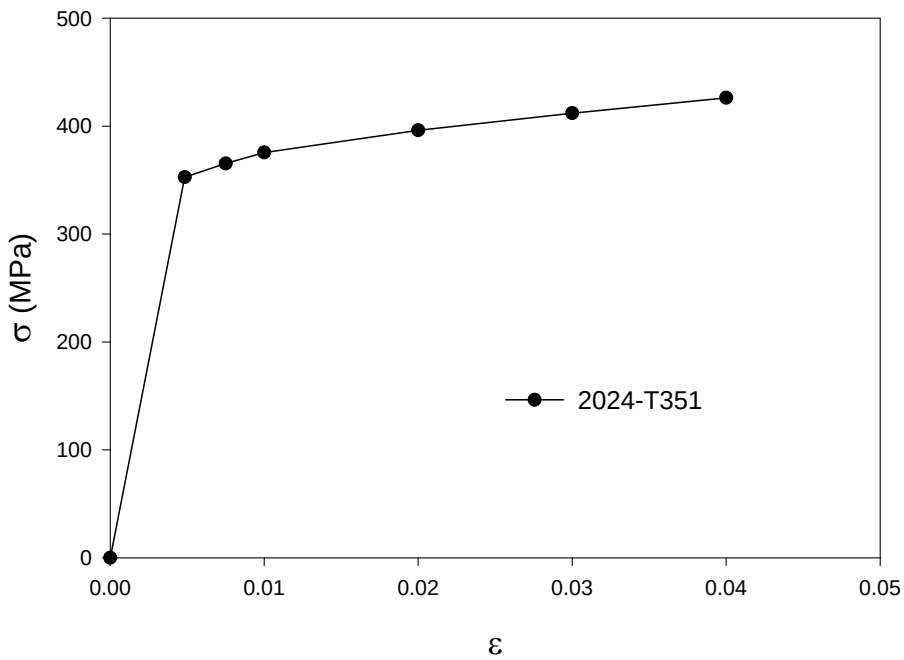

Figure 2. 2024 Stress-Strain Curve

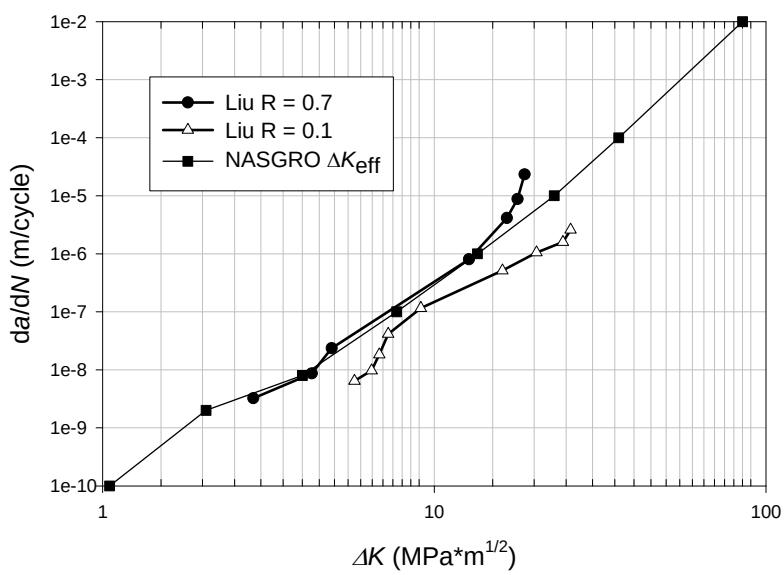

Figure 3. 2024 Baseline Crack Growth Rate Data

3.1.2 Cold Expansion.

Fatigue tests were also performed on plates containing a hole using the specimen shown in figure 1. The test plan called for a 7075-T6 aluminum alloy with t = 2.03 mm, w = 22.23 mm, h = 203.2 mm, and $2r$ = 6.35 mm. An electrical discharge-machined (EDM) notch with notch length l_n = 0.254 mm and notch width w_n = 0.127 mm was inserted into one side of each hole to aid in crack initiation. Overall, ten specimens were tested with constant-amplitude loading with R = 0.1 and σ_{max} = 117.2 MPa. Six specimens were tested with no residual stress. The test plan initially called for specimens with cold-expanded holes, with a final $2r$ = 6.35 mm to be tested. The cold expansion process was applied using the following steps:

a. Initial hole cut with $2r$ = 5.979 mm

b. A mandrel with diametrical interference d_i = 0.268 mm, corresponding to 4.48% cold expansion, was pulled through hole to induce the residual stress

c. Cold-expanded hole reamed to $2r$ = 6.35 mm

A fatigue test was performed on a cold-expanded hole with a final $2r$ = 6.35 mm, with no crack growth after one million cycles. The test plan was adjusted so that a reasonable failure time could be obtained. To relieve some residual stress around the hole, the final ream was increased so that the final $2r$ = 8.738 mm, and this value was used for all cold-expanded specimens. In addition, failure at the grip was a problem with the cold-expanded specimens, so the specimen widths were reduced to w = 21.59 mm, and fiberglass shims were used to minimize damage to the specimens in the gripping area. Four cold-expanded specimens with a final ream $2r$ = 8.738 mm were successfully tested. Fatigue cracks were measured visually with a 25X magnification traveling microscope and an electronic micrometer.

No tensile or baseline crack growth rate tests were performed on the 7075-T6 material used for these tests. The stress-strain relationship was taken from the MIL Handbook 5D [37] for the plasticity-induced crack closure simulations. This relationship is shown in figure 4. The baseline crack growth rate data for R = 0.1 was taken from the NASGRO material database, and the baseline crack growth rate data for R = 0.7 was taken from the MIL Handbook 5. The NASGRO da/dN—ΔK_{eff} relationship is also plotted. This data is shown in figure 5. As this figure shows, the data for the R = 0.1 and the NASGRO da/dN—ΔK_{eff} relationship intersect, but the two lines should be parallel. This issue may be a problem with the data or with NASGRO, but was ignored in this work.

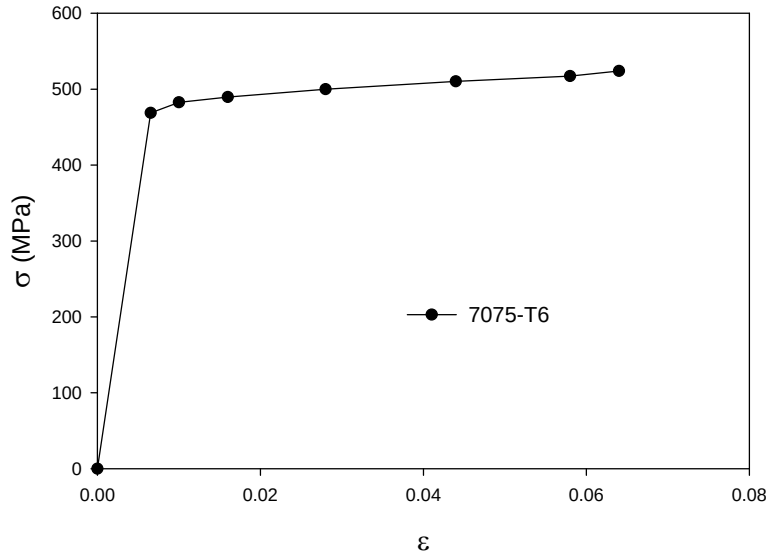

Figure 4. 7075 Stress-Strain Curve

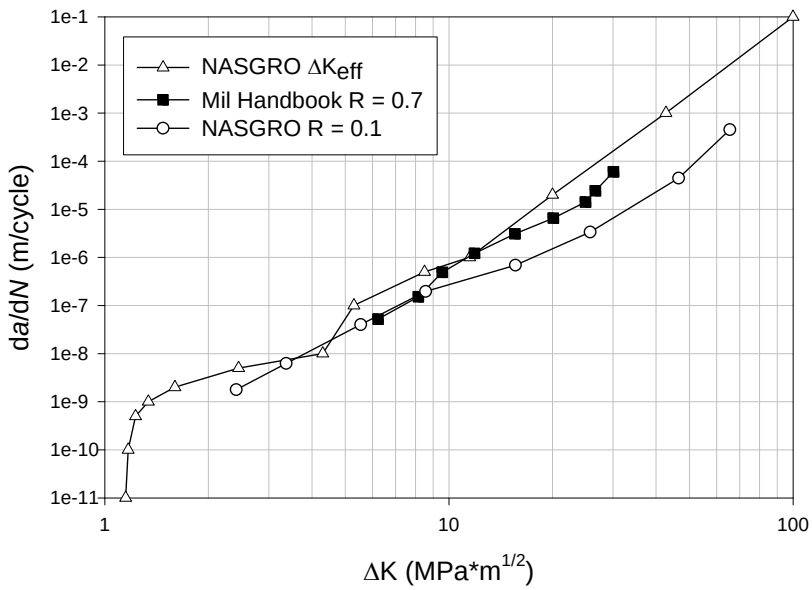

Figure 5. 7075 Baseline Crack Growth Rate Data

3.2 FINITE ELEMENT ANALYSIS.

Finite element analysis was used to simulate the fatigue crack growth in all specimens tested. The commercial finite element program ANSYS version 8.0 [36] was used. To simulate the elastic-plastic constitutive behavior of the material, the stress-strain relationships shown in figures 2 and 4 were input into the finite element code for the two materials. A two-dimensional

mesh was built using four-node plane stress elements, with one half of the specimen modeled because of symmetry. Plane stress was used since both geometries tested were relatively thin, although the assumption is more suited for the 7075 simulation since the test specimens were thinner. The plane stress assumption may lead to opening stress values that are too high for the 2024 simulations. The mesh used in the simulation of the tensile overload contained 6529 elements and 6687 nodes, and is shown in figure 6. The mesh used in the simulation of the cold expansion was similar, with more axisymmetric refinement around the hole to enable the reaming process to be simulated.

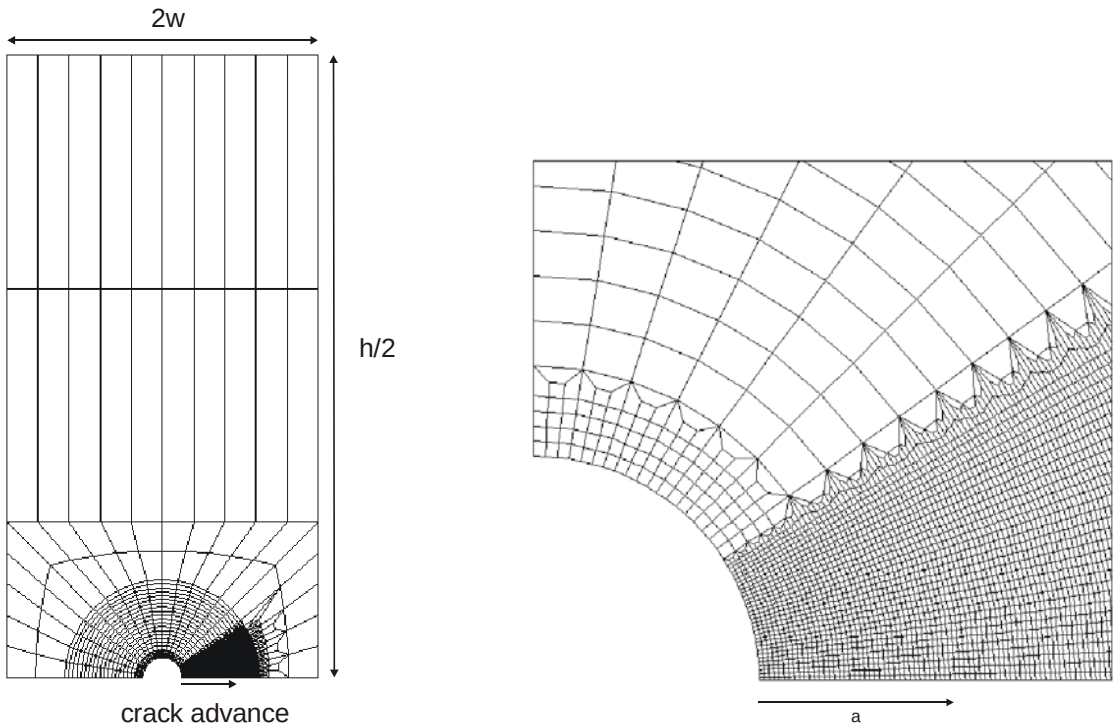

Figure 6. Finite Element Model Mesh

3.2.1 Tensile Overload Simulation.

To simulate the overload and induce the residual stress, a uniform stress of 250 MPa was applied and removed. After the overload, elements were removed from the mesh using the Element Kill command in ANSYS to simulate the slotting process. This command gives the removed elements a negligible stiffness to simulate the removal of material [36].

3.2.2 Cold Expansion Simulation.

To simulate the cold expansion process, three steps were taken. A uniform displacement r_i = 0.134 mm was applied to all nodes on the hole surface. The displacement was then removed to simulate the unloading of the mandrel. The reaming process and EDM notching were then simulated by again using the Element Kill command to give the final residual stress state before the crack growth simulation.

3.2.3 Crack Growth Simulation.

After the residual stress and the slotting were simulated, fatigue crack growth was modeled by repeatedly loading, advancing the crack, and then unloading. The model was incrementally loaded to the maximum load, at which time the crack tip node was released, allowing the crack to advance one element length per load cycle. The applied load was then incrementally lowered until the minimum load was attained. Crack surface closure was modeled by changing the boundary conditions on the crack surface nodes. During each increment of unloading, the crack surface nodal displacements were monitored. Between any two increments, if the nodal displacement became negative, the node was closed and a node fixity was applied to prevent crack surface penetration during further unloading. During incremental loading, the reaction forces on the closed nodes were monitored, and when the reaction forces became positive, the nodal fixity was removed. A command listing for all the routines involved is included in appendix A. A sample input file is included in appendix B. The purpose of this analysis was the computation of the crack-opening stress S_o. The crack-opening stress was found as the applied stress that first fully opened the crack, regardless of the location along the crack that was last to open. A more detailed discussion of this type of analysis can be found in Solanki, et al. [31].

3.3 FATIGUE CRACK GROWTH PREDICTION METHODOLOGIES.

3.3.1 Superposition Prediction Methodology.

To apply the superposition technique, the stress-intensity factors were calculated. From Tada and Paris [38], for a crack of length a growing from a hole in an infinite plate under a uniform stress S:

$$[K(a)]_{\inf} = S\,F(a)\sqrt{\pi a} \tag{9}$$

$$\begin{aligned} F(a) = {} & [1 + 0.2\left(1 - \frac{a}{r+a}\right) + 0.3\left(1 - \frac{a}{r+a}\right)^6]\cdot \\ & [2.243 - 2.64\left(\frac{a}{r+a}\right) + 1.352\left(\frac{a}{r+a}\right)^2 - 0.248\left(\frac{a}{r+a}\right)^3] \end{aligned} \tag{10}$$

A finite-width correction factor $f(a)$was taken from Isida [39] such that the stress-intensity factor from the applied load is given by

$$(K)_L = f(a)[K(a)]_{\inf} \tag{11}$$

$$f(a) = \sqrt{\frac{1}{\cos\left(\frac{\pi}{2}\frac{2r+a}{2W-a}\right)} \cdot \frac{\sin\left(2\frac{2r+a}{2W-a}\frac{a}{W}\right)}{\left(2\frac{2r+a}{2W-a}\frac{a}{W}\right)}} \tag{12}$$

The stress-intensity factors for the initial residual stress $(K)_R$ were determined using a weight function computation and the residual stress resulting from the simulation of the overload or cold expansion and subsequent slotting. Denoting the weight function as $m(x,a)$ and the residual stress in the uncracked slotted body as $\sigma(x)$, the stress-intensity factor was computed as:

$$K_R = \int_0^a \sigma(x) \cdot m(x,a) dx \tag{13}$$

The weight function was taken from Wu and Carlsson [40]. The stress-intensity factors due to the applied loading and the residual stress were then added to give a resultant stress intensity at the maximum and minimum load. If any resultant stress intensity was less than zero, it was taken to be zero.

$$\begin{aligned} K &= (K_L) + (K_R) \quad & K > 0 \\ K &= 0 & K < 0 \end{aligned} \tag{14}$$

The ΔK was then computed as the difference between the maximum and minimum resultant stress-intensity factors, creating an effective $R = 0$ loading. A center crack baseline crack growth rate curve for $R = 0$ was not determined by Liu, and the curve for $R = 0.1$ was used as an approximate replacement to determine the corresponding crack growth rates from the computed ΔK. The crack growth rate was then used with a prescribed small da to find a corresponding dN, and these incremental values were added to the previous values of a and N to give the life prediction.

3.3.2 Finite Element Prediction Methodology.

The crack growth was also predicted using the opening stresses from the finite element analysis, as shown in figure 7. Equation 11 was used to find the maximum stress-intensity factor K_{max} and the opening stress-intensity factor K_o, using $S = S_{max}$ and $S = S_o$, respectively. The ΔK_{eff} was then calculated as the difference between the maximum and opening stress-intensity factors. Both the baseline crack growth curve for the Liu $R = 0.7$ data and the NASGRO da/dN—ΔK_{eff} curve were used as an effective crack growth rate curve $da/dN = g(\Delta K_{eff})$, and each curve was used to determine crack growth rates for the computed ΔK_{eff}. These crack growth rates were used to determine the crack length as a function of the number of cycles.

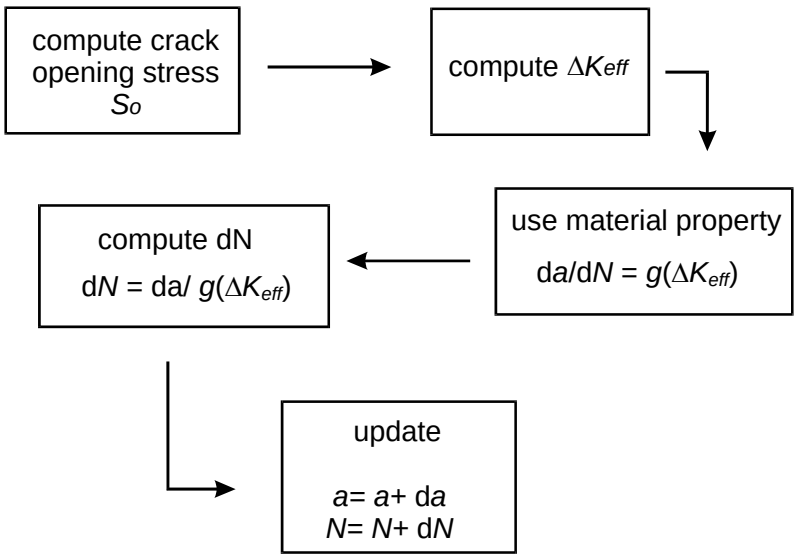

Figure 7. Crack Closure-Based Crack Growth Prediction Methodology

3.4 RESULTS.

3.4.1 Tensile Overload Results.

The residual stress determined from the finite element analysis is shown in figure 8. The initial residual stress from the overload shows a maximum compressive stress at the edge of the hole nearly the same magnitude as yield strength of the material. After the slotting process was simulated, the compressive residual stress at the notch edge was increased. Since the slot is modeled as an idealized rectangle with sharp corners, the residual-stress predictions may be overestimated near the notch end.

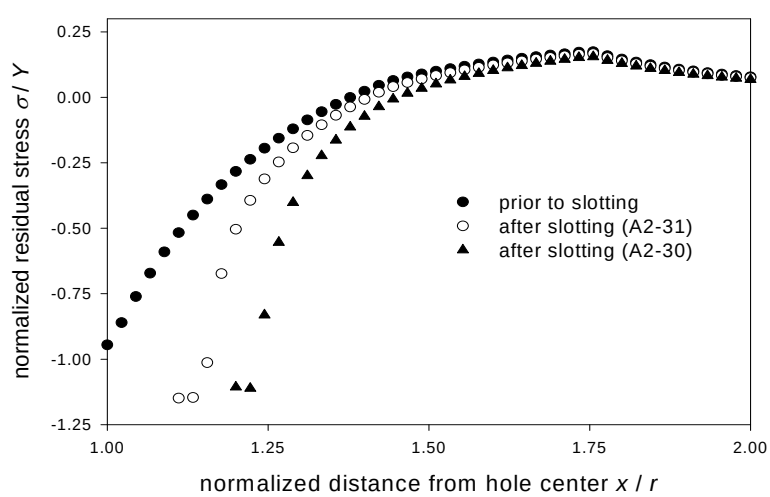

Figure 8. Residual-Stress Results From Finite Element Simulation of the Tensile Overload

The opening stress results given by the finite element crack growth analysis are shown in figure 9. Both plots illustrate opening stresses that initially exhibit a sharp increase, then decrease gradually before again rising slowly. The initial sharp increase indicates that the crack growth is slower initially, due to the residual stress at the edge of the notch. For test A2-31, the opening stress for a residual stress-free specimen is shown for comparison. The opening stresses merge after approximately 5.2 mm of crack growth.

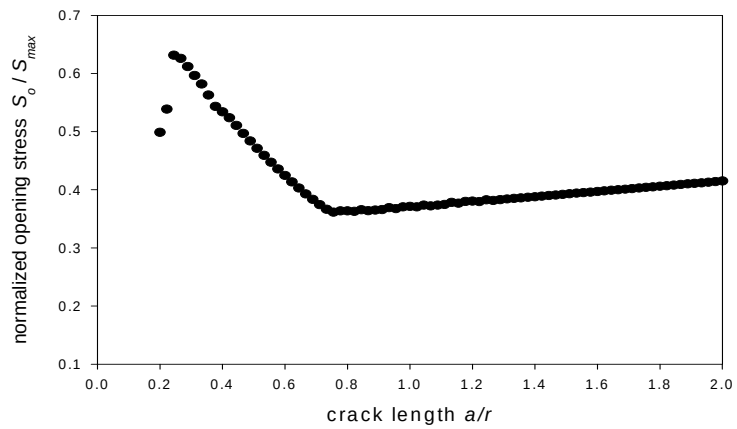

(a)

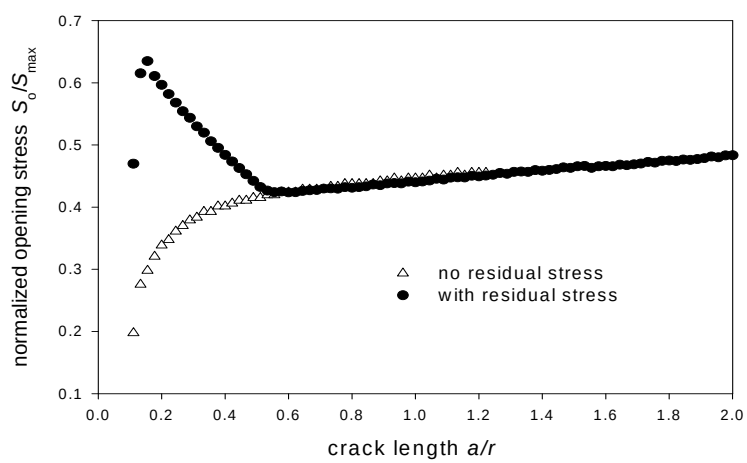

(b)

Figure 9. Predicted Crack-Opening Stress, (a) Test A2-30 and (b) Test A2-31

Figure 10 shows the predicted crack growth as a function of the number of cycles for test A2-30 from both the superposition and finite element methods. The results from each method are compared to the experimental data. The plot indicates that the superposition method predicts lives much longer than the experimental data. The finite element predictions are more conservative, leading to shorter lives than seen in the experiment. When the NASGRO *da/dN*—ΔK_{eff} curve is used, the finite element analysis prediction compares better with the experimental data when compared with the finite element analysis prediction that uses the Liu $R = 0.7$ data to define the *da/dN*—ΔK_{eff} relationship. The NASGRO curve extends to larger ΔK_{eff} values and does not exhibit a nonlinearity in the higher ΔK_{eff} region as seen in figure 3. This nonlinearity is

often seen in high R tests and its presence likely produced the poor fatigue crack growth predictions observed when using the $R = 0.7$ baseline data.

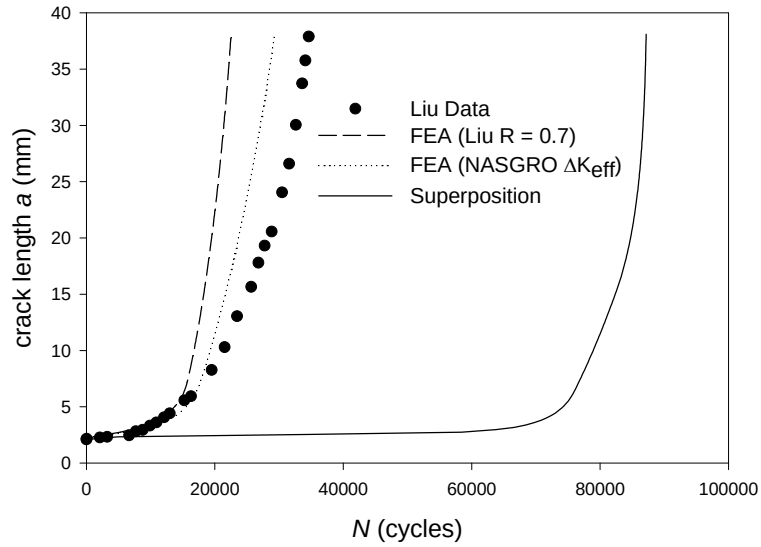

Figure 10. 2024 Fatigue Crack Growth: Predicted and Actual, Test A2-30

Figure 11 shows the predicted crack growth rate for test A2-31 from both the superposition and finite element methods, compared with the experimental data. Again, the NASGRO da/dN—ΔK_{eff} curve results are in good agreement with the data. The superposition method again overestimates the actual life, but for this test, the difference is much smaller.

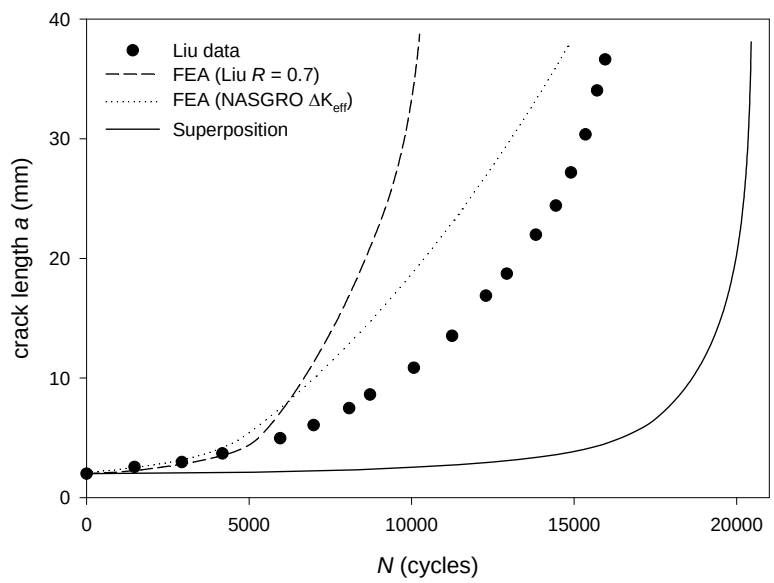

Figure 11. 2024 Fatigue Crack Growth: Predicted and Actual, Test A2-31

To further justify the use of one *da/dN*—ΔK_{eff} relationship over the other, a simple verification was employed. Fatigue crack growth in center-cracked specimens tested by Liu with R = 0.1 was predicted using a plane-strain (α = 3) opening stress value S_o/S_{max} = 0.265, from Newman [41] and calculating ΔK_{eff} using a center crack stress-intensity factor solution taken from Tada and Paris [38]. The specimen tested was relatively thick, with t = 6.35 mm, so plane strain is a reasonable assumption. Both the NASGRO *da/dN*—ΔK_{eff} and Liu *da/dN*—ΔK_{eff} were used to predict fatigue crack growth. As shown in figure 12, use of the Liu *da/dN*—ΔK_{eff} relationship resulted in better correlation with the experimental data. The conflicting results may be due to the maximum values of ΔK calculated by the finite element method. The highest calculated ΔK is over 21 MPa*m$^{1/2}$, a value outside of the range of the Liu R = 0.7 data. The NASGRO equation is a better option given that no extrapolation is needed when the calculated ΔK values extend outside of the region of the Liu data.

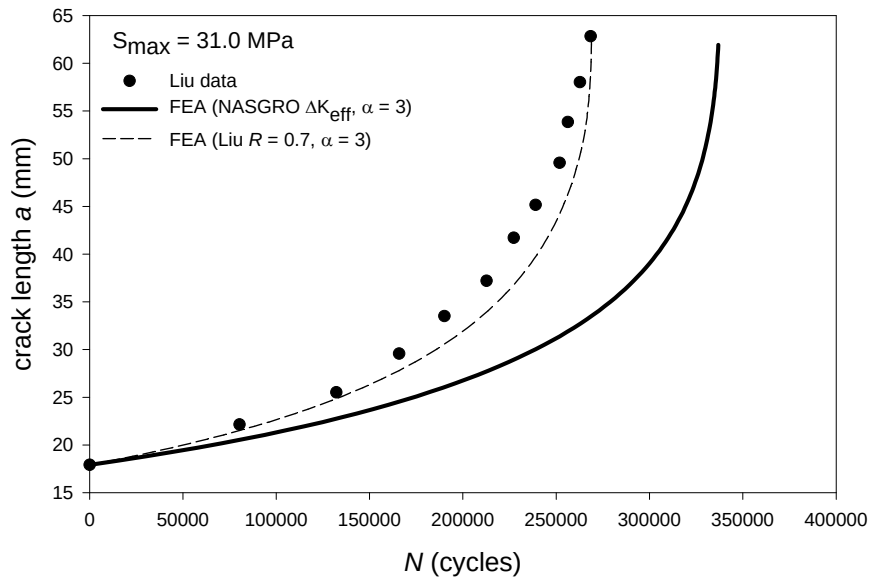

Figure 12. 2024 Center Crack Specimen Fatigue Crack Growth: Predicted and Actual

Next, consider the effect of the notching process on the fatigue life. Figure 13 compares superposition-based predictions made using the initial residual stress and the redistributed residual stress after slotting. The difference is fairly small when comparing the results given by each residual stress. The redistribution is not significant here, but it may have a much greater influence in other cases.

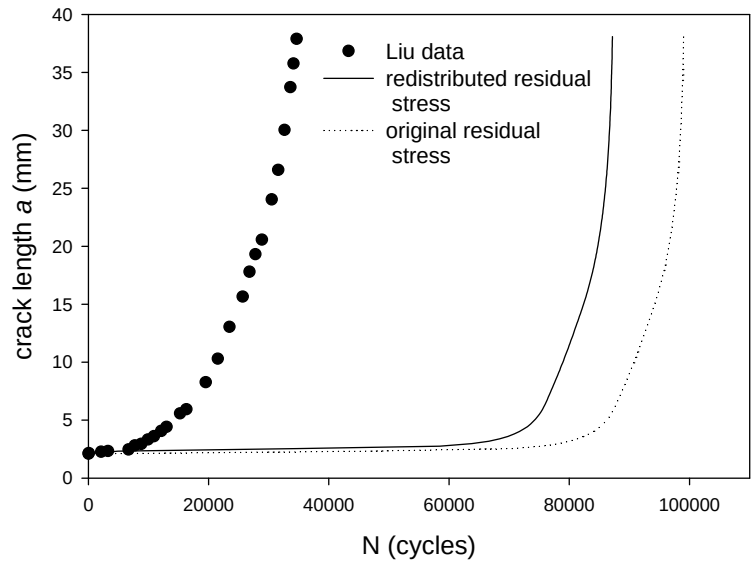

Figure 13. 2024 Fatigue Crack Growth, Superposition Predictions With Slotted and Unslotted Residual Stress and Actual, Test A2-30

In addition to opening stresses, the finite element analysis also provided profiles of the crack as it opened and closed. Figures 14 and 15 give predicted profiles for short and long cracks for test A2-31 to illustrate the different crack-opening behavior at different crack lengths. Figure 14 shows that for short cracks, remote closure occurs and the crack mouth is the last to open. Figure 15 indicates that remote closure does not occur when the crack becomes longer, with the crack tip being the last location to open. No distinction between these two different crack-opening behaviors was made in the fatigue crack growth predictions presented here.

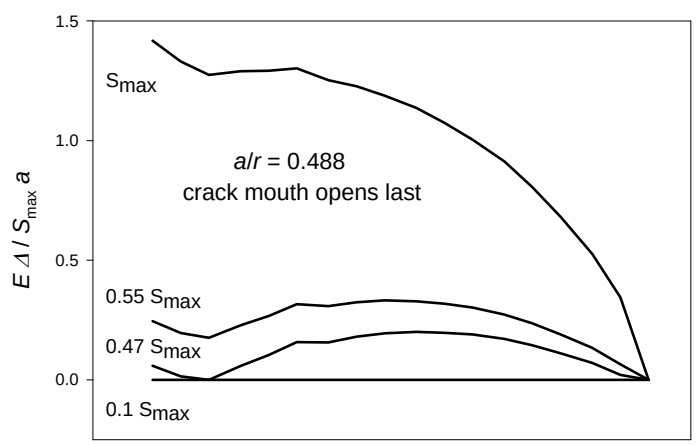

Figure 14. Test A2-31 Short-Crack Profile

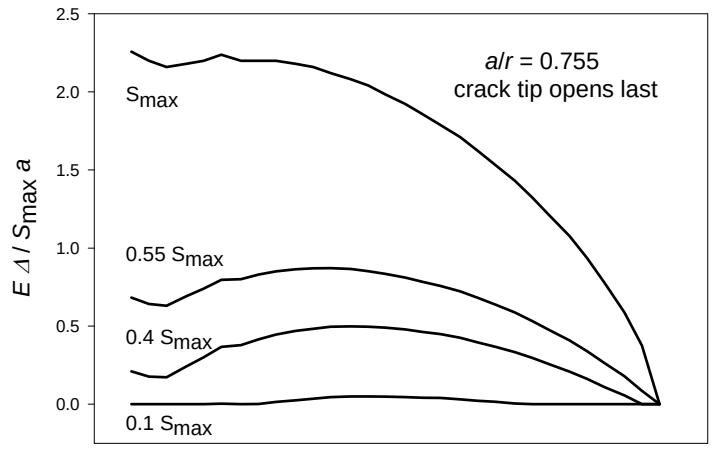

Figure 15. Test A2-31 Long-Crack Profile

3.4.2 Cold Expansion Results.

The residual stress determined from the finite element analysis for the cold-expanded specimens is shown in figure 16. After the cold expansion, the residual stress shows a maximum compressive stress at the edge of the hole near the magnitude of the yield strength of the material. This residual stress corresponds to the first cold-expanded test that resulted in no crack growth. After reaming, the residual stress is relaxed considerably, with the magnitude reduced by a factor of two. After the slotting process is simulated, the peak residual stress increases to reach the yield strength again. This residual stress may be overestimated because the slot was modeled as a rectangular notch. The finite element analysis predicted a high strain gradient at the corners of the slot, which would likely not be seen if a slot with more realistic rounded corners was considered.

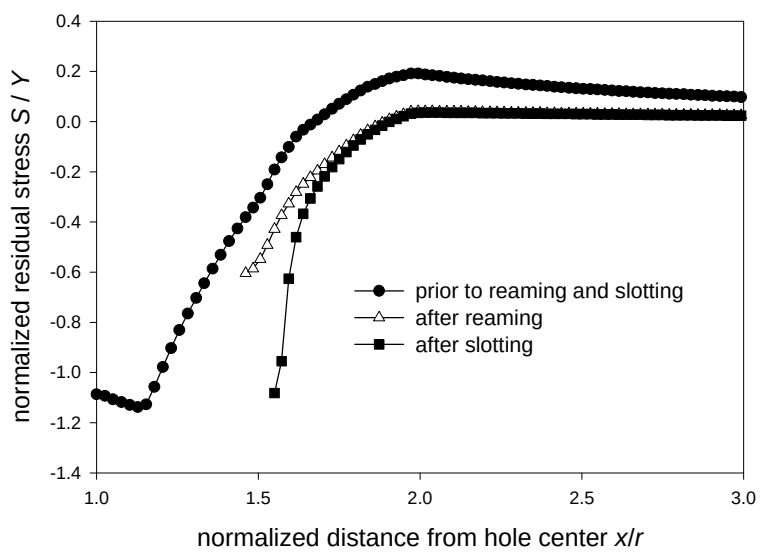

Figure 16. Residual-Stress Results From Finite Element Simulation of the Cold Expansion Process

The opening stress results given by the finite element crack growth analysis are shown in figure 17. The results are similar to those from the tensile overload simulation. The opening stresses from the cold-expanded simulation show an initial increase before decreasing to approximately the steady-state value. The high initial opening stress values are a result of remote crack closure. The crack mouth node is the last to open until the opening stress value reaches steady state, which indicates the crack tip node is now the last to open. The opening stress values for the non-cold-expanded hole start at zero and climb to the steady-state value.

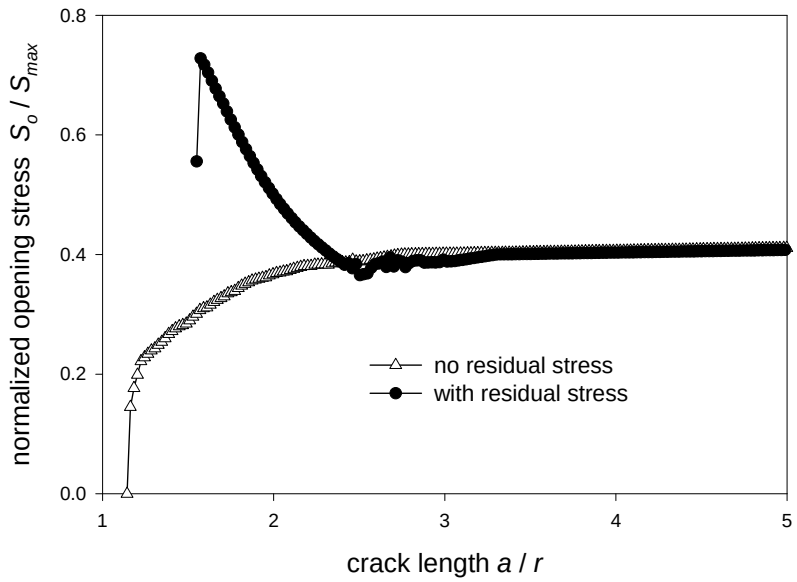

Figure 17. Predicted Opening Stress for the 7075-T6 Simulations

Figure 18 shows the predicted crack growth as a function of the number of cycles for the cold-expanded tests from the superposition and finite element methods. The results are compared with the experimental data. The superposition method predicts the crack growth much better than the finite element method. The finite element prediction is in error by a factor of approximately 4 when the NASGRO da/dN—ΔK_{eff} relationship is used, but this error is reduced to around 2 when the da/dN—ΔK_{eff} relationship, taken from MIL-Handbook 5, is used. This error questions the reliability of the opening stress calculations. A more refined mesh may give better results, but the crack growth algorithm had convergence problems with smaller elements. Although all predictions were conservative, the superposition method compared fairly well with the experimental data.

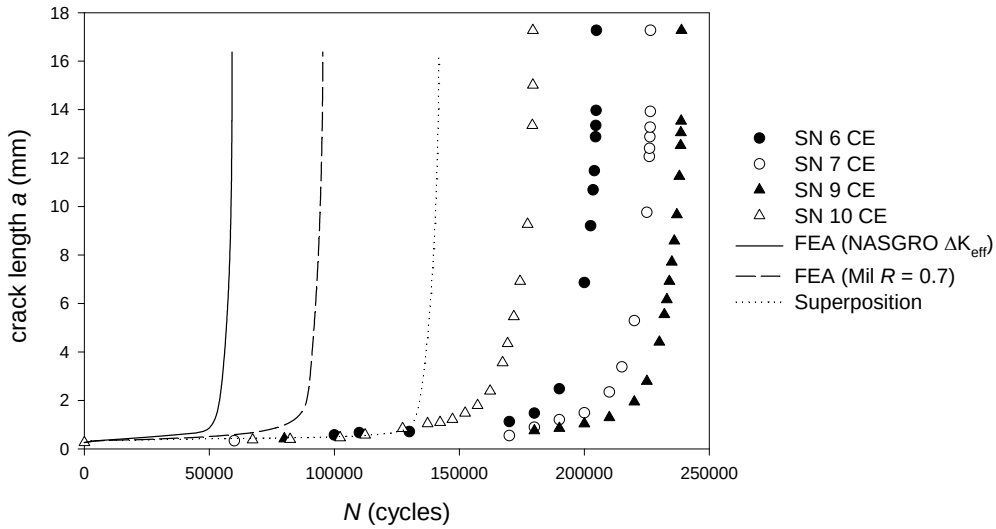

Figure 18. 7075 Fatigue Crack Growth for Cold-Expanded Hole: Predicted and Actual

The predicted crack growth for the non-cold-expanded hole is compared with experimental data in figure 19. Since the test simulated is simple constant amplitude with no residual stress, more accuracy was expected from the finite element predictions when compared with the data, but as the plot illustrates, the comparison is fairly poor with the prediction differing from the data by a factor of 2 with the NASGRO da/dN—ΔK_{eff} relationship. Again, the use of the da/dN—ΔK_{eff} relationship, taken from MIL-Handbook 5, reduces this error, but the results again point to the opening stress calculations as the probable cause of the poor agreement. A more refined mesh may produce the higher opening stress values needed to allow the prediction to agree better with the data. Any attempts to run a more refined mesh were unsuccessful because of convergence issues in the finite element code.

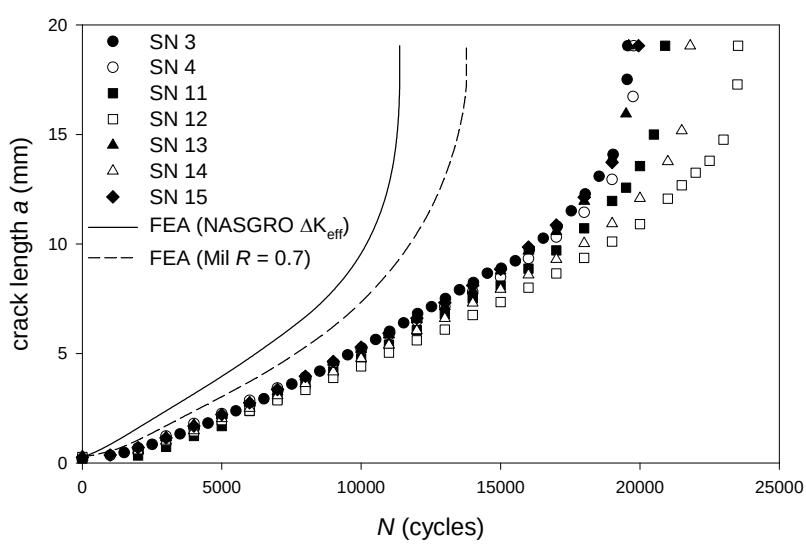

Figure 19. 7075 Fatigue Crack Growth for Non-Cold-Expanded Hole: Predicted and Actual

The residual-stress redistribution from the slotting process was also investigated by using the slotted and unslotted residual stress with the superposition method to predict the fatigue crack growth. Figure 20 shows the predictions compared with the experimental data. The unslotted residual stress led to a better comparison than the slotted residual stress. The difference is small and demonstrates that simulating the slotting process does not make a considerable difference in the resulting life predictions.

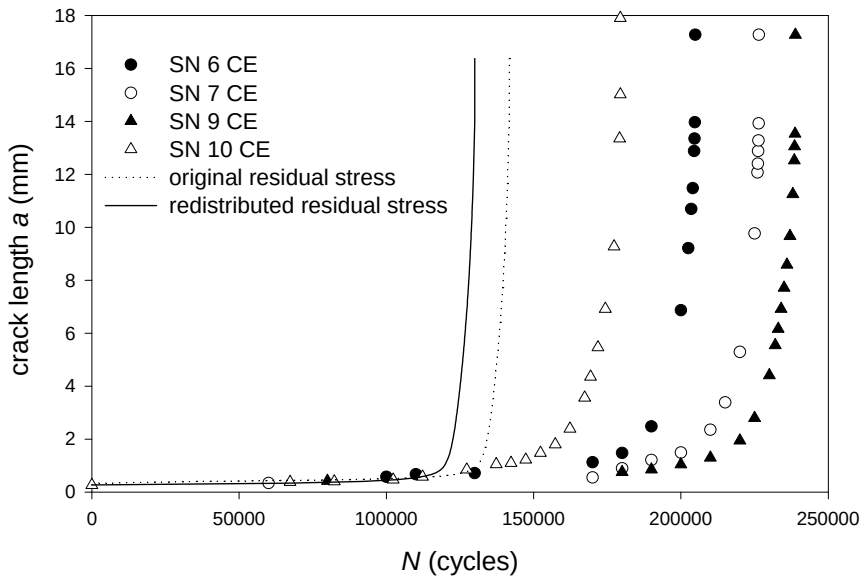

Figure 20. 7075 Fatigue Crack Growth, Superposition Predictions With Slotted and Unslotted Residual Stress and Actual

3.4.3 Convergence Issues.

Fatigue crack growth simulations were performed with varying levels of mesh refinement in an attempt to verify that the computed opening stresses were mesh independent. As the elements in the mesh near the crack tip are made smaller, the opening stress values should not change if convergence is achieved. Three different meshes were used in the simulation of test A2-30, with crack growth element sizes *da* of 0.635, 0.2117, and 0.0706 mm. To attach a physical significance to these values, they were compared to the Dugdale plane stress monotonic crack tip plastic zone ρ.

$$\rho \cong \frac{\pi}{8}\left(\frac{K_{\max}}{Y}\right)^2 \tag{15}$$

$K_{\max}$ was calculated with and without residual stress included, using the precrack crack length of a = 2.095 mm. For physically realistic results, one would expect that $da < \rho$ would be necessary. When the residual stress was not included in the $K_{\max}$ calculation, ρ = 1.078 mm, which implies that even the largest crack growth element size is potentially sufficient. When the residual stress is included, ρ = 0.166 mm. This smaller value suggests that only the smallest crack growth element size will give realistic results.

Figure 21 gives the opening stress predictions for the three different meshes in the simulation of test A2-30. For the meshes corresponding to a crack growth element size *da* of 0.6350 and 0.2117 mm, the opening stress values appear to be approaching convergence. The third mesh with the smallest element size, *da* = 0.0706, exhibited results that were considered excessively noisy. It is believed that the noise is an artifact of a numerical difficulty, and not representative of a physical phenomenon. Consequently, the results predicted with *da* = 0.2117 mm were considered satisfactory.

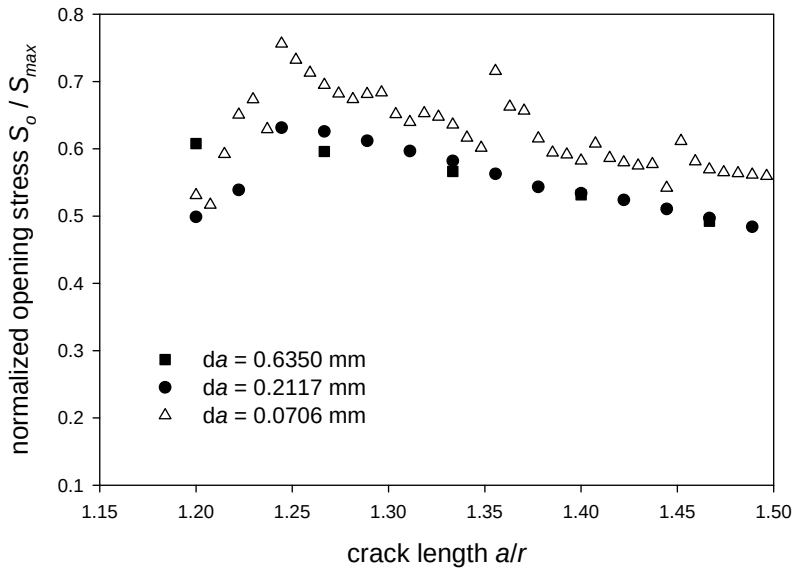

Figure 21. Opening Stresses for Different Element Sizes in Test A2-30 Simulation

4. SUMMARY.

Fatigue crack growth predictions in the presence of residual stress using elastic superposition are simple and relatively accurate. Increased accuracy can be obtained using a closure-based approach, but at the expense of increased modeling complexity. A slotting process for purposes of starting a fatigue crack introduces a redistribution of the residual stress, although this did not have a considerable effect on the subsequent fatigue life for the geometry considered here.

Crack growth predictions using elastic superposition are relatively simple and accurate. A slotting process for purposes of starting a fatigue crack introduces a significant redistribution of the residual stress, and this may have a considerable effect on the subsequent fatigue life. The finite element method presented here created conflicting results for the two different tests simulated. The finite element method worked well in predicting the tensile overload tests, but resulted in less accurate predictions for the cold-expanded tests.

Crack growth simulations using plasticity-induced crack closure concepts are sensitive to the crack growth rate relationship $da/dN = f(\Delta K_{\mathrm{eff}})$ used. This represents a potentially serious problem and highlights the need for experimental methods to reliably measure this relationship. For the work presented here (tensile overload tests), the baseline data for R = 0.7 from Liu's

work was initially chosen as the $da/dN = f(\Delta K_{eff})$ relationship. This relationship could have also been defined by closure-free baseline data for $R = 0.6$ or $R = 0.8$, if such data were available, and this could have changed the results significantly. As stress ratio is increased, the data exhibits a nonlinearity at a lower ΔK, which will lead to inaccurate predictions as demonstrated. This nonlinearity occurs because of the specimen size used when generating the baseline data. If a small-width specimen is used, such as the specimen used by Liu, fracture occurs sooner, but if a wider specimen is used, fracture does not occur as soon and this nonlinearity is not seen.

Another concern with the crack growth relationship $da/dN = g(\Delta K_{eff})$ is in the near-threshold region. In the closure-based predictions, the high opening stresses in the regions with compressive residual stress led to low ΔK_{eff} values. These values may lie in the near-threshold regime for the material tested, where data uncertainties may be highest. Accurate predictions will not be produced until the near-threshold regime is properly characterized.

Each tensile overload fatigue crack growth prediction was compared with a single test only, and thus, the comparisons are not a sufficient validation due to the inherent scatter in fatigue crack growth data. More replicate tests are needed to further validate the prediction methodologies used in this study.

5. REFERENCES.

1. Nelson, D.V., *Residual Stress Effects in Fatigue*, *ASTM STP 776*, American Society for Testing and Materials, 1982, pp. 172-194.

2. Parker, A.P., *Residual Stress Effects in Fatigue*, ASTM STP 776, American Society for Testing and Materials, 1982, pp. 13-31.

3. Besuner, P.M., Harris, D.O., and Thomas, J.M., "A Review of Fracture Mechanics Technology," *NASA Contractor Report 3957*, NASA, 1986.

4. Leis, B., "Effect of Surface Conditioning and Processing on Fatigue Performance," *ASM Handbook, Fatigue and Fracture*, v 19, 1997.

5. SAE Fatigue Design and Evaluation Steering Committee, *Fatigue Design Handbook*, 3rd edition, Society of Automotive Engineers, 1997.

6. Stephens, R.I., Fatemi, A., Stephens, R.R., and Fuchs, H.O., *Metal Fatigue in Engineering*, John Wiley & Sons, New York, 2001.

7. Ozdemir, A.T., Cook, R., and Edwards, L., "Residual Stress Distributions Around Cold Expanded Holes," ICAF Symosium, Stockholm, 1993.

8. Pavier, M.J., Poussard, C.G.C., and Smith, D.J., "A Finite Element Simulation of the Cold Working Process for Fastener Holes," *Journal of Strain Analysis*, Vol. 32, No. 4, 1997, pp. 287-300.

9. FTI, *Extending the Fatigue Life of Metal Structures*, Materials Testing, Fatigue Technology Inc., 150 Andover Park West, Seattle, Washington, 1991.

10. Hsu, Y.C. and Forman, R.G., "Elastic-Plastic Analysis of an Infinite Sheet Having a Circular Hole Under Pressure," *Journal of Applied Mechanics*, Vol. 42, 1975, pp. 347-352.

11. Rich, D.L. and Impellizzeri, L.F., "Fatigue Analysis of Cold-Worked and Interference Fit Fastener Holes," *Cyclic Stress-Strain and Plastic Deformation Aspects of Fatigue Crack Growth*, ASTM STP 637, 1975, pp. 153-175.

12. Chen, P.C.T., "A New Method of Predicting Residual Stresses in Autofrettaged Gun Barrels," *Technical Report ARCCB-TR-86012*, U.S. Army Armament Research and Development Center, Watervliet, 1986.

13. Zhu, W. and Zha, Z., "An Elastic-Plastic Analysis of Autofrettaged Thick-Walled Cylinders," *Acta Mech. Sinica*, Vol. 19, 1987, pp. 245-255.

14. Poussard, C., Pavier, M.J., and Smith, D.J., "Analytical and Finite Element Predictions of Residual Stresses in Cold Worked Fastener Holes," *Journal of Strain Analysis*, Vol. 30, No. 4, 1995.

15. Kang, J., Johnson, W.S., and Clark, D.A., "Three-Dimensional Finite Element Analysis of the Cold Expansion of Fastener Holes in Two Aluminum Alloys," *Transactions of the ASME*, Vol. 124, 2002, pp. 140-145.

16. Underwood, J.H., Pook, L.P., and Sharples, J.K., *Flaw Growth and Fracture*, ASTM STP 631, American Society for Testing and Materials, 1977, pp. 402-415.

17. Fukuda, S. and Tsuruta, Y., *Transactions of JWRI*, Vol. 7, 1978, pp. 67.

18. Chandawanich, N. and Sharpe, W.N., Jr., "An Experimental Study of Fatigue Crack Initiation and Growth From Coldworked Holes," *Engineering Fracture Mechanics*, Vol. 11, 1979, pp. 609-620.

19. Lam, Y.C. and Lian, K.S., "Effect of Residual Stress and its Redistribution on Fatigue Crack Growth," *Theoretical Applied Fracture Mechanics*, Vol. 12, No. 1, 1989, pp. 59-66.

20. Wilks, M.D.B., Nowell, D., and Hills, D.A., "The Evaluation of Stress-Intensity Factors for Plane Cracks in Residual-Stress Fields," *Journal of Strain Analysis*, Vol. 28, No. 3, 1993, pp. 145.

21. Kiciak, A., Glinka, G., and Burns, D.J., "Analysis of Fatigue Growth of Semi-Elliptical Cracks Through Residual-Stress Fields," *Proceedings of 6th International Fatigue Congress (Fatigue 96)*, G. Lüjenry and H. Nowack, eds., Pergamon, Vol. II, 1996, pp. 1207-1212.

22. Lee, Y., Chung, C., Park, Y., and Kim, H., "Effects of Redistributing Residual Stress on the Fatigue Behavior of SS330 Weldment," *International Journal of Fatigue*, Vol. 20, No. 8, 1998, pp. 565-573.

23. Todoroki, A. and Kobayashi, H., "Prediction of Fatigue Crack Growth Rate in Residual-Stress Fields," *Key Engineering Materials, Fracture and Strength '90*, Vol. 51-52, 1991, pp. 367.

24. Bueckner, H.F., "The Propagation of Crack and the Energy of Elastic Deformation," *Transactions of the ASME*, Series A-D 80, 1958, pp. 1225-1230.

25. Heaton, M.D., "On the Calculation of Stress-Intensity Factors Due to Thermal and Residual-Stress Fields," *CEGB Research Report NW/SSD/RR/158*, 1976.

26. Rice, J.R., *Fatigue Crack Propagation*, ASTM STP 415, American Society for Testing and Materials, 1967, pp. 247-311.

27. Broek, D., *Elementary Engineering Fracture Mechanics*, 4th ed., Kluwer Academic Publishers, Dordrecht, The Netherlands, 1986.

28. Elber, W., "Fatigue Crack Closure Under Cyclic Tension," *Engineering Fracture Mechanics*, Vol. 2, 1970, pp. 37-44.

29. Elber, W., "Damage Tolerance in Aircraft Structures," *ASTM STP 486*, American Society for Testing and Materials, 1971, pp. 230-242.

30. McClung, R.C. and Sehitoglu, H., "On the Finite Element Analysis of Fatigue Crack Closure—1. Basic Modeling Issues," *Engineering Fracture Mechanics*, Vol. 33, No. 2, 1989, pp. 237-252.

31. Solanki, K., Daniewicz, S.R., and Newman Jr., J.C., "Finite Element Modeling of Plasticity-Induced Crack Closure with Emphasis on Geometry and Mesh Refinement Effects," *Engineering Fracture Mechanics*, Vol. 70, 2003, pp. 1475-1489.

32. Skinner, J.D. and Daniewicz, S.R., "Simulation of Plasticity-Induced Fatigue Crack Closure in Part-Through Cracked Geometries Using Finite Element Analysis," *Engineering Fracture Mechanics*, Vol. 69, No. 1, 2001, pp. 1-11.

33. Beghini, M. and Bertini, L., "Fatigue Crack Propagation Through Residual-Stress Fields With Closure Phenomena," *Engineering Fracture Mechanics*, Vol. 36, No. 3, 1990, pp. 379-387.

34. Choi, H.C. and Song, J.H., "Finite Element Analysis of Closure Behaviour of Fatigue Cracks in Residual-Stress Fields," *Fatigue and Fracture of Engineering Materials & Structures*, Vol.18, No. 1, 1995, pp. 105-117.

35. Liu, A.F., "The Effect of Residual Stresses on Crack Growth From a Hole," *NOR 79-74*, Northrop Corporation Aircraft Group, 1979.

36. *ANSYS User's Manuals*, Revision 8.0, 2003

37. MIL-Handbook 5, Vol. 1, Department of Defense, Washington DC, 1983.

38. Tada, H., Paris, P.C., and Irwin, G.R. *The Stress Analysis of Crack Handbooks*, 3rd ed., ASME, 2000.

39. Isida, M., "Laurent Series Expansion for Internal Crack Problems," *Methods of Analysis and Solutions of Crack Problems*, G. C. Sih, ed., Noordhoff International Publishing, 1973.

40. Wu, X. and Carlsson, A.J., Weight Functions and Stress-Intensity Factor Solutions, Pergamon, 1991.

41. Newman J.C., Jr., "A Crack-Opening Stress Equation for Fatigue Crack Growth," *International Journal of Fracture*, Vol. 24, 1984, pp. R131-R135.

APPENDIX A—SIKORSKY FINAL REPORT

TITLE	Crack Growth and Life Enhancement Methods Cold Work Specimen Testing Performed at Sikorsky Aircraft
DOCUMENT NUMBER	Final Report
PREPARED UNDER	Subcontract # 061700 300109 01 from Mississippi State University FAA Prime Agreement # DTFA03-02-C-0043
DOCUMENT DATE	April 12, 2005
PERIOD COVERED	February 18, 2003– March 31, 2005

PREPARED BY: Darron Kannenberg CHECKED BY: Jeffery Schaff

Steve Daniewicz
Dept. of Mechanical Engineering
Mississippi State University
Mississippi State, MS 39762-5925

Table of Contents

Section	Page
Background	A-4
Overview of Testing	A-4
Test Specimen Geometry, Non-Cold Worked Specimens	A-6
Test Specimen Geometry, Cold Worked Specimens	A-6
Test Specimen Geometry, Cold Work Parameters	A-10
Test Results, Non-Cold Worked Specimens	A-12
Test Results, Cold Worked Specimens	A-13
Analysis of Test Results	A-18
Conclusions	A-24
Appendix: Photo Documentation of Fracture Surfaces	A-25

List of Tables	Page
Table 1.a Specimen Summary Table, Geometry and Test Results.	A-5
Table 1.b Specimens Delivered to MSU	A-6
Table 2 Cold Work Dimensions per Machining Operation	A-10
Table 3 Cold Work Specimen Test Results, .190” Thick Specimen,	A-13

List of Figures		Page
Figure 1	Non-Cold Worked Crack-Growth Test Specimens	A-6
Figure 2	Cold Worked Crack-Growth Test Specimens	A-7
Figure 3	Second .030” EDM Corner Notch Applied to Cold Worked Hole	A-8
Figure 4.a	080” Cold Worked Specimens: Iterative Test Method to Obtain .344” Final Ream Diameter EDM Through-thickness notch set-up also shown	A-9
Figure 4.b	.080” Cold Worked Specimen Test Result, .344” final ream DIA	A-9
Figure 5	Cold Work Expansion Tool, Specimen, and Sleeve	A-11
Figure 6	Cold Work Processing of Specimen	A-11
Figure 7	7.2 ksi Lower-Stress Non-Cold Worked Specimens	A-12
Figure 8	9.25 ksi Higher-Stress Non-Cold Worked Specimens	A-12
Figure 9	22.0 ksi Cold Worked Specimens (specimen 3)	A-14
Figure 10	18.0 ksi Low-Stress Cold Worked Specimens (specimens 4 and 5)	A-15
Figure 11	20.0 ksi High-Stress Cold Worked Specimens (specimens 7 and 8)	A-18
Figure 12.a	Non-Cold Work Test Results Comparison, High Stress vs Low Stress	A-19
Figure 12.b	Non-Cold Work Test Life vs Cold Work Test Life	A-19
Figure 13	Primary Crack in Cold Worked Specimen 3	A-21
Figure 14	Cold Work Specimen 3, Cracks in Bore	A-21
Figure 15	Cold Work Specimen 3, End of Crack on Back Side of Specimen	A-21
Figure 16	Cold Worked Specimen 3, Crack Diagram	A-22
Figure 17	Fractured Cold Work Specimen 5 in Test Facility	A-23
Figure 18	Microscope and Test Facility with Cold Work Specimen 3	A-23

Reference 1 ASTM E 466 (fatigue test spec) alignment.	A-16

Background:

Mechanical joints and fastener holes are common airframe structural elements that cause stress concentration under applied load. These structural elements are, therefore, a prime concern for fatigue and crack growth. A number of life enhancement techniques have been developed in the aircraft industry to improve the fatigue and crack growth life of components with fastener holes, such as installing interference fit fasteners and bushings, or cold working the material surrounding the holes. A major benefit of cold working is the reduction of vibratory stresses and/or introducing compressive residual stresses in the material surrounding the holes through cold working.

In this work, Sikorsky collaborated with Mississippi State University (MSU) and the Federal Aviation Administration (FAA) to evaluate life enhancement techniques on crack growth for structural components with cold working fastener holes.

This report provides a summary of cold work specimen crack growth testing performed at Sikorsky Aircraft. The report contains test data from both non-cold worked and cold worked aluminum 7075-T6 bare plate-with-hole specimens. Sikorsky fabricated all non-cold worked and cold worked test specimens in two thicknesses, .080" and .190", and performed EDM notching for purpose of crack initiation in tests. The .080" thick test specimens with a .010" EDM through-thickness notch were sent to MSU for crack growth testing. The .190" thick specimens with a .030" EDM corner notch were tested at Sikorsky. NASGRO analysis was utilized to investigate suitable geometry for the cold work specimens, but the results of the analysis showed significant variability with respect to *da/dN* curve shapes. Hence, iterative testing was chosen as the optimal method of obtaining suitable specimen geometry for cold work specimen testing. Iterative test method and results leading to a final cold work specimen geometry are included in this report. The crack growth data generated in this work enables verification of crack growth analysis and provides baseline data on beneficial effects of cold working of rotorcraft joints.

Photo documentation of fracture surfaces (cold worked and non-cold worked) was performed after this report was written and is therefore included in the appendix.

Overview of Testing:

Sikorsky produced a total of 36 test specimens for the purpose of crack growth testing. Eighteen of these specimens were .080" thick (nine cold worked, nine non-cold worked) and had a .010" EDM through-thickness notch. Two of the cold work .080" specimens were tested at Sikorsky to determine a ream hole diameter that produced crack growth data. The remaining sixteen .080" thick specimens were shipped to MSU (see table 1.b) for crack-growth testing. In addition, Sikorsky produced eighteen .190" thick specimen (nine cold worked, nine non-cold worked) and had a .030" EDM corner notch. Of these eighteen .190" thick specimens, sixteen were tested at Sikorsky and the test loads and results are summarized in table 1.a. The specimens, testing, and test results are presented in more detail in this report.

Table 1.a. Specimen Summary Table, Geometry and Test Results

Specimen Thickness (in)	Condition	EDM Notch	Approximate EDM Notch Size **	Number of Specimens	Number of Spares	Number of Specimens Tested	Applied Max Load (lb)	Load Ratio
0.08	non-cold worked	thru thickness	0.010	3	3	MSU	MSU	MSU
0.08	non-cold worked	thru thickness	0.010	3		MSU	MSU	MSU
0.08	cold worked	thru thickness	0.010	3	3	MSU	MSU	0.1
0.08	cold worked	thru thickness	0.010	3		5 *a	2381	0.1
0.19	non-cold worked	corner	0.030	3	3	5	2362 *b	0.1
0.19	non-cold worked	corner	0.030	3		3	3111 *c	0.1
0.19	cold worked	corner	0.030	3	3	3	5985 *f, h	0.1
0.19	cold worked	corner	0.030	3		5	6650 *d, e, g, I, j	0.1

Notes to Table 1.a:

*a: 2 at MSU (unrepresentative failures),
3 at Sikorsky (.279" DIA and .312" DIA stopped after 1e6 cycles, .344" DIA failed at 211,059 cycles) ***

*b: 7.2 ksi gross stress (far field)

*c: 9.25 ksi gross stress

*d: at Sikorsky (.344" DIA at 17 ksi stopped after 1e6 cycles. Increased stress to 22 ksi (7315 lb), failed at 178,645 cycles)

*e: at Sikorsky (.344" DIA at 20 ksi failed at 941,706 cycles).

*f: at Sikorsky (.344" DIA at 18 ksi (5985 lb) failed at 789,815 cycles; 18 ksi (5985 lb) failed at 681,789 cycles)

*g: at Sikorsky (.344" DIA at 22 ksi (7315 lb) failed at 161,713 cycles)

*h: at Sikorsky (.344" DIA at 18 ksi (5985 lb) at 2.96e6 cycles)

*I: at Sikorsky (.344" DIA at 20 ksi (6650 lb) at 290,553 cycles)

*j: at Sikorsky (.344" DIA at 20 ksi (6650 lb) at 334,633 cycles)

** EDM notch size is defined as radial length from hole true edge to corner of notch at specimen surface

*** Only 2 of these 3 specimens are totaled in Table 1.a. Sikorsky tested 1 additional spare cold worked .080” thick specimen with .010” EDM notch that was not included in Table 1.a. specimen totals. This was possible since the original plan called for 18 specimens per thickness of sheet stock (.080” and .190” thickness), but twenty was actually the optimal number of specimens that fit on a sheet (4 specimens high by 5 specimens across equals 20 specimens). Hence, there were actually 4 spare specimens for the cold worked and non-cold worked specimens in both the .080” and .190” specimen thicknesses.

Table 1.b. Specimens Delivered to MSU

Specimen Thickness (in)	Condition	EDM Notch	Approximate EDM Notch Size **	Number of Specimens
0.08	non-cold worked	thru thickness	0.010	9
0.08	cold worked	thru thickness	0.010	7

Test Specimen Geometry, Non-Cold Worked Specimens:

Sikorsky Aircraft fabricated non-cold worked crack growth test specimens from Aluminum 7075-T6 bare plate in two thicknesses, .080" and .190". Each specimen was 1.75" wide and 8.0" long and had a .25" DIA reamed hole. The .080" thick specimens had a .010" EDM through-thickness notch. The .190" thick specimens had a .030" EDM corner notch (see figure 1). The nine non-cold worked .080" thick specimens were delivered to MSU for crack growth testing. The nine non-cold worked .190" thick specimens were kept at Sikorsky for crack growth testing. In coordinating with MSU to harmonize specimen preparation, Sikorsky began polishing the .190" specimens local to the EDM notch (non-cold work specimens 6, 7, 8, 9) to improve crack visibility for detection and growth measurement.

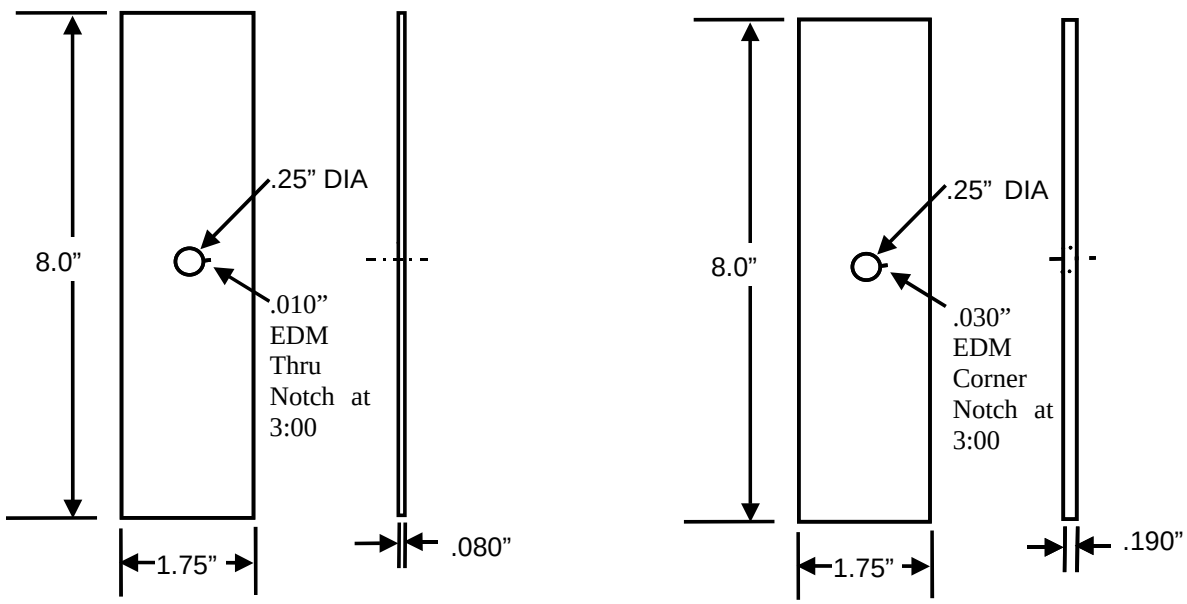

Figure 1. Non-Cold Worked Crack-Growth Test Specimens, .080" and .190" Thick

Test Specimen Geometry, Cold Worked Specimens:

Sikorsky Aircraft fabricated cold worked crack growth test specimens from Aluminum 7075-T6 bare plate in two thicknesses, .080" and .190". Each specimen was 1.75" wide and 8.0" long and

had a .344” DIA final reamed hole. The .080” thick specimens had a .010” EDM thru notch. The .190” thick specimens had a .030” EDM corner notch (see figure 2).

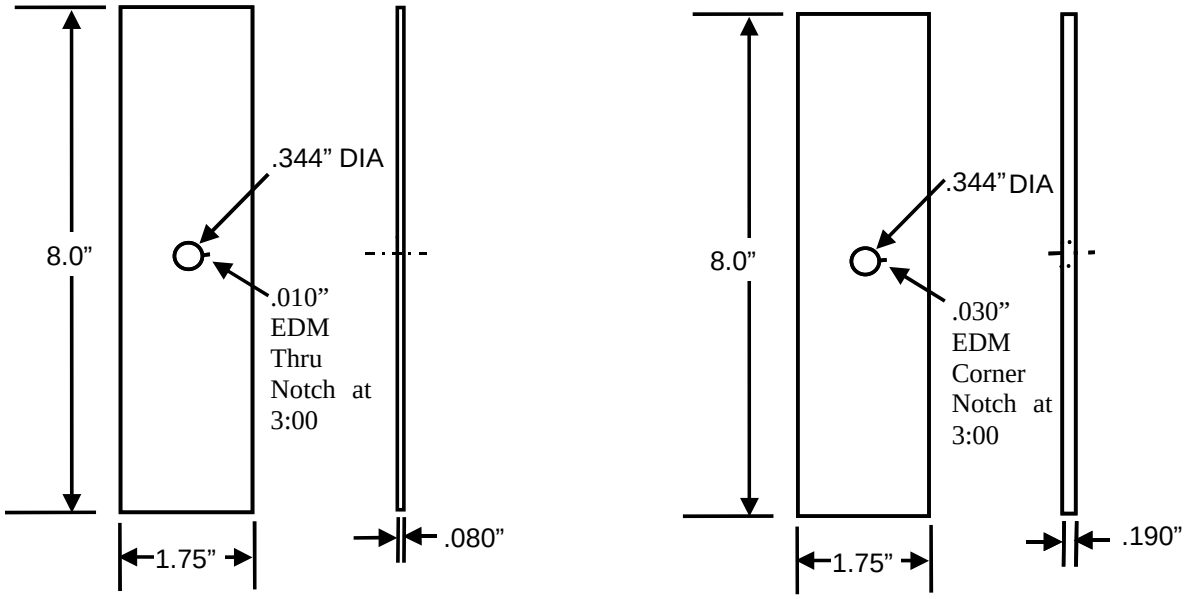

Figure 2. Cold Worked Crack-Growth Test Specimens, .080” and .190” Thick

The .190” thick cold worked specimens initially had only one corner notch on the nose-side of the specimen, the side that interfaced the nose of the cold work tool (figures 5, 6). Initial crack growth tests of these specimens showed that crack initiation occurred on the back side of the specimens (figure 6). This was assumed to be due to variation in the through thickness residual stress distribution provided by the cold work process. Hence, a second notch (see figure 3) was added to the .190” thick specimen to help ensure a .030” corner crack initiation.

The final ream hole diameter of the cold worked specimens was initially .250”, same as the final ream diameter of the non-cold worked specimens. The final ream diameter was increased to .344” DIA in an effort to obtain a geometry that would allow for crack initiation of the .080” thick specimens that were to be tested at MSU. This required a series of test and specimen modifications with iterative increases in the hole diameter as summarized in figure 4.a. Inspection of figure 4.a. also shows finite element results (performed by MSU) for residual stress distribution on a .25” DIA cold worked hole. It also shows the EDM notch method and approximate region of the cold worked specimen containing significant residual compressive stress. The method of test iterations toward obtaining a feasible cold work specimen geometry are provided in the following paragraph.

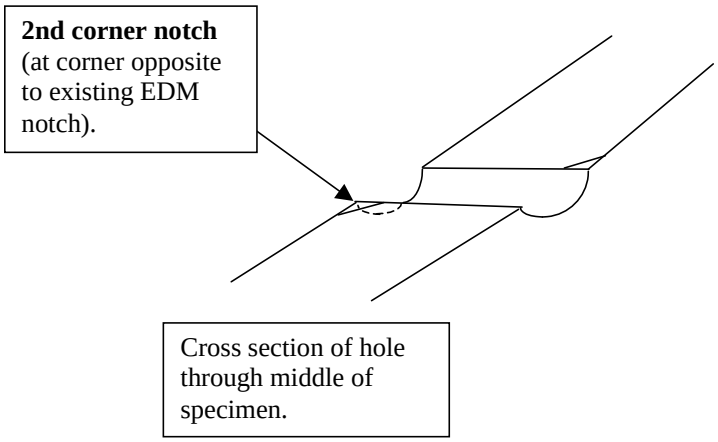

Figure 3. Second .030” EDM Corner Notch Applied to .344” DIA Cold Worked Hole of .190” Thick Cold Worked Specimen (both notches at the 3:00 location)

The .080” thick specimens were tested first at MSU with a .250” DIA hole. The initial tests were performed at 17.0 ksi max stress (R=0.1) and led to unrepresentative failures due to grip-to-specimen interface damage. Sikorsky then tested a .080” thick cold worked specimen with nylon shims at the grip interface in order to mitigate concerns of grip damage, stress concentration, and chafing. Also, since testing by MSU had shown difficulty in obtaining crack growth, the hole size was increased to .279” final ream diameter thereby removing about .015” radially of the residual compressive zone. The .279” final ream diameter represented the maximum allowable final ream diameter per Sikorsky specification. The .080” thick specimen with .279” final ream diameter and .010” EDM through thickness notch was tested at 17.0 ksi max stress (R=0.1) to 2e6 cycles and initiated a crack, but the crack did not grow beyond .02”. The hole on a new .080” thick cold worked specimen was then final reamed to .312” to provide a significant reduction in residual stress at the notch based on FEA residual stress distribution (see figure 4.a). This geometry was tested to 1e6 cycles, but did not initiate a crack. The hole on a new .080” thick cold worked specimen was then final reamed to .344” DIA to reduce the residual stress to approximately -30 ksi at the notch. This geometry was tested to fracture at 211,059 cycles at 17 ksi max stress, R=0.1 (see figures 4.a, 4.b). Inspection of the fracture surface (figure 4.b) showed the specimen had about .050” of residual compressive zone extending radially beyond the .010” EDM notch. The series of test iterations toward obtaining a suitable cold work geometry showed the benefit of cold working in that final ream diameter had to be increased beyond the specification limit (.279” DIA) in order to obtain crack growth in fewer than one million cycles.

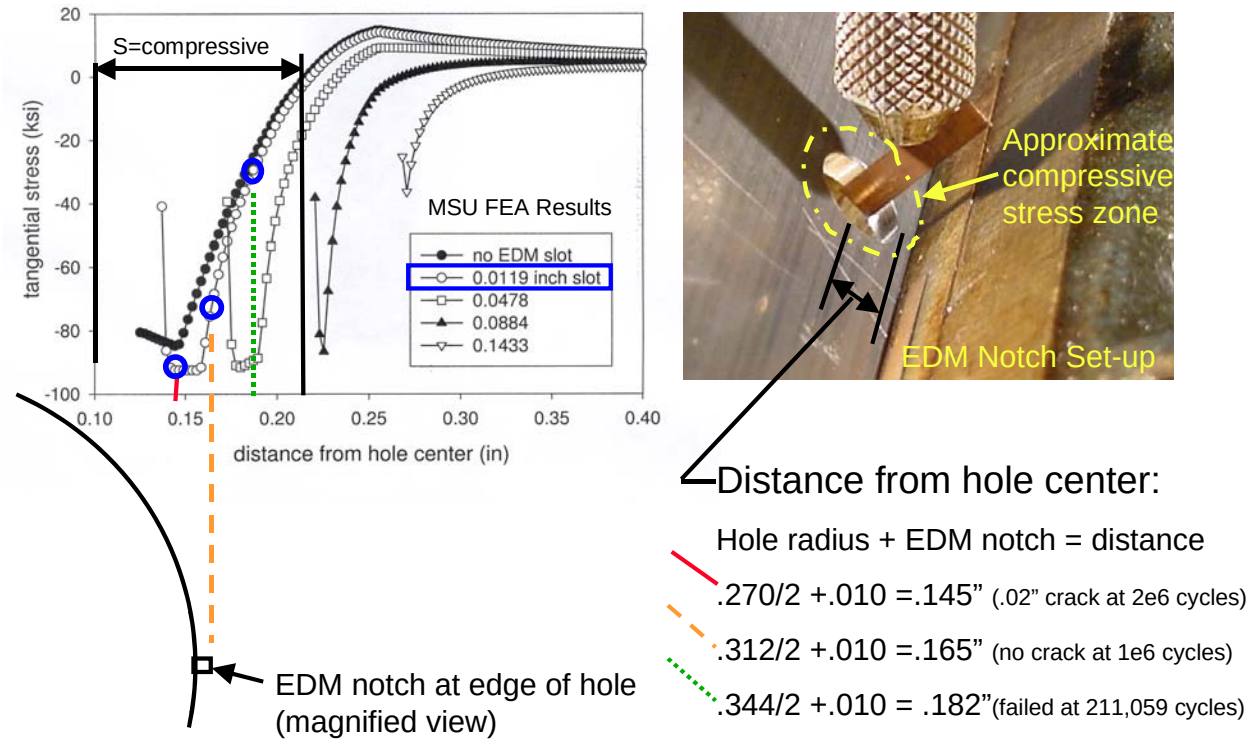

Figure 4.a. .080" Cold Worked Specimens: Iterative Test Method to Obtain .344" Final Ream Diameter for Crack Growth Testing (EDM Through-thickness notch set-up also shown).
Note: .270" is discrepant vs .279" on machine shop order, though not significant to results.

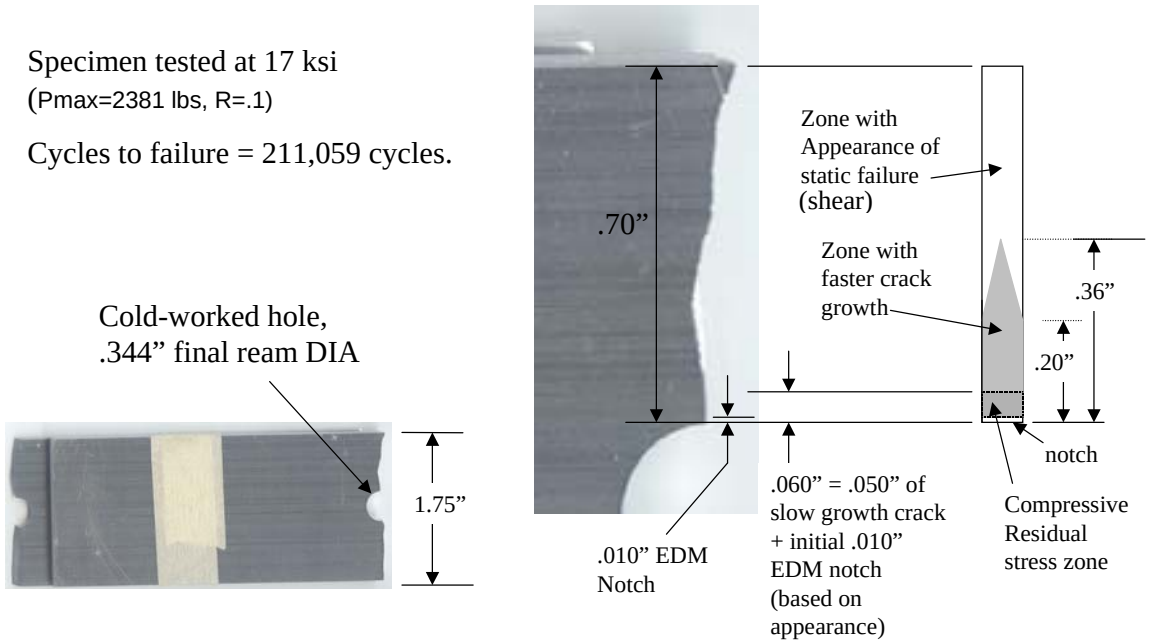

Figure 4.b. .080" Cold Worked Specimen Test Result, .344" final ream DIA

After determining the acceptable final ream diameter to be .344”, the 5 remaining cold worked .080” thick specimens were final reamed to .344” diameter and shipped to MSU (with nylon shims for use at grip interface). The ten .190” thick cold worked specimens were then final reamed to .344” final ream diameter and EDM corner notched to .030” for crack growth testing at Sikorsky Aircraft.

Test Specimen Geometry, Cold Work Parameters:

Cold work parameters for .080” and .190” thick specimen were for a ¼” fastener size. These parameters include initial ream diameter, diameter after cold working, and final ream diameter (Table 2).

Table 2. Cold Work Dimensions per Machining Operation

Cold Worked Data

	S/N	Initial Reamed Dia.	After Cold Work	Final Ream, 3-9 o'clock
	1	0.2352	0.2422	0.2499
	2	0.2355	0.2423	0.25
	3	0.2355	0.2423	0.25
	4	0.2355	0.2422	0.25
.080”	5	0.2355	0.2423	0.25
	6	0.2354	0.2424	0.2503
	7	0.2355	0.2425	0.2503
	8	0.2354	0.2426	0.2501
	9	0.2355	0.2425	0.25
Thin Sheet	10	0.2355	0.2425	0.2501
	S/N			
	1	0.2354	0.242	0.25
	2	0.2354	0.2421	0.25
	3	0.2354	0.242	0.2498
	4	0.2355	0.2418	0.25
.190”	5	0.2355	0.2418	0.2498
	6	0.2355	0.2421	0.2498
	7	0.2354	0.242	0.2499
	8	0.2354	0.242	0.25
	9	0.2355	0.2419	0.25
Thick Sheet	10	0.2355	0.2419	0.2498

Note: The final ream diameter of the cold worked specimen was increased to .344” DIA as detailed in the section ‘Test Specimen Geometry, Cold Worked Specimens’.

Cold work processing equipment and process is shown in the figures 5 and 6.

Note: Blue handles of pliers in background not part of tool.

Figure 5. Cold Work Expansion Tool, Specimen, and Sleeve

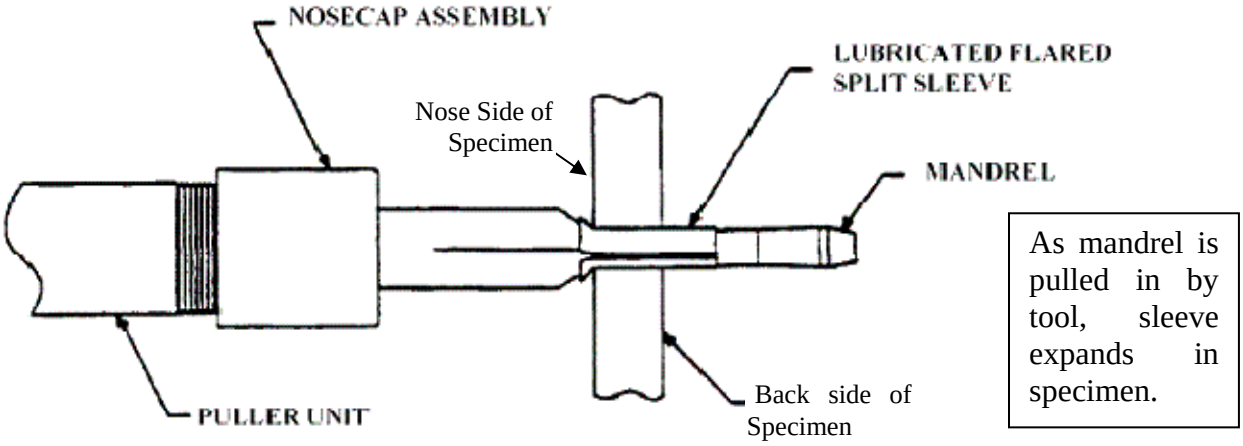

Figure 6. Cold Work Processing of Specimen

Test Results Non-Cold Worked Specimens:

The crack growth test results for the .190” thick non-cold work EDM .030” corner notch test specimens are based on a 7.2 ksi (low-stress) test level and a 9.25 ksi (high stress) test level. For each specimen, the crack initiated at the .030” EDM corner notch located at 3:00 on the edge of the bore azimuth (figure 1). Each fracture surface was straight and planar (slight shear visible at free edge) and propagated to the free edge of the specimen as shown in figure 7. The results for the 7.2 ksi test level are provided for four specimens as plotted on the ‘a vs N’ curves in figure 7.

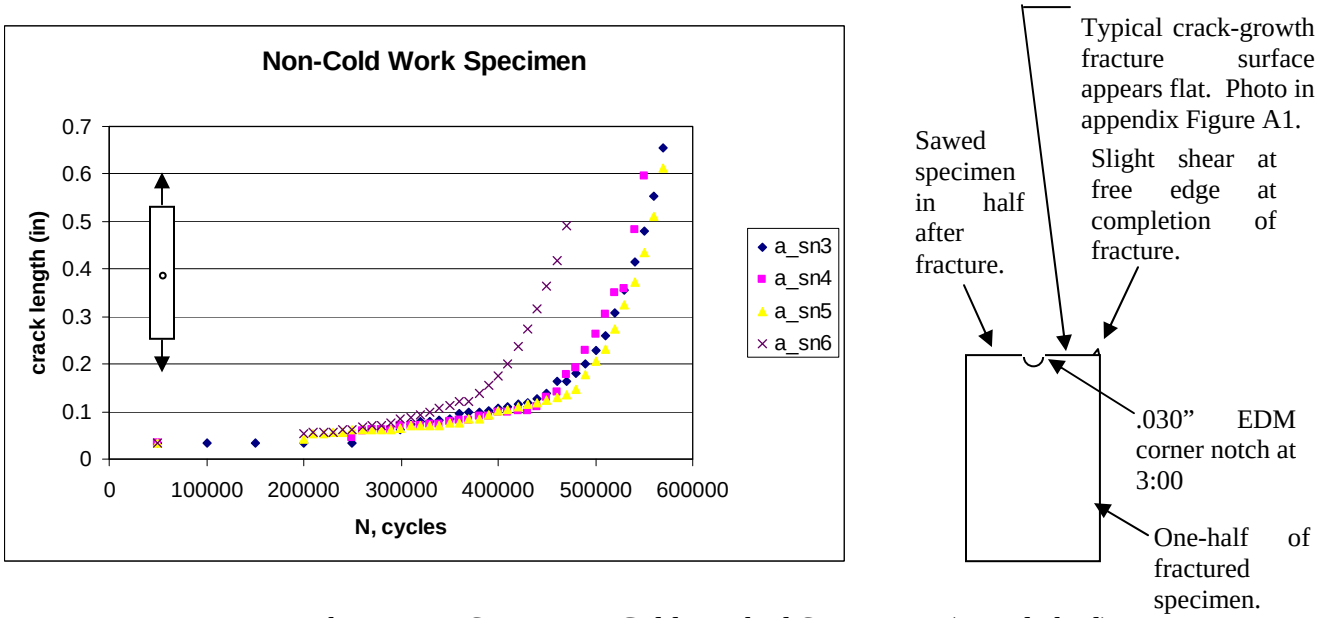

Figure 7. 7.2 ksi Lower-Stress Non-Cold Worked Specimens (P=polished)

The results for the 9.25 ksi test level are provided for three specimen as plotted on the ‘a vs N’ curves in figure 8. Crack growth path and fracture surface similar to that shown in figure 7.

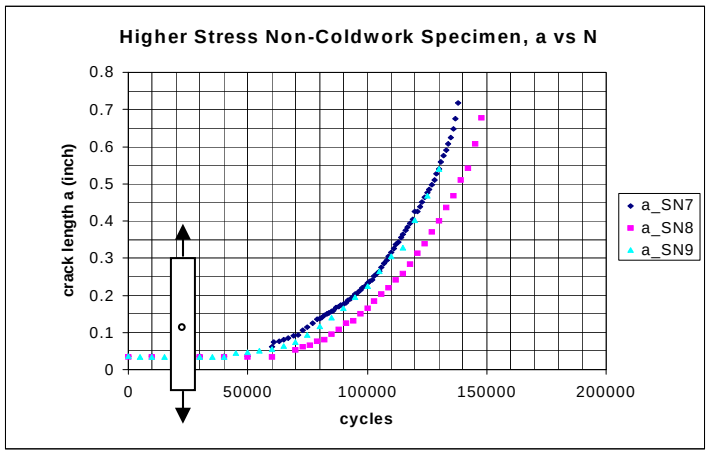

Note: Photo documentation of fracture surface is provided for specimen 7 in appendix Figure A2.

Figure 8. 9.25 ksi Higher-Stress Non-Cold Worked Specimens (specimens 7, 8, and 9 polished local to notch)

Test Results Cold Worked Specimens:

The test results for the .190" thick cold work EDM .030" corner notch test specimens are provided in summary table 3. This table also includes the initial test spares (cold work specimens 1 and 2) which were run to fracture to determine high stress (22.0 ksi, R=0.1) and low stress (20.0 ksi, R=0.1) levels that would initiate a crack and be suitable for obtaining crack growth data. Crack initiation sites are discussed in the test results and refer to the 'nose side' of the specimen and the 'back side' of the specimen (see figure 6). The nose side of the specimen interfaces the nose-cap assembly of the tool.

Table 3. Cold Work Specimen Test Results, .190" Thick Specimen, .030" EDM corner notch

CW S/N	R=0.1, max stress (ksi)	crack detection method	a,init.	N,init.	N,fracture	crack initiation (notch or no notch)	crack initiation (nose side or opposite)	a,thru bore initiation	crack growth data
1	22	run to fracture	no	n/a	178,645	no notch	back	n/a	no
2	20	run to fracture	no	n/a	941,706	no notch	back	n/a	no
3	22	20k cycle insp.	0.046	100,000	161,713	no notch	back	n/a	yes
4	18	25k cycle insp.	0.1205	750,000	789,815	notched	nose	0.190	yes
5	18	microwire	0.02	385,000	681,789	no notch	back	0.133	yes
6	18	microwire	0.01	1,424,607	2,962,482	no notch	back	n/a	no
7	20	microwire	0.1545	280,197	290,553	notched	back	0.095	partial
8	20	microwire	0.031	87,774	334,633	notched	nose	n/a	partial

Notes: Table 3, crack growth data (no, partial):

Specimen 1, 2: No growth data. Ran to fracture to ensure specimen would fracture within 1e6 cycles.

Specimen 6: No growth data. Crack stopped growing. Ran to fracture to avoid unproductive data collection.

Specimen 7. Partial growth data. Crack grew past microwire before stopping test facility.

Specimen 8: Partial growth data. Crack stopped growing, later fractured without warning.

Note on Fracture Surfaces for Specimens listed in Table 3: Each of the .190" cold-worked specimens had fracture surfaces similar to that diagramed in figure 4.b for the .080" specimen in that the residual compressive stress zone was visible and transitioned to a triangular 'zone with faster crack growth' that led to crack growth along shear surfaces. The general appearance of the fracture surface of the cold work specimens is also diagrammed in figure 9, though initiation sometimes occurred at notch (diagram in figure 9 is based on specimen 3, for which crack initiated at unnotched location at back). Photo documentation of fracture surfaces is provided in the appendix figures A3.a, A3.b, A4, A5, and A6 for cold work specimens in which crack growth data was obtained (specimens 3, 4, 5, 7).

The third .190” thick cold worked test specimen (specimen number 3) cracked at the un-notched back side and grew to fracture at 161,713 cycles. Figure 9 includes the crack growth data for the radial direction and the through-bore direction. Figure 9 also includes a diagram of the fracture surface for specimen 3. A summary of the test results for specimen 3 are provided in table 3. Microscope inspection of the fracture surface of the prior two specimens (1 and 2) showed these two fractures also started from the un-notched back side (appendix figures A3.a and A3.b). Hence, a second EDM notch was then added to the back side of all .190 specimen per figure 3.

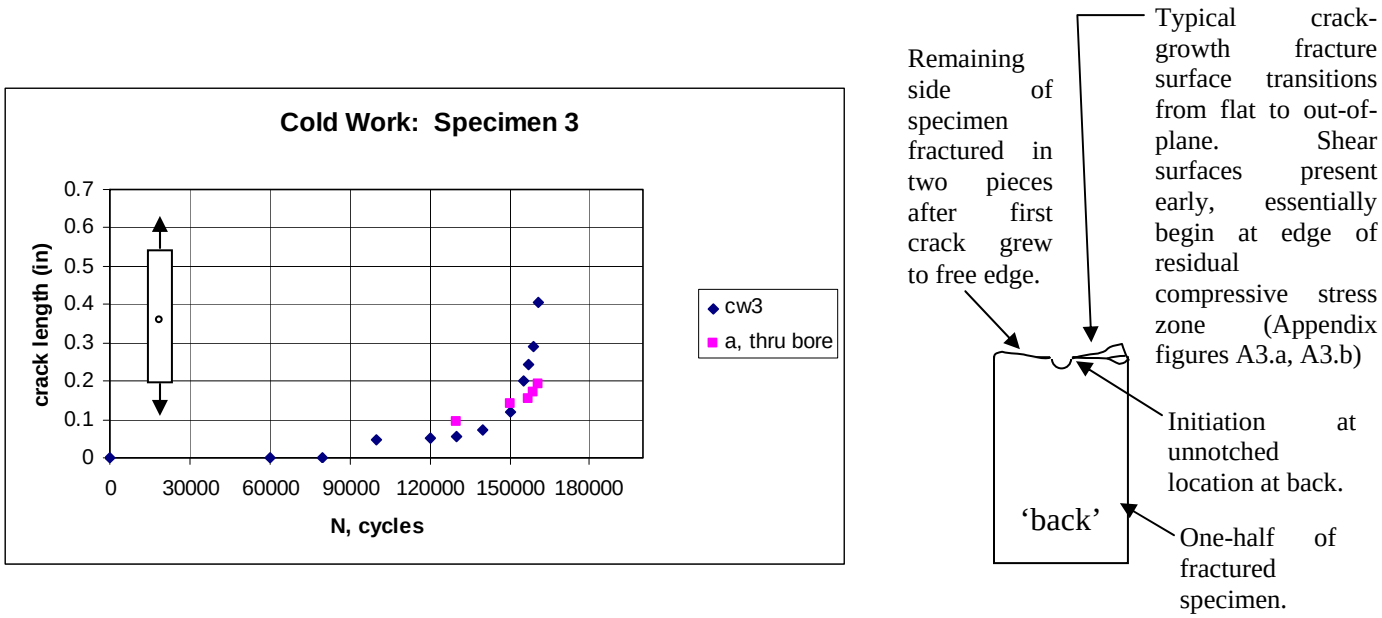

Figure 9. 22.0 ksi Cold Worked Specimens (specimen 3)

Specimen 4 was tested with two notches per figure 3, at 18 ksi, R=0.1. A crack was observed at the notched nose side of the specimen and at the unnotched back side. The crack from the notched nose side of the specimen was dominant and is included in table 3. Both cracks grew to significant crack length before meeting in bore. The specimen fractured at 789,815 cycles. The crack growth curve is provided in figure 10. Note on fracture surface is provided in table 3. Appearance of fractured specimen is similar to that shown in figure 9. End view of fracture surface is provided in appendix figure A4.

Microwire was added to specimen 5 to allow continuous cycling until wire breakage. This was to reduce the time spent performing cycle iteration and inspection in effort to detect crack initiation. Prior to testing specimen 5, a dummy specimen was instrumented and loaded to determine if the test facility was introducing bending into the specimen. Strain measurement from lab data was as follows:

Dummy specimen: 7075-T6, .250" thick x 2.00" wide.

Strain, front = -111 ustrain (with zero axial load after clamping)
Strain, back = +107 ustrain (with zero axial load after clamping)

The bending did not change when the specimen was cycled +/- 2000 lbs.

Stress = strain X Modulus
= (107e-6)*(10 E+6)
= 1070 psi

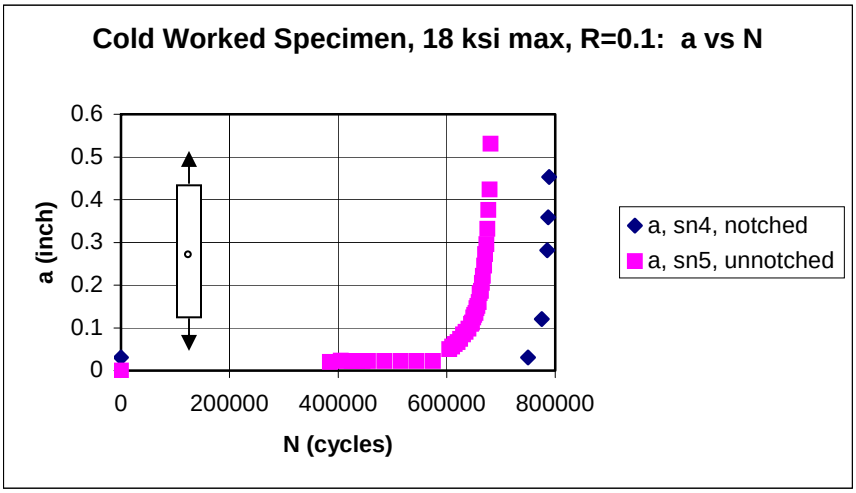

Note: Specimen 5 was notched in two places. Crack initiated at unnotched location.

Fracture surface photo documentation in appendix Figures A4 and A5.

Figure 10. 18.0 ksi Low-Stress Cold Worked Specimens (specimens 4 and 5)

After strain data for the dummy specimen was recorded for bending, concentricity and angle of clamp were adjusted to align the specimen grips with the specimen axis with the assumption that bending strains would be lower for the thinner .190" thick specimen. Although actual amounts of concentricity and angular adjustment were not recorded, beam theory can be utilized to approximate the amount of bending strain present in the .190" thick specimens based on the strain recorded for the dummy specimen.

For rotational end deflection of a beam with an end moment,

$$\theta = (M*L)/(E*I)$$

Assume the same rotational deflection for clamping .190" thick and .250" specimens, both of same E modulus (AL 7075-T6) and same clamped length (L):

$$\theta,_{.190} = \theta,_{.250}$$
$$(M/I)_{.190} = (M/I)_{.250}$$
$$M_{.190} = M_{.250}*(I_{.190} / I_{.250})$$

Where $I=(1/12)*b*h^3$

And $b,_{.190} = 1.75$ in $h,_{.190} = .190$ in
$b,_{.250} = 2.00$ in $h,_{.250} = .250$ in

$M_{.190} = M*(I_{.190} / I_{.250})$

$= M*(b * h^3)_{.190} / (b * h^3)_{.250}$
$= .384*M_{.250}$

In terms of bending strain,

$\varepsilon,_{.190} = .384*\varepsilon,_{.250}$

The bending strain of interest is at the .190" thick specimen cross section with the notch. Hence, the specimen width 'b' is reduced to account for the hole.

$b,_{.190} = (1.75 - .25) = 1.5$ in (non-cold worked specimen)
$b,_{.190} = (1.75 - .344) = 1.406$ in (cold worked specimen)

The actual strain would have been closer to

$\varepsilon,_{.190} = .384*\varepsilon,_{.250} * 1.5/1.75$
$= .329*\varepsilon,_{.250}$ (non-cold work specimen)

$\varepsilon,_{.190} = .384 * 1.406/1.75$
$= .309*\varepsilon,_{.250}$ (cold work specimen)

The same result can be shown for bending strain due to lateral deflection at end of beam with applied moment.

$\delta = (M*L^2)/(2E*I)$

or bending strain due to rotational deflection at end of beam with an applied shear load,

$\theta = (P*L^2)/(2E*I)$

or bending strain due to lateral deflection at end of beam with applied shear load.

$\delta = (P*L^3)/(3E*I)$

Bending stress due to the test facility should be within 5 percent of the maximum gross stress (Reference 1).

Stress, bending $= .329*\varepsilon,_{.250}*E,mod$
$= .329*107\ \mu strain*10.3e6$
$= 363$ psi (non-cold work specimen)

Stress, bending $= .309*\varepsilon,_{.250}*E,mod$
$= .309*107\ \mu strain*10.3e6$
$= 341$ psi (cold work specimen)

Stress ratio = σ,bend / σ,axial
= 363 / 7200
= .050 (non-cold work specimen)

Stress ratio = σ,bend / σ,axial
= 341 / 18000
= .019 (cold work specimen)

The approximated 363 psi bending stress for the non-cold work specimens would have been close to 5 percent of the maximum gross stress, though still acceptable. The approximated 341 psi bending stress for the cold work specimens would have been about 1.9 percent of maximum gross stress, also acceptable. This assumes that bending due to lateral displacement was sufficiently small such that vibratory bending moment (axial load multiplied by any steady lateral displacement) remained small during testing. The recorded data from the lab measurements does not provide the quantity of concentricity that may have been removed. It only provides data in terms of strain that existed due to both concentricity and angle of clamp, both of which were then adjusted to reduce the strain due to clamp up.

Specimen 5 was tested at 18 ksi (R=0.1), and microwire shutdown the facility at 344,058 cycles. Crack on specimen face was not detectable until 385,000 cycles, when a .020" crack was measured on the back side at an unnotched location of the bore. Crack growth data was recorded and the specimen fractured at 681,789 cycles. The test results are summarized in table 3. Crack growth data is plotted in figure 10. End view of the fracture surface is provided in appendix figure A5.

Specimen number 6 was tested at 18 ksi (R=0.1) with microwire, which shutdown the test facility at 1.42 million cycles. The initial crack size was measured to be .010" at the un-notched back side of specimen. The crack grew to .015", showed no growth for 200,000 cycles, and was then run to fracture at 2.96 million cycles. The test results are summarized in table 3. Since the crack growth data for specimen 6 is essentially limited to initial crack size data and number of cycles to fracture, this specimen is not included in figure 10.

Cold work specimen 7 was tested at 20 ksi max stress (R=0.1) in an effort to obtain crack growth data for a higher stress level. The crack in specimen 7 initiated at the notch, grew beyond the microwire, and measured .155" when the microwire broke and shutdown the test facility. Specimen 7 crack growth data was obtained from crack detection at 280,197 cycles and specimen fracture at 290,553 cycles. Crack growth data is plotted in figure 11. Fracture surface is noted in table 3 and is similar to fracture diagram shown in figure 9. End view of the fracture surface is provided in appendix figure A6.

Cold work specimen 8 was also tested at 20 ksi max, R=0.1. The microwire shut down the facility at 87,774 cycles. The crack measured .031" and was on the back side at an unnotched location. The crack grew to .0545" at 137,000 cycles, but then experienced no growth up to 307,000 cycles. The specimen fractured unexpectedly at 334,633 cycles. Therefore abbreviated crack growth data is shown in figure 11.

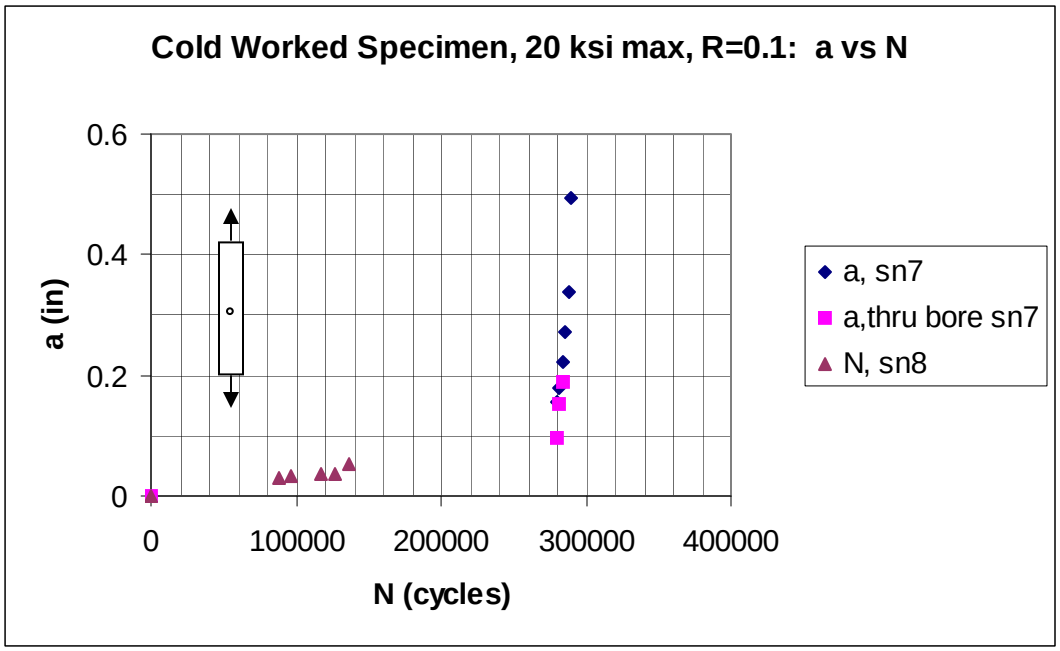

Fracture surface photo documentation in appendix Figure A6.

Figure 11. 20.0 ksi High-Stress Cold Worked Specimens (specimens 7 and 8)

Analysis of Test Results:

The test results for the .190" thick non-cold work EDM .030" corner notch test specimens show that the low stress 7.2 ksi test level life (about 500,000 cycles) well exceeded the high stress 9.25 ksi test level life (about 150,000 cycles) thereby providing two different sets of crack growth data. This is indicated in figure 12.a. The cold work (cw) test specimen crack growth plots are all from maximum test stress levels of 18, 20, and 22 ksi (R=0.1) and are also included in figure 12.a.

The benefit of cold work on the test specimen is clearly evident in figure 12.b. Although the tested stress level of the cold work specimens (18 to 22 ksi) was about two times higher than the non-cold work specimen test level (9.25 ksi), the test lives of the cold work specimens were similar or significantly higher than the non-cold work specimens. All eight cold work specimen test lives (table 3) exceeded the 150,000 cycle life of the non-cold worked specimens. In addition, the non-cold work test specimen were tested with a .250" reamed hole. In testing a .279" final ream diameter for the .080" thick cold work test specimen, a .010" through thickness EDM notch would not grow a crack beyond .02" at 2e6 cycles of testing (figure 4.a) at 17 ksi maximum stress (R=0.1) test level. With the hole enlarged to .312" final ream diameter to remove material with compressive residual stress in a new .080" thick specimen, a crack would not grow from the .010" through thickness notch. Only after removing more of the compressive residual stress zone (final ream diameter of .344") from a new specimen was the .080" thick cold worked .010" through thickness notch specimen finally able to grow a crack at a 17 ksi maximum stress (R=0.1) test level.

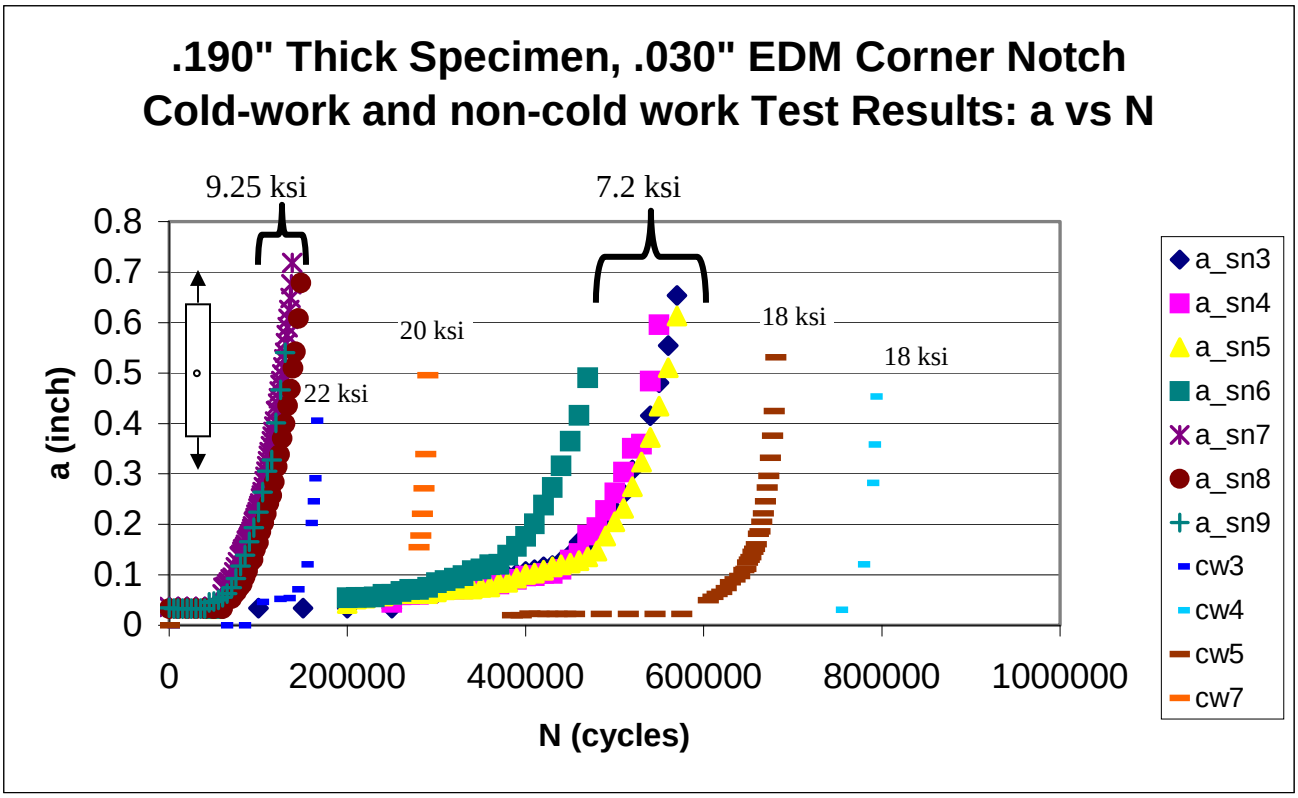

Figure 12.a. Non-Cold Work Test Results Comparison, High Stress vs Low Stress (Cold Work Test Results also shown)

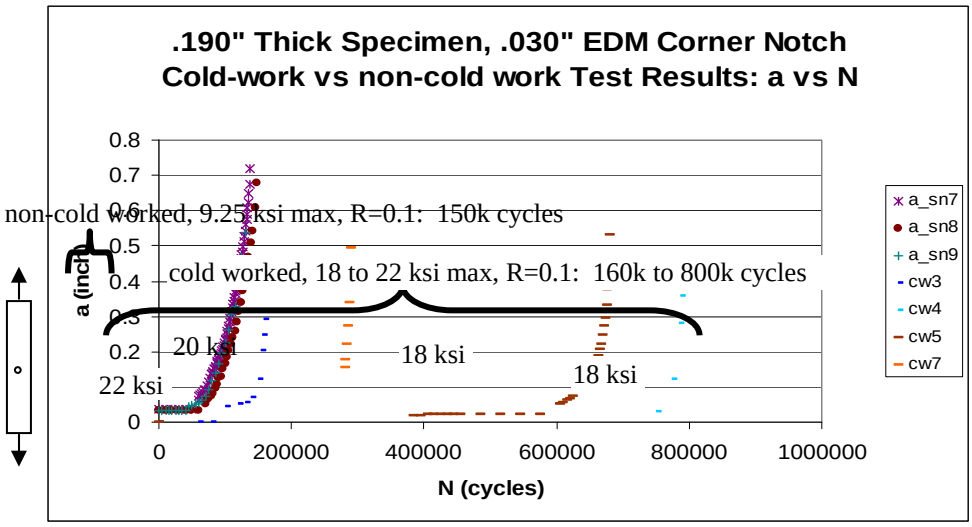

Figure 12.b. Non-Cold Work Test Life vs Cold Work Test Life

It would be reasonable to assume that cold work specimen data would show more variance than non-cold work specimen data due to the additional processing that works the material local to the

cold worked hole. However, the cold work specimen data in table 3 does show correlation with applied stress level as evidenced by specimens 1 and 3 (both tested at 22 ksi and fractured at about 170,000 cycles), specimens 4 and 5 (both tested at 18 ksi and fractured at about 750,000 cycles), and specimens 7 and 8 (both tested at 20 ksi and fractured at about 300,000 cycles). Specimen 6 was tested at 18 ksi and fractured at 2.96 million cycles, well beyond the 750,000 cycles of specimens 4 and 5.

Variance in crack initiation (life in cycles and initiation location) was apparent in the cold work specimen test data and inspection of fracture surfaces. This can be attributed to several factors and considerations detailed in the paragraphs below.

Crack initiation was typically detected on the 'back side' of the specimen (See figure 6 and table 3). This suggests that the back side of the specimen has a lower magnitude compressive residual stress than the nose side. Therefore, a three-dimensional residual-stress field is evident due to the cold work process.

Crack initiation was typically at an unnotched location. This suggests that the .030" EDM notch may experience a residual compressive stress due to the surrounding cold worked material such that crack initiation is favored at unnotched locations near the hole Kt. Recall, that a .030" corner notch was present at the nose side and back side of the cold work specimens 4, 5, 6, 7, and 8 as shown in figure 3 and figure 6. The effect of the existing cold work residual-stress field relative to the introduction of a .030" corner notch could be investigated with finite element analysis to compare stress along notch geometry versus stress at bore edge and bore surface. Test results also suggest that a notch size larger than .030" would have been necessary to provide consistent crack initiation at the notch in the cold work specimen.

Test results could also indicate that at high gross stress levels (18 to 22 ksi), inclusions and other material imperfections local to a hole can be more critical than an EDM notch at the same hole. Microscope inspection of the fracture surface of cold worked specimen number 5 (appendix figure A5) showed that the primary crack initiated at a flaw or inclusion internal to the bore wall. During the cold worked specimen testing, five out of the eight primary cracks grew from unnotched locations on the bore (table 3). Pictures from cold work specimen number 3 are included to show the occurrence of multiple crack initiation sites at locations other than the .030" EDM corner notch (figures 13, 14, and 16), the primary crack initiating at the unnotched back side. A close up of the crack tip on the back side of specimen 3 at 155,000 cycles is provided in figure 15. Photos of the fracture surface of specimen 3 are provided in appendix figure A3.a and A3.b.

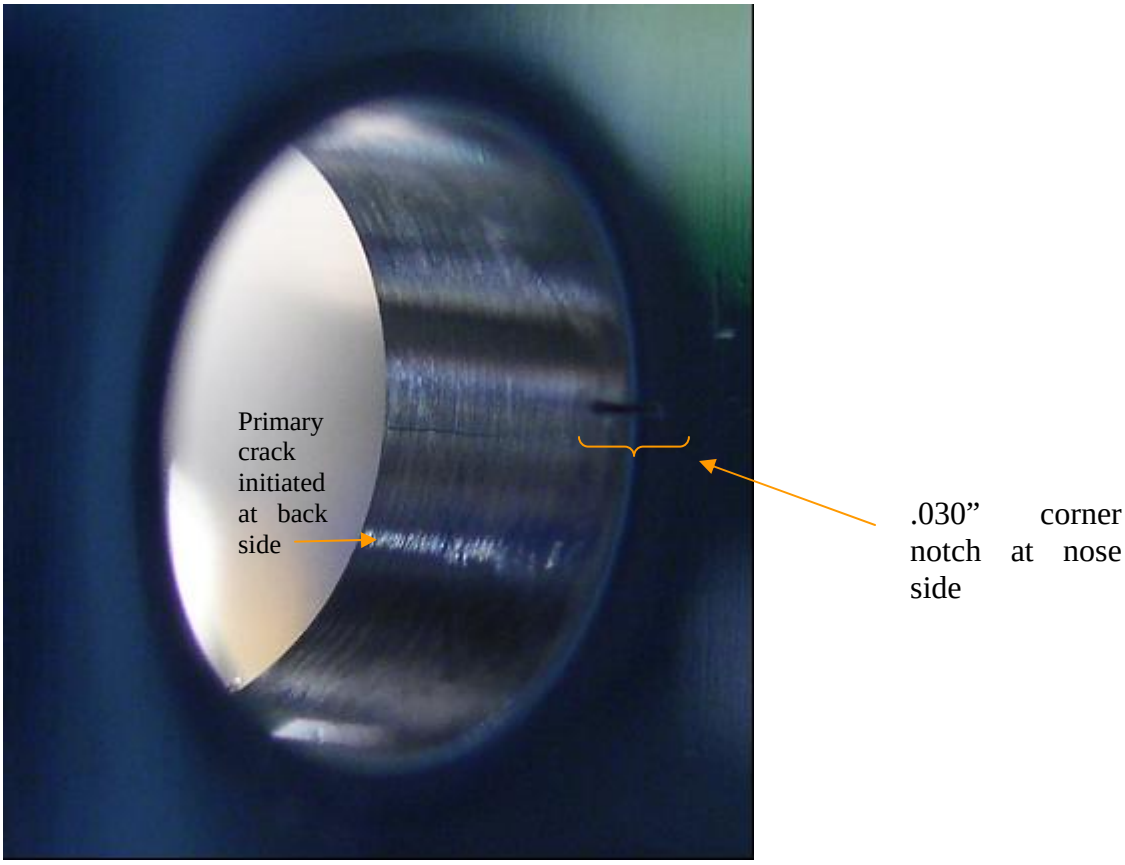

Figure 13. Primary Crack in Cold Worked Specimen 3 in the Test Facility (photo taken at 155,000 cycles)

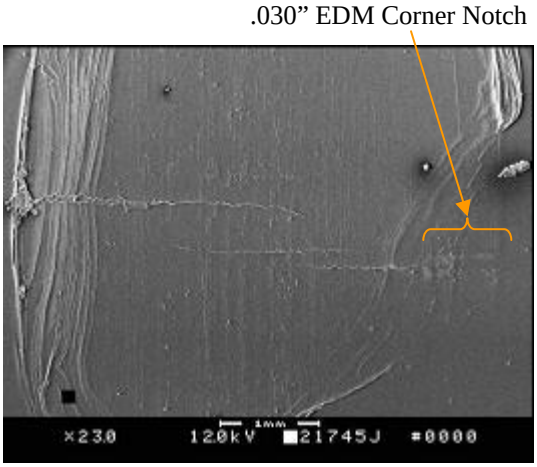

Figure 14. Cold Work Specimen 3, Cracks in Bore (notch visible at right) (Specimen at 155,000 cycles)

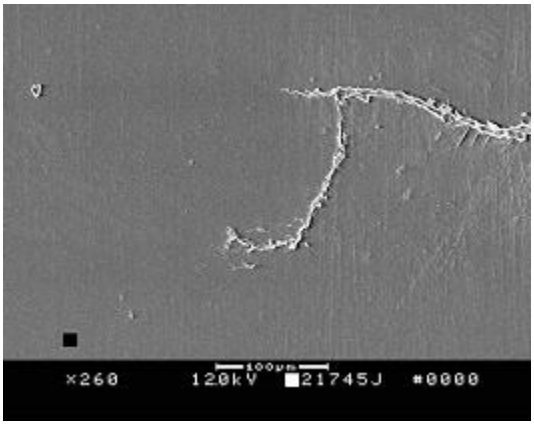

Figure 15. Cold Work Specimen 3, End of Crack on Back Side of Specimen (Specimen at 155,000 cycles)

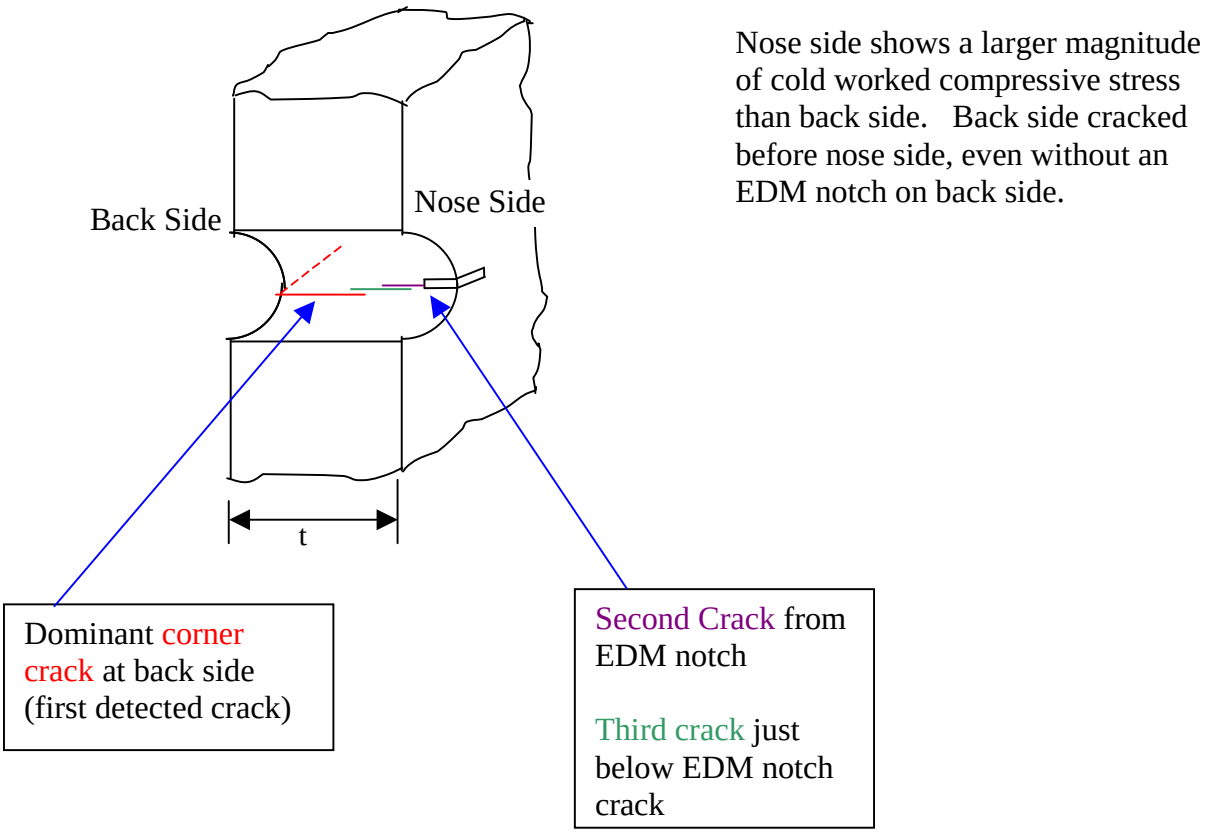

Figure 16. Cold Worked Specimen 3, Crack Diagram (Cracks not shown to scale) Cracks are vertically opposite to relative positions shown in figure 14

A microscope inspection of the fracture surface of cold work specimen number 4 (appendix figure A4) showed that the primary crack initiation was at the nose side 0.030" corner notch on the bore wall. Microscope inspection also showed that the primary crack for specimen number 6 initiated at the unnotched back edge of the hole, the primary crack for specimen number 7 initiated at the EDM notch at the back side of the specimen, and the primary crack for specimen number 8 initiated at the nose side notch.

The typical location of the un-notched crack initiation sites observed during testing of the eight cold-work .190" thick specimens was approximately the 3:00 position of the bore azimuth on the back side of the specimen (figure 17). Only one of the cold-work .190" thick specimen initiated a crack at the notch on the back side. Two of the cold-work .190" thick specimen initiated a crack at the notch on the nose side.

A picture of the test facility is provided in figure 18. The microscope utilized for crack growth measurement is included in the foreground. Cold work specimen 3 and the nylon shims are shown gripped by the jaws of the test facility.

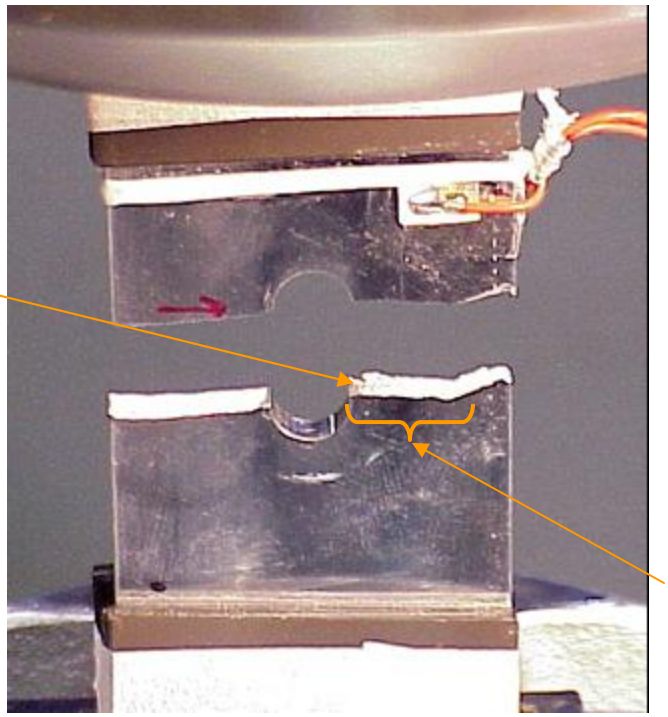

Figure 17. Fractured Cold Work Specimen 5 in Test Facility
Crack initiated internal to bore wall (back side shown)

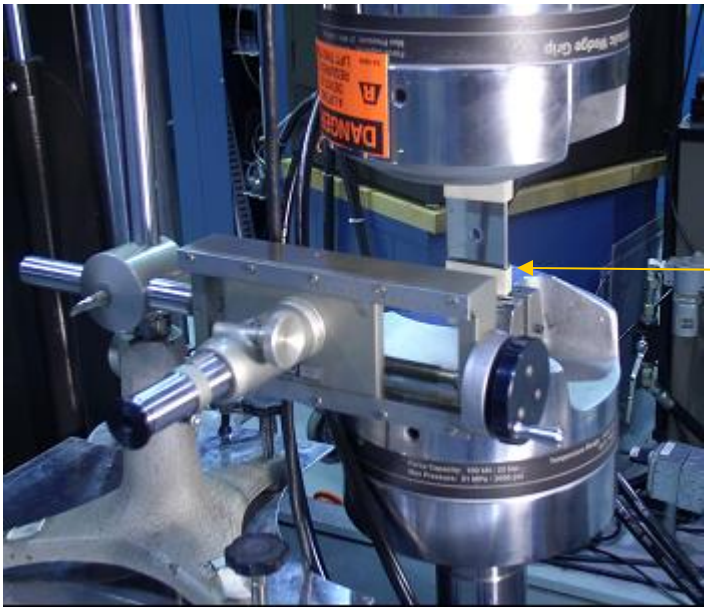

Figure 18. Microscope and Test Facility with Cold Work Specimen

3. Conclusions

1. Cold working of a .250” fastener hole in .190” thick AL7075-T6 improves the fatigue stress capability of the specimen by at least a factor of two (2x) against crack growth. This is evidenced by cold work hole specimens final reamed to .344” final diameter, tested at 18 to 22 ksi maximum stress (R=0.1), and shown to have significantly higher lives than non-cold work specimens tested at 9.25 ksi maximum stress (R=0.1) as presented in figure 12.b. In addition, the cold-work specimens tested at 18 ksi maximum stress demonstrated a life that was at least 4 times (4x) longer than the non-cold worked specimens that were tested at 9.25 ksi maximum stress (figure 12.b.).

2. The maximum final ream diameter per Sikorsky specification was .279”, smaller than the .344” final ream diameter of the test specimens. Hence, the testing presented in this report conservatively under predicts the life improvement that would be anticipated for a .250” fastener hole that is final reamed to within specification limits (.279” maximum final ream diameter). Evidence of this is presented in figure 4.a. for final ream diameter of .279”, for which the crack would not grow past .02” at 17 ksi maximum stress (R=0.1) and 2e6 cycles, whereas cold work specimens tested at .344” final ream diameter and 18 ksi maximum stress (R=0.1) fractured at about 750,000 cycles (figure 12.b). Additional support is based on the finite element plots of residual stress distribution in figure 4.a, which predicts a larger magnitude of compressive residual stress for cold worked material at a final diameter of .279” (.14” radial) as compared to .344” (.172” radial).

3. The back side of a cold worked specimen typically has a lower magnitude of residual compressive stress than the nose side as evidenced by location of crack origins presented in table 3.

4. Crack initiation at inclusions and other imperfections is of increased concern when testing at high stress levels (18 to 22 ksi gross). Cold worked specimens initiated cracks at inconsistent unnotched locations at the bore edge and internal to bore wall. (table 3 and figure 16).

5. A .030” EDM corner notch is not effective at initiating a crack in a cold worked hole of AL7075-T6 of the tested geometry and stress level. Most cold worked specimens initiated cracks at unnotched locations (table 3).

6. The EDM corner notch would have to be larger than .030” to obtain consistent crack initiation at the notch. This is supported by occurrence of multiple crack origins of intersecting paths along bore in cold work specimen (figure 16).

7. Nylon shims were effective against unrepresentative failures at the grip-to-specimen interface during crack growth testing.

8. The series of test iterations toward obtaining a suitable cold work geometry showed the benefit of cold working in that final ream diameter had to be increased beyond the specification limit (.279” DIA) in order to obtain crack growth in fewer than 1 million cycles.

Appendix: Fracture Surface Photos

Fracture surfaces are provided for two non-cold work specimens (figures A1, A2) and four of the cold work specimens (figures A3.a, A3.b, A4, A5, A6) to provide additional understanding of the crack initiation sites and fracture surface characteristics. Crack initiation of non-cold work specimens occurred at the notch as shown in figures A1 and A2.

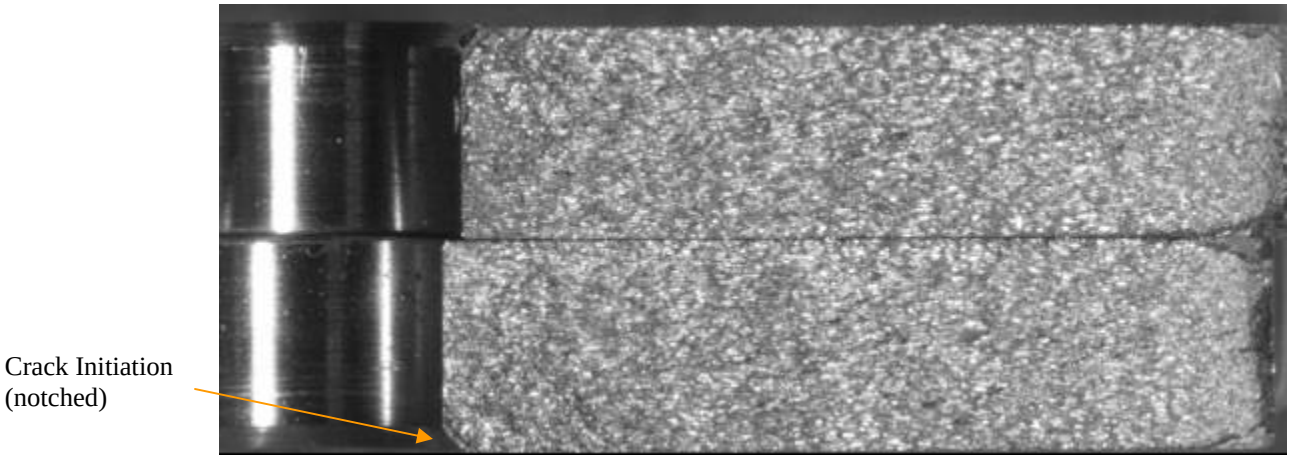

Figure A1. Fracture Surface, Non-Cold Work Specimen 5

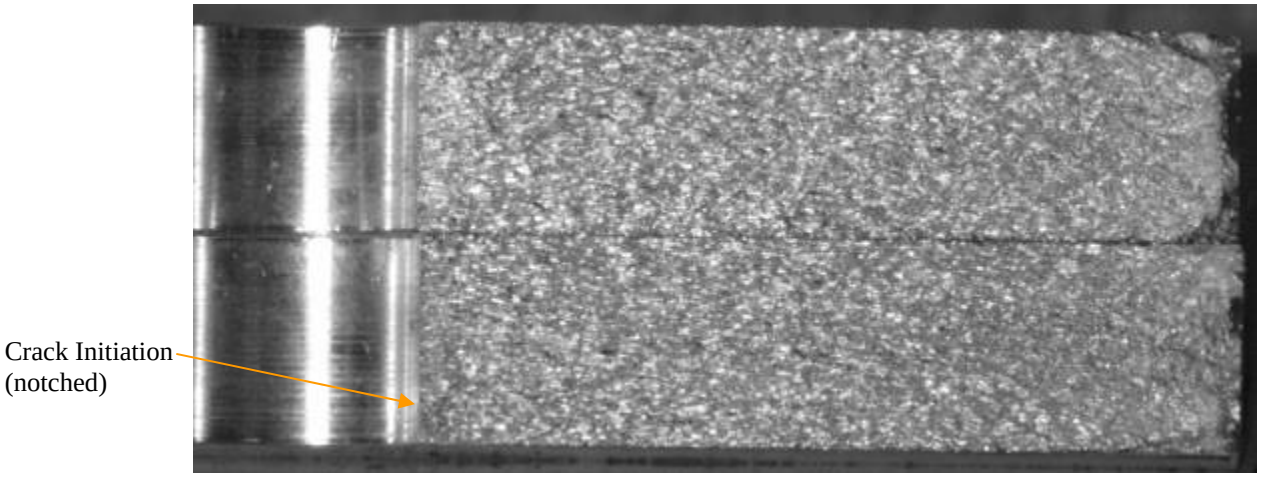

Figure A2. Fracture Surface, Non-Cold Work Specimen 8

Crack initiation in the cold work specimens varied between notched and unnotched locations and between nose side and back side of the specimen (figures A3.a, A3.b, A4, A5, A6). Fracture surface was significantly rougher in cold worked specimens (figure A3.a) than in non-cold work specimens (figure A1). The crack characteristic in cold work specimens changed from tensile fatigue growth to shear failure as the crack progressed beyond the residual stress zone (figure A3.a).

Figure A3.a. Fracture Surface, Cold Work Specimen 3

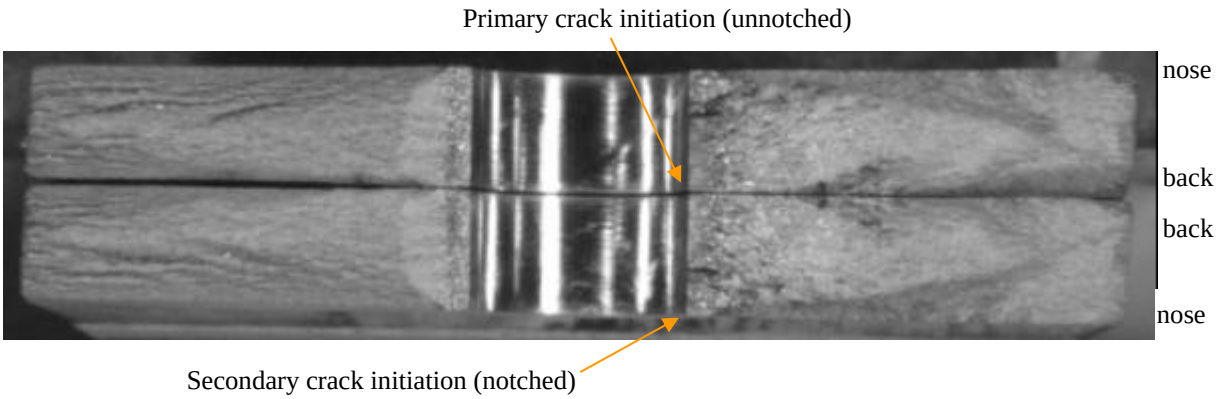

Figure A3.b. Complete Fracture Surface, Cold Work Specimen 3

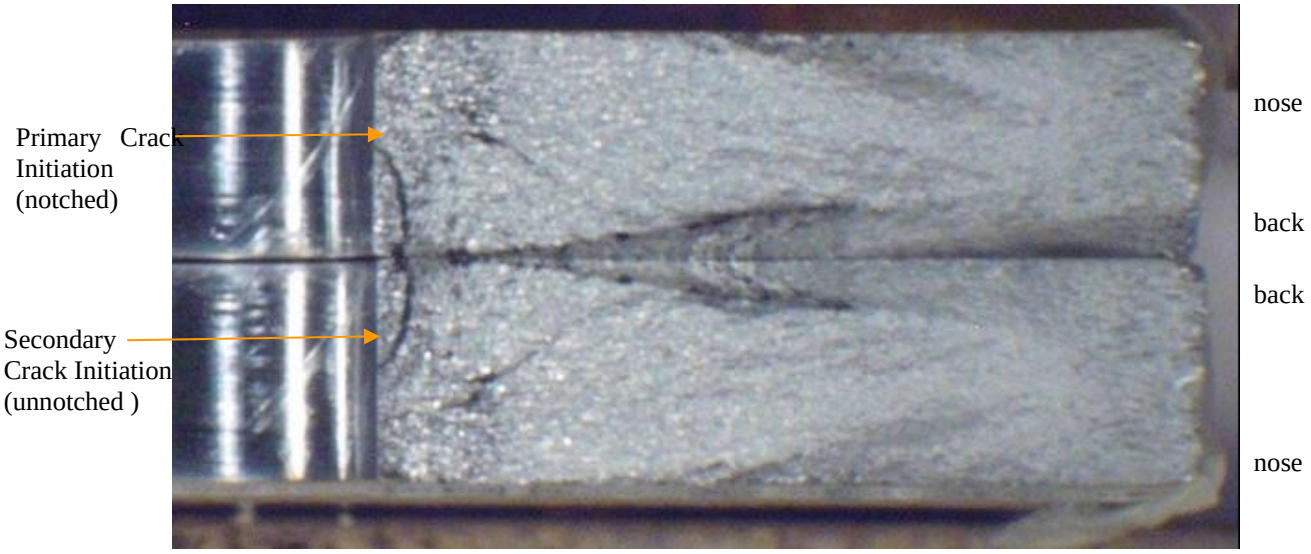

Figure A4. Fracture Surface, Cold Work Specimen 4

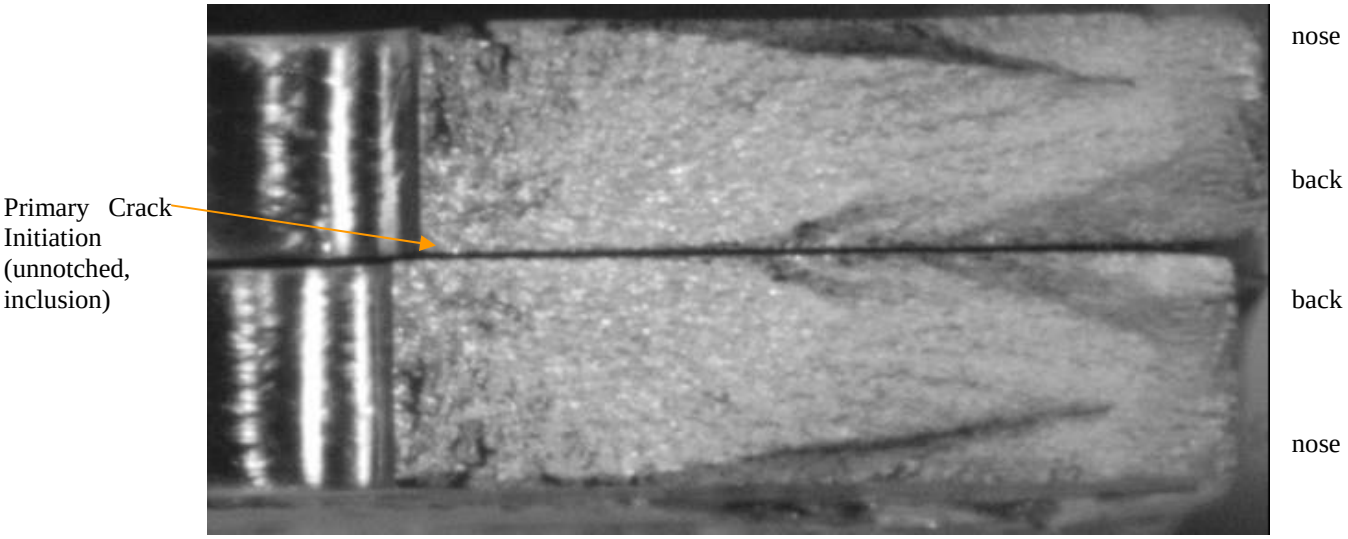

Figure A5. Fracture Surface. Cold Work Specimen 5

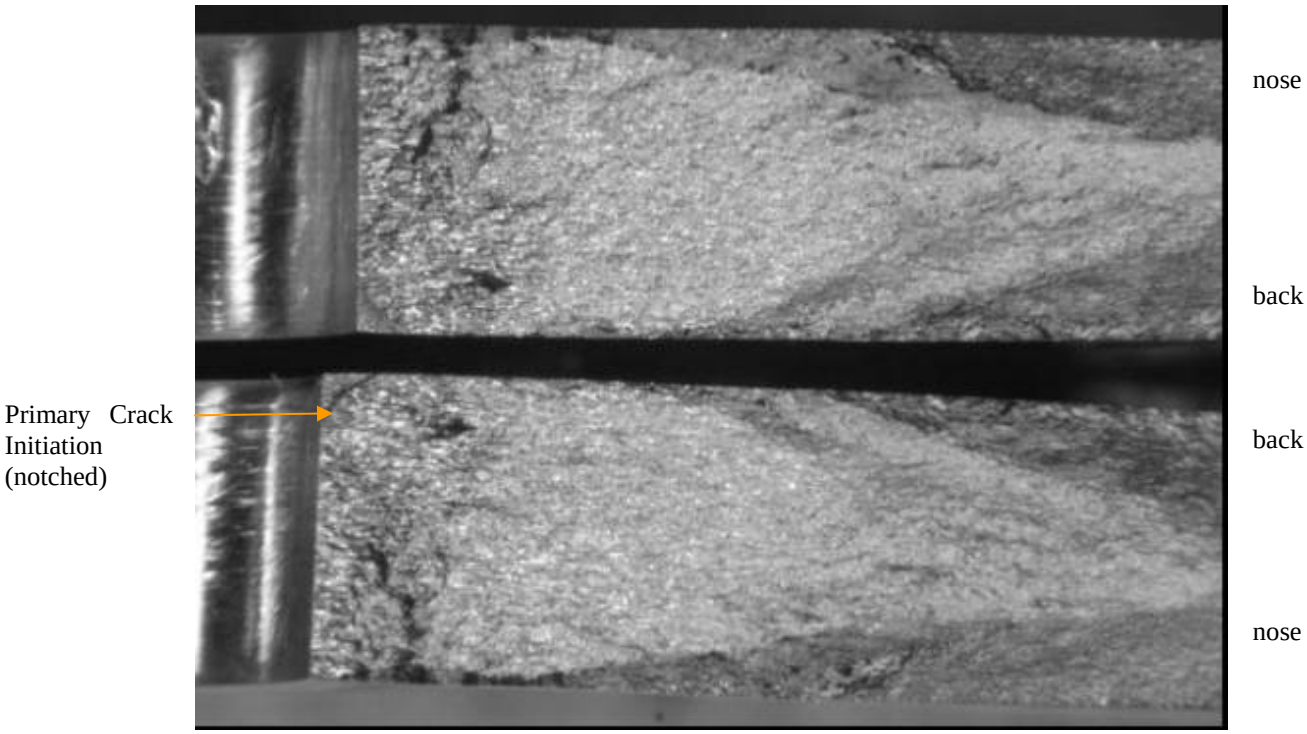

Figure A6. Fracture Surface, Cold Work Specimen 7

APPENDIX B—FASTRAN ANALYSES OF OVERLOADED AND COLD-WORKED HOLE SPECIMENS

B.1. INTRODUCTION.

The application of overloads on cracked structural components or cold-worked holes in structural joints induce "compressive" residual stresses at the crack fronts or at the edges of a hole. These compressive residual stresses greatly enhance the fatigue crack growth characteristics (crack growth retardation) or the fatigue life of these components. In the past, elastic superposition methods have been used in crack growth models to account for these effects. However, this approach assumes that the residual-stress field is unaffected by crack growth and loading history. Because crack growth involves severe plastic deformations around the crack fronts and plastic deformations along the crack surfaces, there is a distinct possibility that the compressive residual-stress fields will diminish as the crack grows through the plastic region (or zone) caused by the overload or cold working, thus negating some of the benefits of the residual stresses.

The primary objective of this study was to enhance the FASTRAN crack closure model [B-1 and B-2] to simulate the introduction of compressive residual stresses due to cold-worked holes. The crack closure model was initially developed in the late 1970s to predict crackgrowth during variable-amplitude load spectra [B-3], which models the plastic deformations and residual stresses during changing load histories, such as after an overload. Thus, overloads may be used to simulate the plastic deformations that are generated during the process of cold-working holes. The cold-working process plastically overloads the material around the hole by inserting a mandrel of slightly larger diameter than the original hole diameter. Thus, plastically deforming the material concentrically around the hole. Once the mandrel is removed, a compressive residual stress develops at the edge of the hole due to the elastic material surrounding the hole. This is the same mechanism that causes crack closure and compressive stresses to develop at the crack front and along the crack surfaces.

Fatigue crack growth rate data generated on specimens with various forms of compressive residual stresses on two aluminum alloy materials, 2024-T351 and 7075-T6, will be studied. All tests were conducted on specimens with a single crack emanating from an open hole. The 2024 alloy test data was generated by Liu [B-4 and B-5]; and the 7075 alloy test data was generated in the current study [B-6]. Liu conducted two types of tests on specimens with a central hole. First, he subjected the specimen to a very high overload (2/3 of the material tensile yield stress), cut an electrical discharge machining (EDM) slot into one side of the hole, and then subjected the specimen to constant-amplitude loading. Second, he cut an EDM slot into one side of the hole, fatigue precracked the specimen to obtain a crack of a specified length, subjected the specimen to the very high overload, and then subjected the specimen to constant-amplitude loading. In the present study, LaRue [B-6] obtained specimens from Sikorsky made of 7075-T6 thin-sheet material with a central hole that had been cold worked (4.5%), reamed, slotted with a small notch (0.25 mm in length). The specimens were then subjected to constant-amplitude loading.

The specimens tested by Liu induced compressive residual stresses by a remote overload; whereas, the cold-worked hole specimens (Sikorsky) induced residual stresses by pressure

loading in the hole. Elastic-plastic finiteelement analyses of the cold-working process [B-6] were used to generate residual stresses around the open hole. Overloads of specific magnitudes were then applied to the FASTRAN model to generate residual stresses that simulate those calculated from the finite element method. Comparisons were made between residual stresses calculated from both the finite element method and the crack closure model. FASTRAN was then used to make fatigue crack growth predictions under the various residual-stress fields. Predictions made by the improved FASTRAN model were compared with experimentally measured fatigue crack growth behavior under the prescribed residual-stress fields.

B.2. FASTRAN LIFE-PREDICTION MODEL.

During the past two decades, the FASTRAN life-prediction code has been successfully used to predict the fatigue crack growth lives for a wide variety of materials under a wide range of load histories (constant amplitude and spectrum loading), see references B-7 to B-12. Using the baseline fatigue crack growth rate data for the material of interest over a wide range in stress ratios and in rates from threshold to near fracture, the code has been able to predict the fatigue crack growth rate behavior under a variety of load histories. The FASTRAN model is based on "plasticity-induced" deformations around a crack front and the crack closure concept [B-13].

Residual stresses are induced by various forms of plastic deformation, such as cold working and shot peening. Thus, it would be a natural extension of the crack closure model to simulate the residual stresses through plastic deformation. The model would naturally change the residual-stress distribution due to the applied loading and crack growth. Current methods, such as linear superposition, which are used to account for the influence of residual stresses on crack growth, do not account for any decay in the residual-stress field with crack growth [B-14].

The FASTRAN crack growth and closure model, shown in figure B-1, is based on the "strip-yield" model concept of Dugdale [B-15], but modified to leave residual-plastic deformation along the crack surfaces. The plastic zone size, ρ, (region 2) is composed of plastic elements that model the crack tip plastic deformations and supports the flow stress of the material. Three-dimensional effects on the flow stress are approximated by using a constraint factor, α, which ranges from 1 (plane stress, very thin sheets) to 3 (plane strain, very thick plates). As the crack grows, plastically deformed material is left along the flank of the crack (region 3). During cyclic loading, these elements may come into contact (close) and some may yield in compression, especially those near the crack tip. During crack growth and cyclic loading, these elements form the residual-plastic deformations that support crack closure. The crack-opening stress level, S_{op}, at which the crack tip opens, is calculated from the contact stresses. Once the crack tip opens, the very high-strain concentration at the crack tip causes damage on the crack tip element and the crack extends. The effective stress range, $\Delta S_{eff} = S_{max}-S_{op}$, is used to calculate the effective stress-intensity factor range (ΔK_{eff}), which controls the amount of fatigue crack growth.

The FASTRAN model is used to correlate large crack growth rate data on a particular material over a very wide range in rates from threshold to fracture. From this correlation, a baseline effective stress-intensity factor range against rate (ΔK_{eff}-rate) curve is generated for the material and environmental condition of interest. (The ΔK_{eff} is the stress-intensity factor range calculated

from K_{max}-K_{op}.) These relationships have been obtained for a wide range of materials (aluminum alloys, titanium alloys, and steels).

The following model enhancements were used:

- K-analogy was activated for all crack configurations. The FASTRAN model has two basic models: one for a central crack in a finite-width plate, and one for two symmetric cracks emanating from a circular hole in a finite width plate. The model for a crack growing from a hole is shown in figure B-1. To model a crack growing in a plate or from a hole in a different configuration and under different loading conditions than the model(s), the concept of K-analogy [B-2 and B-16] is used to transfer the crack-opening stress information from the model to the actual crack configuration.

- The plastic zone region in the model (region 2 in figure B-1) was refined to have 20 elements in the plastic zone instead of 10. Ten elements were used in the original model to save computer time. However, it has been shown that 10 elements give essentially the same crack-opening stress results as 20 elements, but the 20-element model was used to more accurately simulate the residual-stress distributions, which exhibit very high stress gradients.

- For crack emanating from a hole or notch, the hole (or notch) radius-to-plate-thickness ratio control constraint, i.e., the elevation of material flow stress due to multiaxial stress states. In the original model, the crack was assumed to always control the constraint level, whether the crack was growing from a hole or in a plate. This approach was done for simplicity, and the results were generally conservative. However, to improve the life calculations for a crack growing from a hole, the hole radius-to-thickness ratio will control constraint, and on the first load cycle, the state-of-stress is nearly “plane stress”. This will cause more yielding at the hole than in the original model, but will simulate more accurately the state of yielding at an open hole, which will have lower constraint than a crack.

- The stress-intensity factor solution for a single crack at an open hole in a finite plate (finite width and height) was recalculated using the FADD2D code [B-17], and the current solution in FASTRAN for remote uniform stress was verified as being very accurate (±0.2%). However, the test specimen used for the cold-worked hole experiments was gripped in friction grips, which impose a more uniform displacement boundary condition on the specimen. The stress-intensity factor solution for remote uniform displacement applied to the particular test specimen configuration indicated that the stress-intensity factors were lower than the uniform stress case for cracks greater than about 1/2 of the ligament from the hole to the edge of the plate.

- The basic FASTRAN model for two symmetric cracks emanating from an open hole was modified to allow reaming of the hole to increase the hole radius and to remove some of the plastically deformed material caused by cold working. The plastically deformed material away from the reamed hole was transferred to a new set of model elements in the

plastic zone region. Thus, reaming has modified the residual stresses induced by the original cold working.

- Similar to the reaming option, an option was developed to induce a cut or notch, like an EDM notch, at the edge of the hole, which would also eliminate some of the plastically deformed material.

B.3 TEST SPECIMENS.

The test specimens used in this study are shown in figure B-2. The middle-crack tension specimen, M(T), was used to obtain the basic fatigue crack growth rate data on the two materials. The specimen with the central hole was used in the studies of the various residual-stress distributions. The latter specimen was subjected to either remote uniform stress (S) or uniform displacement (δ).

B.3.1 UNIFORM REMOTE APPLIED STRESS.

The stress-intensity factor for a single crack emanating from an open hole in a finite-width plate subjected to a remote uniform stress is given by

$$K_s = S \sqrt{(\pi a)}\, F_{hs} \tag{B-1}$$

where S is the remote applied stress, a is the crack length measured from the hole, and F_{hs} is the boundary-correction factor, which accounts for the influence of the hole and finite-width plate. The function F_{hs} is given by

$$F_{hs} = F_n\, F_w \tag{B-2}$$

and

$$F_n = 0.707 + 0.765\,\lambda + 0.282\,\lambda^2 + 0.74\,\lambda^3 + 0.872\,\lambda^4 \tag{B-3}$$

where $\lambda = 1/(1 + a/r)$ for $0 < \lambda \leq 1$. Equation B-3 is within 0.2 percent of the results in reference 18. The finite-width correction, F_w, is given by

$$F_w = \{\sec[\pi/2\,(r + a/2) / (w - a/2)]\}^{1/2} \tag{4}$$

which agrees well with Isida's solution [B-19 and B-20] for an eccentric crack in a finite-width plate. Note that the crack length in Isida's crack configuration, $2a$, is assumed to be equal to the crack length, a, plus hole diameter ($a + 2r$) in figure 2.

B.3.2 UNIFORM REMOTE APPLIED DISPLACEMENT.

The stress-intensity factor for a single crack emanating from an open hole in a finite-width plate subjected to a remote uniform displacement is

$$K_d = S \sqrt{(\pi a)}\, F_{hd} \tag{B-5}$$

where S is the remote applied stress due to a uniform displacement, δ, a is the crack length measured from the hole, and F_{hd} is the boundary-correction factor, which accounts for the influence of the hole, finite width and finite height of the plate. The function F_{hd} is given by

$$F_{hd} = F_n\, F_w\, F_d \tag{B-6}$$

where F_n and F_w are given by equations B-3 and B-4, respectively. The function F_d accounts for the influence of the uniform applied displacement and is a function of hole radius, specimen width and specimen height. Herein, the function F_d was developed for only r/w = 0.143 and h/w = 2, the values used in the current test program. The function F_d is given by

$$F_d = 1 - 0.2\, \beta^2 - 0.1\, \beta^3 - 0.05\, \beta^{16} \tag{B-7}$$

where $\beta = (a + r)/w$. Equation B-7 is within 0.5 percent of the results calculated from the boundary-element code, FADD2D [B-16].

Figure B-3 shows a comparison of the boundary-correction factor, F_h, for remote uniform applied stress or remote uniform applied displacement as a function of the normalized crack length, $(a+r)/w$. The solid and open symbols show recent results calculated from the FADD2D [B-17] code on the specific crack configuration with r/w = 0.143 and h/w = 2. The solid and dashed curves are the results of equations developed by Newman [B-7] and in the NASGRO code [B-21], respectively, which agreed very well with each other. The dash-dot curve is the equations developed herein (equation B-6) for the case of uniform applied displacement. Figure B-4 shows the ratio of the stress-intensity factor for the uniform displacement case to that for the uniform stress case (equation B-7). These results demonstrate that the stress-intensity factor is greatly reduced for the larger crack length-to-width ratios.

B.4 MATERIALS.

Fatigue crack growth rate data on the two materials were obtained from the literature. The data on the 2024-T351 alloy were obtained from the Liu report [B-5]; whereas, the data for the 7075-T6 alloy were obtained from reports from National Aeronautics and Space Administration (NASA) [B-22 and B-23].

B.4.1 ALUMINUM ALLOY 2024-T351.

The fatigue crack growth rate data for the 2024 plate (B = 6.35 mm) is shown in figure B-5 for stress ratios ranging from R = 0.1 to 0.7. (The yield stress was 372 MPa and the ultimate tensile strength was 490 MPa.) For a given ΔK value, the higher R ratio results exhibit faster crack grow rates than the low R ratio results. The solid curve shows the ΔK_{eff}-rate relationship for a thin-sheet 2024-T3 material [B-10]. These results were obtained from an analysis of Hudson's

[B-22] and Phillips' [B-24] data. The ΔK_{eff} curve is the results for a fully open crack, and these results should agree with the high R ratio data, such as $R = 0.7$.

Figure B-6a shows a crack-closure analysis of Liu's data, which shows ΔK_{eff}-rate using the crack-opening stress equations developed from FASTRAN analyses [B-25]. For rates lower than 10^{-9} m/cycle, the plate material was assumed to agree with the thin-sheet material (dashed curve). For rates greater than 10^{-5} m/cycle, the plate material was, again, assumed to agree with the thin-sheet material and match a point taken from a K_R-curve on 6-mm-thick material (NASGRO database). (The extremely high-rate relationship was needed to model the large amount of crack extension exhibited in the test specimen that was fatigue precracked and then overloaded to 2/3 of the material yield stress.)

Cracks growing in thin-sheets and plates show a flat fatigue crack surface at low rates and, usually, a slant (45 degrees) fatigue crack surface at high rates. This transition from flat-to-slant crack growth is characteristic of a constraint loss, in that the constraint changes from plane strain to plane stress during this transition. The vertical dashed line (figure B-6) shows the transition location in terms of ΔK_{eff} that was calculated using an equation developed in reference B-10, $(\Delta K_{eff})_T = 0.5\ \sigma_o \sqrt{B}$. The data correlated within a fairly tight band, except in the region around 10^{-7} m/cycle. Here, some spread in the data was apparent as a function of the R ratio. The baseline curve (solid curve with open symbols) was chosen to fit the average of these data. Normally, the high R ratio results, such as 0.7, are used to obtain the ΔK_{eff}-rate relationship. The results for only $R = 0.7$ are shown in figure B-6b. Note that the $R = 0.7$ data falls in between the thin sheet and the current baseline relation. The results for only $R = 0.1$ are shown in figure B-6c. The low R data is significantly higher than the baseline curve around a rate of 10^{-7} m/cycle.

The baseline ΔK_{eff}-rate relationship used in the FASTRAN code is the solid lines with open symbols in figure B-6a. A table lookup form with a simple power-law relation is used between each data point, as shown by the lines between each data point. The table lookup form is used because many materials show transitions in rates at various locations along the curve. These transitions have been associated with microstructure and environment. The baseline relation for the 2024-T351 alloy is given in table B-1.

Table B-1. Effective Stress-Intensity Factor Against Rate Relationship for 2024-T351.

ΔK_{eff}, MPa-m$^{1/2}$	*da/dN*, m/cycle
0.80	1.00e-12
1.10	5.00e-11
2.05	2.00e-9
4.00	8.00e-9
7.70	1.00e-7
13.5	1.00e-6
23.0	1.00e-5
36.0	1.00e-4
85.0	1.00e-2
α = 2.0	4.00e-7
α = 1.0	1.50e-5

B.4.2 ALUMINUM ALLOY 7075-T6.

An ΔK_{eff}-rate relationship had previously been obtained on the thin-sheet 7075 alloy [B-10 and B-23]. (The yield stress was 520 MPa and the ultimate tensile strength was 575 MPa.) Figure B-7a shows this correlation on the data generated in reference B-22. The data generated for three stress ratios correlated extremely well, except in the near-threshold regime. The baseline relation is fitted to the mean of these data, as shown by the solid curve with solid symbols. The solid symbols are the table lookup values used in the FASTRAN code. Again, the flat-to-slant crack growth regime (constraint loss regime) was defined and the values of constraint (α) were established from variable-amplitude load tests in reference B-23. The location and constraint values for the constraint loss regime are best established using variable-amplitude fatigue crack growth rate tests instead of constant-amplitude tests. Figure B-7b shows another data set on the 7075 alloy. Hudson obtained these data in 1969 [B-22], which exhibited some differences in the high-rate regime. For rates less than about 10^{-9} m/cycle, the baseline curve (solid curve and solid symbols) was fit to small-crack data [B-22], and this relationship will be used herein.

In figure B-7b, the solid lines show the baseline ΔK_{eff}-rate relation used in the FASTRAN code for the 7075-T6 material and is given in table B-2.

Table B-2. Effective Stress-Intensity Factor Against Rate Relationship for 7075-T6

ΔK_{eff}, MPa-m$^{1/2}$	da/dN, m/cycle
0.90	1.00e-11
1.25	1.00e-9
3.40	1.00e-8
5.20	1.00e-7
11.90	1.00e-6
20.0	1.00e-5
50.0	7.00e-4
α = 1.8	7.00e-7
α = 1.2	7.00e-6

B.5 OVERLOAD TESTS.

The tests conducted by Liu [B-4 and B-5] were analyzed with the improved FASTRAN for three loading conditions: (1) crack growth predictions are made under constant-amplitude loading on M(T) specimens; (2) the preyielded holes, and (3) the precracked and overload holes were analyzed. Comparisons are made between test and analyses for many of the test conditions reported by Liu.

B.5.1 CONSTANT-AMPLITUDE LOADING.

Figure B-8 shows the measured and calculated crack length against cycles on two M(T) tests conducted at two remote applied stress levels at R = 0.1. The symbols show the tests and the curves show the calculations. The discrepancy (50% on final life) is partly due to the correlation shown on figure B-6c, which shows that the measured rate data is faster than the baseline relationship. However, the initial rates observed on the test data (first two data points) did not agree with the stress-intensity factor range against rate (ΔK-rate) data (open circles) shown in figure B-6c, so these data may be questioned. Further study would be required to resolve this discrepancy.

B.5.2 PREYIELDED HOLE AND CONSTANT-AMPLITUDE LOADING.

As previously mentioned, FASTRAN has always modeled yielding that occurs at the edge of a hole using the strip-yield model [B-7], as shown in figure B-9(a) and B-9(b). As seen, the modified Dugdale model does not simulate the two-dimensional nature of the yield zone at a hole or even at a crack. But, the model has been successful in modeling crack growth behavior under various load histories as an engineering tool. However, on the initial overload, the state of stress is now assumed to be nearly plane stress; whereas, the crack may be growing under a high-constraint condition, like plane strain. This lower constraint will cause more yielding to occur in the crack closure model at the edge of the hole. After the overload, an EDM notch is machined into one side of the hole of length, a_i, as shown in figure B-9(c). The simulation in

FASTRAN is shown in figure B-9(d). The EDM notch removes some of the plastically deformed material at the edge of the hole.

Figures B-10a to B-10c show comparisons made between the tests and analyses made with FASTRAN. The plots show log crack length against linear cycles, so that the unique behavior of the test and analyses can be observed in the smaller crack regime. (Note that a linear plot of crack length against cycles will not show any distinction between constant-amplitude and preyielded hole results in the early stages of crack growth, i.e., the curves are extremely flat.) The solid and dashed curves are the prediction made with FASTRAN for the preyielded and no overload cases, respectively. FASTRAN was able to accurately describe the influence of the compressive residual stresses on crack growth for most of the test cases. These results show that there is very little difference in total life between the no overload and the preyielded condition, but the shape of the crack length against cycles curves are distinctly different in the early stages of crack growth. However, the results shown in figure B-10c had to have a larger EDM cut, 0.5 mm, than the 0.25 mm stated for the test (A2-24). Again, further study would be required to resolve this issue. But, these results may be similar to the discrepancy observed in the next series of tests.

B.5.3 PRECRACKED, OVERLOADED, AND CONSTANT-AMPLITUDE LOADING.

Several specimens made of the 2024 alloy were EDM cut on one side of the hole, fatigue precracked to a specified initial crack length, a_i, under constant-amplitude loading, and then the specimen was severely overload to 248 MPa (2/3 of the yield stress of the material). Figure B-11 shows the comparison between the test (A2-25) and the FASTRAN simulations. The solid and dashed curves show the overload and no-overload cases, respectively. In this case, there was nearly a factor of 2 difference between the no-overload predictions and the test results. However, FASTRAN predicted that the crack in the precracked and overloaded case (solid curve) would grow and nearly stop (failure predicted at 260,000 cycles).

This type of behavior has been observed in past experiments on fatigue crack growth. Hudson and Hardrath [B-26] observed that after a maximum stress change from 200 to 100 MPa (R = 0), a crack would grow and stop, while another crack would initiate along the fatigue crack surfaces (perpendicular to the main crack) and grow around the plastic zone size created during the higher stress amplitude.

A schematic of the anticipated crack behavior in the precracked and overloaded case is shown in figure B-12. After fatigue precracking to an initial crack length of a_i, the specimen was overloaded to 248 MPa. The predicted crack extension during the overload was the solid symbol (denoted K_R-curve) shown in figure B-6a. Thus, the specimen was in the fracture process and the crack would have developed along shear bands (70 degrees) to the plane of the precrack, i.e., forming the slant fracture behavior through the plate thickness. The plastic zone sizes are scaled to approximate sizes compared to the hole radius. Thus, the crack would have grown around the primary plastic zone caused by the overload and the crack closure behavior would have been dramatically reduced from the FASTRAN predictions. FASTRAN, as in the case of the Hudson-Hardrath test, forced the crack to grow self similar along the dashed line into the overload plastic zone. However, the crack-opening stress levels would reach very high levels and result into

extremely slow crack growth rates. In summary, FASTRAN has not been programmed to model this unique behavior during severe stress amplitude changes, which result into difference fracture modes.

Thus, a trial-and-error procedure was used to find an overload that would cause FASTRAN to fit the final life in the test case. Here, it was found that an overload of 200 MPa would fit the results very well. It would be of future interest to conduct these type of tests and vary the overload to see if FASTRAN could predict the behavior for self-similar crack growth and/or to modify FASTRAN to simulate the fracture process and reduce the residual plastic deformation along the anticipated crack path.

B.6 COLD-WORKED HOLE TESTS.

The tests conducted by LaRue [B-6], using cold-worked specimens obtained from Sikorsky, were analyzed with the improved FASTRAN code for two loading conditions. First, crack growth predictions are made under constant-amplitude loading on single crack at open hole specimens, second, the cold-worked reamed and notched specimens were analyzed. Comparisons are made between all tests and the predicted results from FASTRAN.

B.6.1 CONSTANT-AMPLITUDE LOADING.

Figure B-13 shows the measured and predicted crack length against cycles results on two test specimens conducted at two different remote applied stress levels at $R = 0.1$. The symbols show the tests and the curves show the predictions. Here, the results are presented as a log-log plot, so that both test and analyses can be shown on the same plot, because there is over an order-of-magnitude difference in the test lives. Both test specimens had an initial crack length of 0.25 mm in length from one side of the central hole. The predicted results agreed extremely well with the test data.

All the constant-amplitude tests that were conducted at the higher stress level (117.2 MPa) are shown in figure B-14. Again, the initial crack lengths had an average value of 0.25 mm in length. FASTRAN predictions were made for the case of uniform applied stress (dashed curve). These results indicated that something was causing the predicted results to produce much higher crack growth rates than the tests for crack lengths greater than about 6 mm. At this point, the remote boundary conditions on the test specimen were under question. It was known that remote displacement boundary conditions for an unsymmetrical crack configuration would cause a load transfer to the stiffer ligament that would lower the stress-intensity factors for the cracked ligament. Thus, the FADD2D code [B-17] was used to generate the stress-intensity factor solution for the case of remote uniform displacement. Using these results produced the solid curve in figure B-14. The predicted results are now in better agreement with the test data, but still fall short. It is suspected that there may be something else in the specimen gripping or in the load train that would further reduce the stress-intensity factors.

B.6.2 COLD-WORKED AND CONSTANT-AMPLITUDE LOADING.

Significant modification was required to simulate cold-worked and reamed holes in FASTRAN. The cold-working process plastically overloads the material around the hole by inserting a mandrel of slightly larger diameter than the original hole diameter, r. The plastically deformed material (or yield zone) forms concentrically around the hole, as shown in figure B-15(a). Once the mandrel is removed, a compressive residual stress develops at the edge of the hole due to the elastic material surrounding the hole. In the current study, overloads of specific magnitudes are applied to the FASTRAN model to generate a plastic zone region and compressive residual stresses that simulate those produced during the cold-working process, as shown in figure B-15(b). As in the case of an overload, previously discussed, the modified Dugdale model does not produce the type of yielding that is produced during the cold-working process. Whether the simple model can be used with remote overloads to simulate the compressive residual stresses produced during cold working will be studied. (A similar model could also be developed, which would pressurize the hole, similar to cold working. This model may produce a different residual plastic deformation region, but this would require further study, if the overload method were unsatisfactory.) This approach does require a calibration between either finite element analyses (see reference B-26) or some of the closed-form equations that have been developed for cold working (see reference B-27). Comparisons will be made between the residual stresses calculated from both the finite element method [B-6] and the crack closure model.

In addition, the cold-worked hole was reamed to a radius of r_m. The reaming of the hole removed a large amount of the plastically deformed material at the edge of the hole and greatly reduced the extent of the compressive residual stresses. After reaming the hole, an EDM notch was machined into one side of the hole of length, a_i, as shown in figure B-15(c). The EDM notch, again, removed some of the plastically deformed material at the edge of the hole. The simulation in FASTRAN is shown in figure B-15(d).

A finite element code was used to analyze a cold-worked hole in the test specimen shown in figure B-1 (without a notch or crack). The specimen width (w) was 21.6 mm, and the specimen was friction gripped with an *h/w* ratio was about 2. The details of the analysis are given in the main text [B-6]. The initial radius (r) was about 3 mm. A mandrel with diametrical interference of 0.268 mm, corresponding to 4.5% cold expansion, was pulled through the hole to induce the compressive residual-stress field. In the final specimens, the hole was reamed to a radius of 4.37 mm to relieve some residual stresses around the hole.

The normalized residual stress (σ_{rs}/σ_{ys}) as a function of the distance from the hole (x/r) is shown in figure B-16 as open symbols. The tensile yield zone had extended to about twice the hole radius, and the reverse plastic zone was about 20% of the hole radius. Various tensile overloads (S_{OL}) were applied to the crack closure model, and the resulting residual-stress distributions are shown as curves. The end of each curve shows the extent of the tensile plastic zone. The 350-MPa overload matched the tensile plastic zone, but did not produce enough compressive residual stresses in the plastic zone. The solid curve at 420 MPa tended to match the reverse plastic zone size and approximated the residual-stress distribution on the average. The latter overload will be used to simulate the cold-worked hole.

The finite element analysis was also used to simulate the process of reaming and notching the hole in the cold-worked specimen. The normalized residual stress as a function of the distance from the hole is shown in figure B-17 as open symbols. The circular symbols show the final residual-stress distribution predicted to be present in the test specimens. Again, the curves show the results of the reaming and notching simulations in FASTRAN. The solid curve (420 MPa) tended to match the residual-stress distribution fairly well. Figure B-18 shows the residual plastic deformations in the crack closure model after the overload (solid symbols) and after reaming the hole (open symbols) as a function of the distance to the tip of the tensile plastic zone (x/d_{max}). The reaming process greatly reduced the amount of plastic deformation from the cold-worked hole.

The cold-worked and reamed holes were then notched with a 0.25-mm length cut on one side of the hole, and the specimens were subjected to a constant-amplitude loading (S_{max} = 117.2 MPa; R = 0.1). The results of four tests are shown in figure B-19 as symbols. The initial crack length for each specimen is shown at 100 cycles. The cycles required to initiate a crack at the notch, which is estimated to be less than a few thousand cycles, is included in the crack length against cycles data. The dashed curve shows the predicted results for only constant-amplitude loading (no cold-working), using the larger hole radius and same initial notch size. The solid curve shows the predicted results from FASTRAN, which was a factor of 1.8 short of the average of the four tests. In view of the fact that the residual stresses in the FASTRAN model (figures B-16 and B-17) were less than those from the finite element analyses, the comparison was reasonable. The modified FASTRAN predicted the nearly order-of-magnitude enhancement in life due to cold working.

The enhancement from the crack closure model was due to the higher crack-opening stress levels generated in the cold-worked and reamed specimens. Figures B-20a and B-20b show the crack-opening stress ratio as a function of either crack length or cycles, respectively. The dashed curve shows the calculated crack-opening stress ratio under constant-amplitude loading (no cold working). The rise in the crack-opening stress ratio near the initial crack length was caused by the lower constraint due to the hole. The crack-opening stress ratio reached nearly a constant level for most of the fatigue life. The rapid drop in the crack-opening stress ratio near the end of life was due to the crack rapidly growing to failure (yield zone became large compared to the uncracked ligament). However, the cold-worked and reamed hole simulation exhibited a much larger rise in the crack-opening stress ratio, reaching a value of 87% of the maximum applied stress. As shown in figure B-20b, most of the fatigue life was consumed while the crack-opening stress ratio was at the high level.

B.7 CONCLUDING REMARKS.

The primary objective of this study was to enhance the FASTRAN crack closure model to simulate the introduction of “compressive” residual stresses due to cold-worked and reamed holes. Cold-worked residual stresses were simulated by using a single overload on the crack closure model to induce residual stresses at the edge of the hole that are similar to those from finite element analyses. Several improvements were also made in the crack-closure model: (1) K-analogy was activated for all crack configurations to improve the transferability of the crack-opening stresses from the model to the actual crack configuration; (2) the plastic-zone region was

composed of 20 elements to more accurately model the steep stress gradients in the residual-stress fields; (3) the hole or notch was assumed to control the constraint on the "first" load cycle, subsequently, the crack controlled the constraint level, as in the original model; (4) the stress-intensity factor solution for a single crack at an open hole in a specimen subjected to remote uniform displacement was developed; (5) an option to ream a hole to remove plastically-deformed material was incorporated into the model; and (6) an option to induce a cut or small notch at the edge of a hole to simulate the introduction of crack starters at the edges of holes.

The improved model was demonstrated on crack length against cycles data generated from two test programs to study the influence of residual stresses on crack growth rate behavior on two materials. In the first program, compressive residual stresses were induced by a remote overload on a 2024 alloy; whereas, in the second program, the residual stresses were induced by cold working a hole and reaming on a 7075 alloy. Using the baseline effective stress-intensity factor range against crack growth rate relationship for each material, predictions were made on the various test specimens. The comparison of measured and predicted crack length against cycles behavior for the overload study agreed very well, except for an extreme case where it was suspected that the crack grew around the overload plastic zone. For the cold-worked-hole case, the measured and predicted life from a small initial crack (0.25 mm) to failure was a factor of 1.8 short of the average test lives. This study has provided an improved FASTRAN life-prediction model for durability and damage tolerance life calculations for components that have various forms of residual stresses; and has further verified that the crack closure concept accounts for residual stresses on crack growth rate behavior.

B.8 REFERENCES.

B-1. Newman, J.C., Jr., "A Crack-Closure Model for Predicting Fatigue Crack Growth Under Aircraft Spectrum Loading," *Methods and Models for Predicting Fatigue Crack Growth Under Random Load*, ASTM STP 748,1981, pp. 53-84.

B-2. Newman, J.C., Jr., "FASTRAN-II - A Fatigue Crack Growth Structural Analysis Program," NASA TM 104159, February 1992.

B-3. Newman, J.C., Jr., "Prediction of Fatigue Crack Growth Under Variable Amplitude and Spectrum Loading Using a Closure Model," *Design of Fatigue and Fracture Resistant Structures*, ASTM STP 761, 1982, pp. 255-277.

B-4. Liu, A.F., "Crack Growth at a Pre-yielded Hole," *Journal of Engineering Materials and Technology*, Transactions of ASME, Vol. 104, 1982, pp. 153-154.

B-5. Liu, A.F., "The Effect of Residual Stresses on Crack Growth From a Hole," NOR 79-74, Northrop Corporation, Aircraft Group, Hawthorne, CA, August 1979.

B-6. LaRue, J., "The Effect of Residual Stress on Fatigue Crack Growth," M.S. Thesis, Mississippi State University, 2005.

B-7. Newman, J. C., Jr., "A Nonlinear Fracture Mechanics Approach to the Growth of Small Cracks," *Behavior of Short Cracks in Airframe Components*, AGARD Conference Proceedings No. 328, 1983.

B-8. Newman, J.C., Jr., Swain, M.H., and Phillips, E.P., "An Assessment of the Small-Crack Effect for 2024-T3 Aluminum Alloy," *Small Fatigue Cracks*, The Metallurgical Society, Inc., Warrendale, PA, 1986, pp. 427-452.

B-9. Swain, M.H., Everett, R.A., Newman, J.C., Jr., and Phillips, E.P., "The Growth of Short Cracks in 4340 Steel and Aluminum-Lithium 2090," *AGARD R-767*, 1990, pp. 7.1-7.30.

B-10. Newman, J.C., Jr., "Effects of Constraint on Crack Growth Under Aircraft Spectrum Loading," *Fatigue of Aircraft Materials*, Delft, The Netherlands, Delft University Press, 1992, pp. 83-109.

B-11. Newman, J.C., Jr., Phillips, E.P., and Swain, M.H., "Fatigue-Life Prediction Methodology Using Small-Crack Theory," *International Journal of Fatigue*, Vol. 21, 1999, pp. 109-119.

B-12. Everett, R.A., Jr., Newman, J.C., Jr., and Phillips, E.P., "The Effects of Machining-Like Scratch on the Fatigue Life of 4340 Steel," *Proceedings of the American Helicopter Society*, 55th Annual Forum, Montreal, Quebec, Canada, May 25-27, 1999.

B-13. Elber, W., "The Significance of Fatigue Crack Closure," *Damage Tolerance in Aircraft Structures*, ASTM STP 486, American Society for Testing and Materials, Philadelphia, 1971, pp. 230-242.

B-14. Lam, Y.C. and Lian, K.S., "Effect of Residual Stress and its Redistribution on Fatigue Crack Growth," *Theoretical Applied Fracture Mechanics*, Vol. 12, No. 1, 1989, pp. 59-66.

B-15. Dugdale, D.S., "Yielding of Steel Sheets Containing Slits," *Journal of the Mechanics and Physics of Solids*, Vol. 8, 1960, pp. 100-104.

B-16. McClung, R.C., "Finite-Element Analysis of Specimen Geometry Effects on Fatigue Crack Closure," *Fatigue and Fracture of Engineering Materials and Structures*, Vol. 17, 1994, pp. 861-872.

B-17. Chang, C. and Mear, M.E., "A Boundary-Element Method for Two-Dimensional Linear Elastic Fracture Analysis," *International Journal of Fracture*, Vol. 74, 1996, pp. 219-251.

B-18. Shivakumar, V. and Forman, R.G., "Green's Function for a Crack Emanating From a Circular Hole in an Infinite Sheet," *International Journal of Fracture*, Vol. 16, No. 4, 1980, pp. 305-316.

B-19. Isida, M., "Stress-Intensity Factors for the Tension of an Eccentrically Cracked Strip," Trans. ASME, Series E, *Journal of Applied Mechanics*, Vol. 33, 1965, pp. 674.

B-20. Tada, H., Paris, P.C., and Irwin, G.R., *The Stress Analysis of Cracks Handbook*, Third Edition, American Society of Mechanical Engineers, 2000, pp. 233.

B-21. NASGRO Reference Manual 4.02, Southwest Research Institute and NASA Johnson Space Center, 2002.

B-22. Hudson, C.M., "Effect of Stress Ratio on Fatigue-Crack Growth in 7075-T6 and 2024-T3 Aluminum Alloy Specimens," NASA TN D-5390, August 1969.

B-23. Newman, J.C., Jr., Wu, X.R., Venneri, S.L., and Li, C.G., "Small-Crack Effects in High-Strength Aluminum Alloys," A NASA/CAE Cooperative Program, NASA RP-1309, May 1994.

B-24. Phillips, E.P., "The Influence of Crack Closure on Fatigue Crack Growth Thresholds in 2024-T3 Aluminum Alloy," ASTM STP 982, 1988, pp. 505-515.

B-25. Newman, J.C., Jr., "A Crack-Opening Stress Equation for Fatigue Crack Growth," *International Journal of Fracture*, Vol. 24, 1984, pp. R131-R135.

B-26. Hudson, C.M. and Hardrath, H.F., "Effects of Changing Stress Amplitude on the Rate of Fatigue-Crack Propagation in Two Aluminum Alloys," NASA TN D-960, September 1961.

B-27. Pavier, M.J., Poussard, C., and Smith, D.J., "A Finite-Element Simulation of the Cold Working Process for Fastener Holes," *Journal of Strain Analysis*, Vol. 32, No. 4, 1997, pp. 287-300.

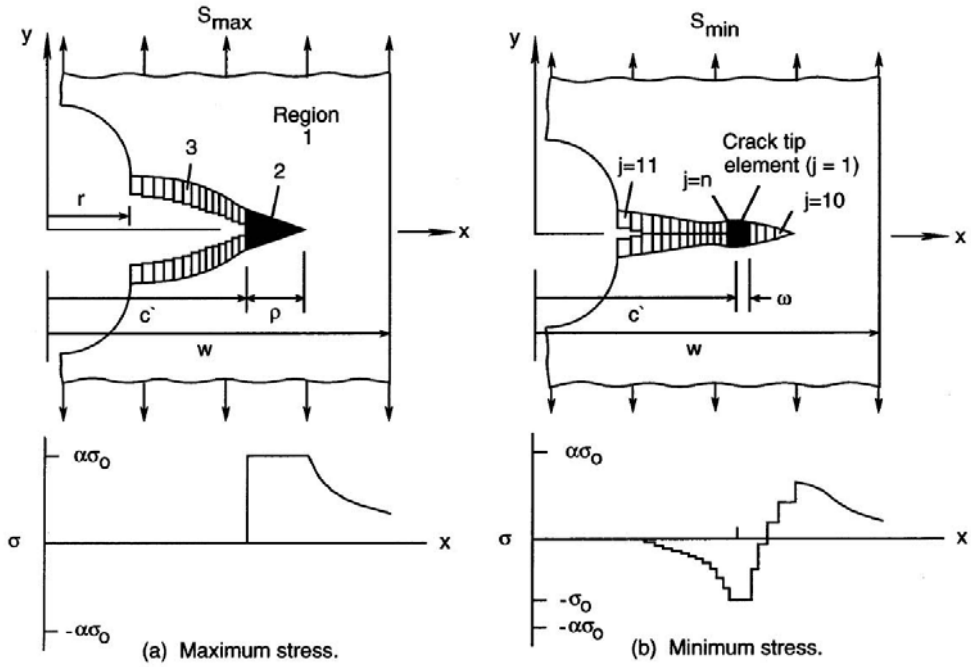

Figure B-1. Schematic of the FASTRAN Crack-Closure Model for Cracks Emanating From Holes

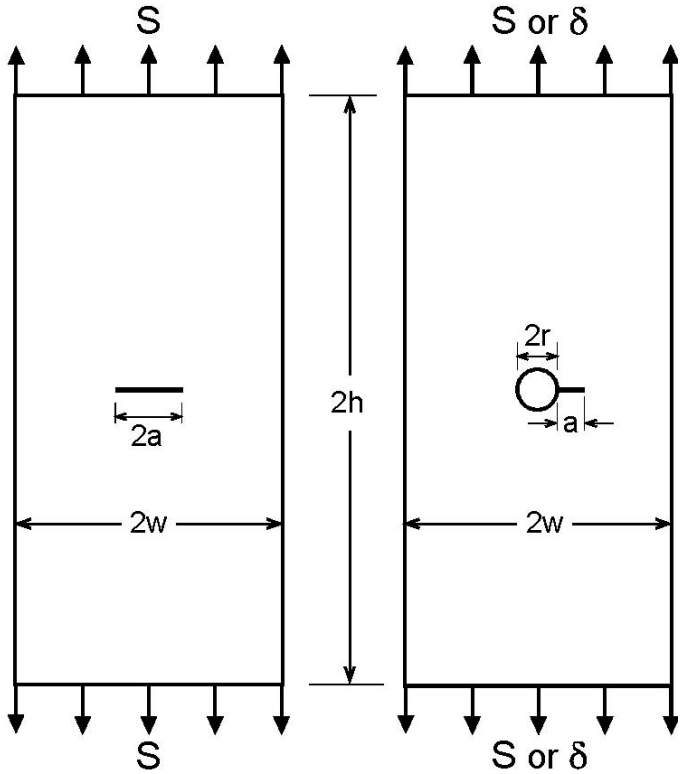

Figure B-2. Crack Configurations Tested and Analyzed

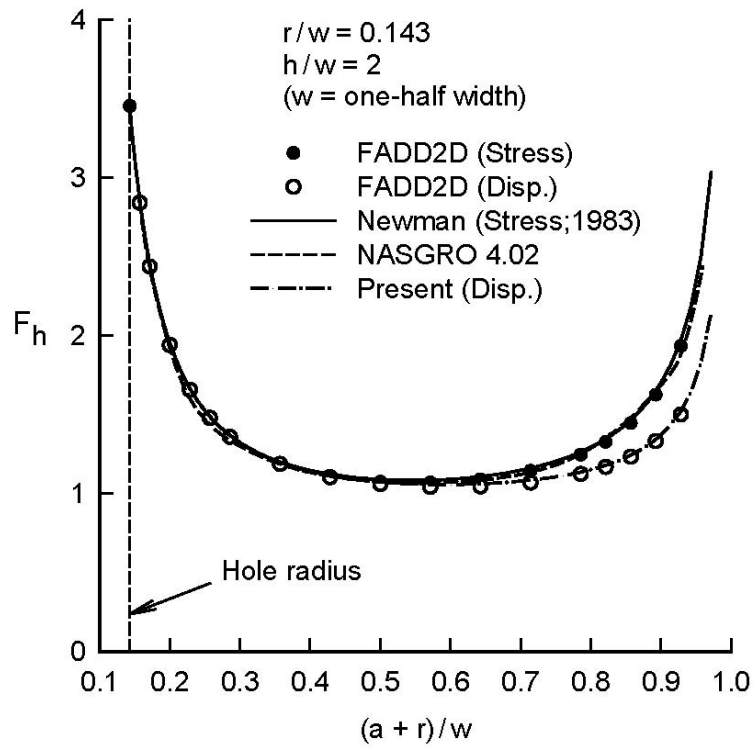

Figure B-3. Stress-Intensity Factor Solutions for a Single Crack at Open Hole in a Finite Plate

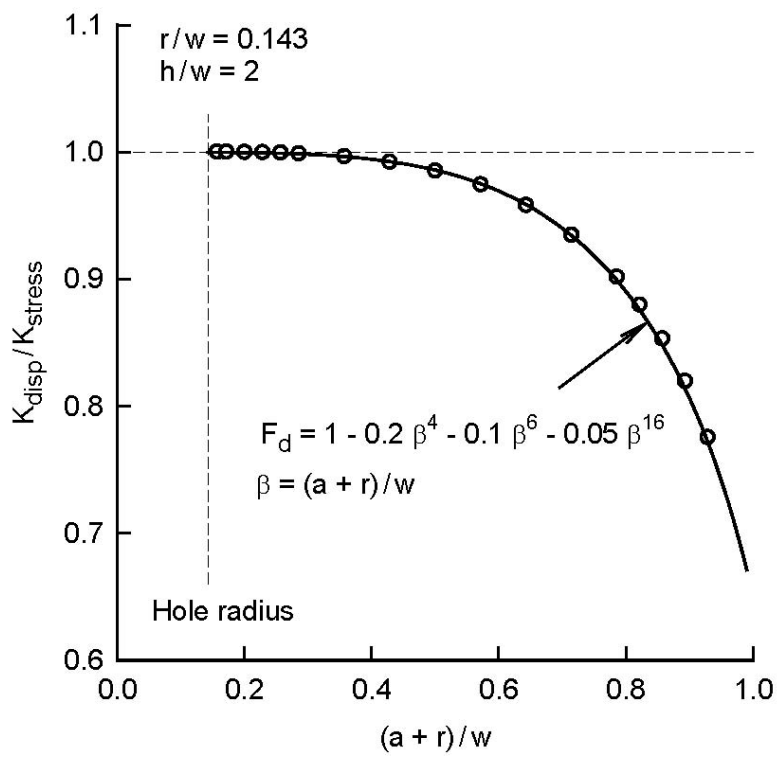

Figure B-4. Ratio of Stress-Intensity Factors for Uniform Displacement to Uniform Stress for a Single Crack at Open Hole in a Finite Plate

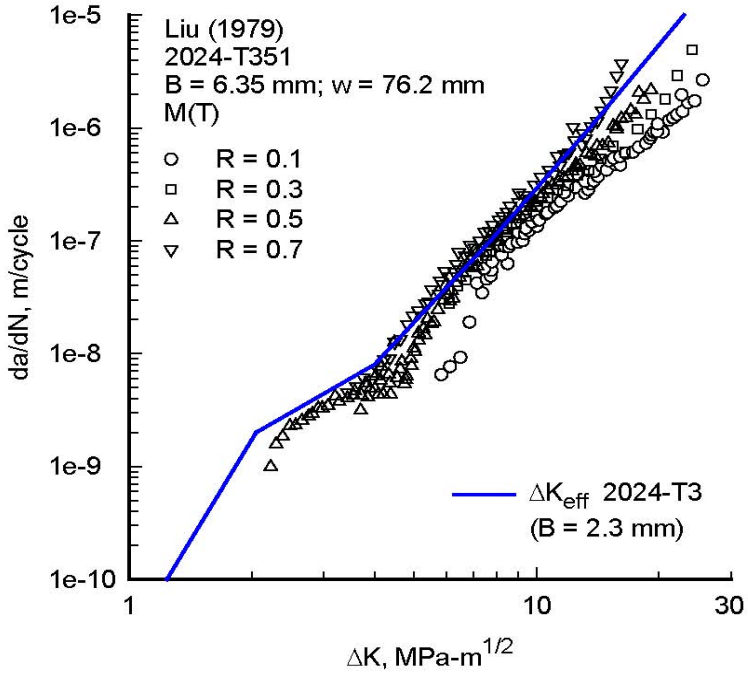

Figure B-5. Fatigue Crack Growth Rate Against Stress-Intensity Factor Range for 2024-T351 Plate at Various Stress Ratios

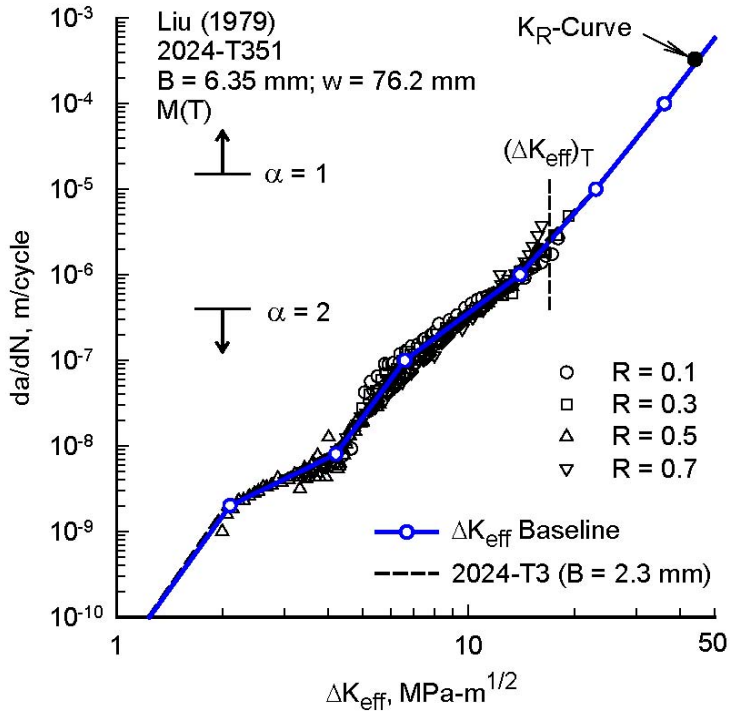

Figure B-6a. Effective Stress-Intensity Factor Range Against Rate for 2024-T351 Plate for Various Stress Ratios

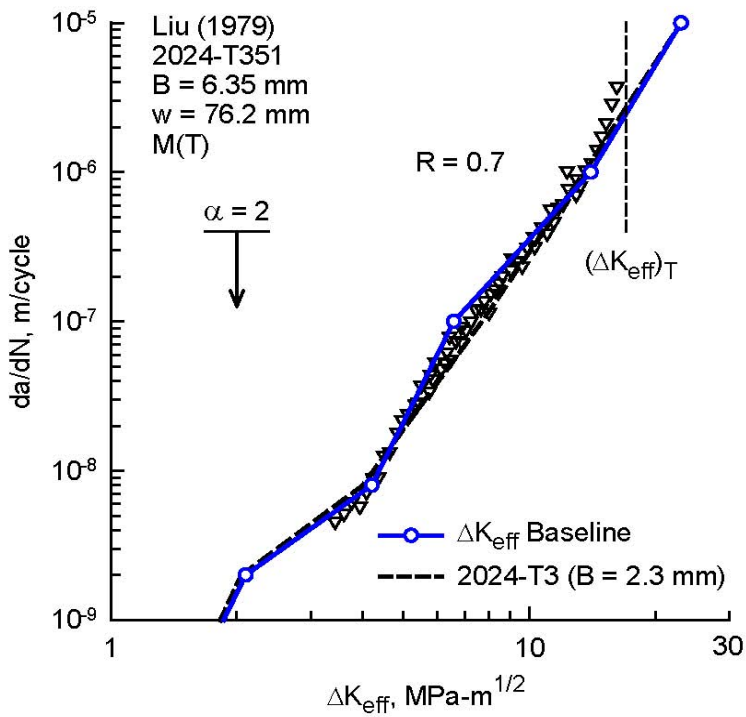

Figure B-6b. Effective Stress-Intensity Factor Range Against Rate for 2024-T351 Plate for R = 0.7

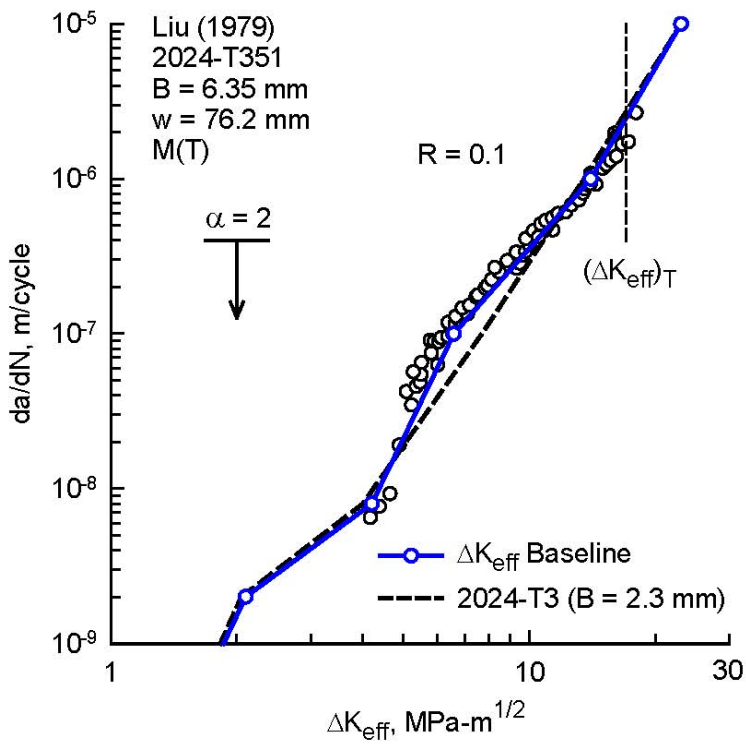

Figure B-6c. Effective Stress-Intensity Factor Range Against Rate for 2024-T351 Plate for R = 0.1

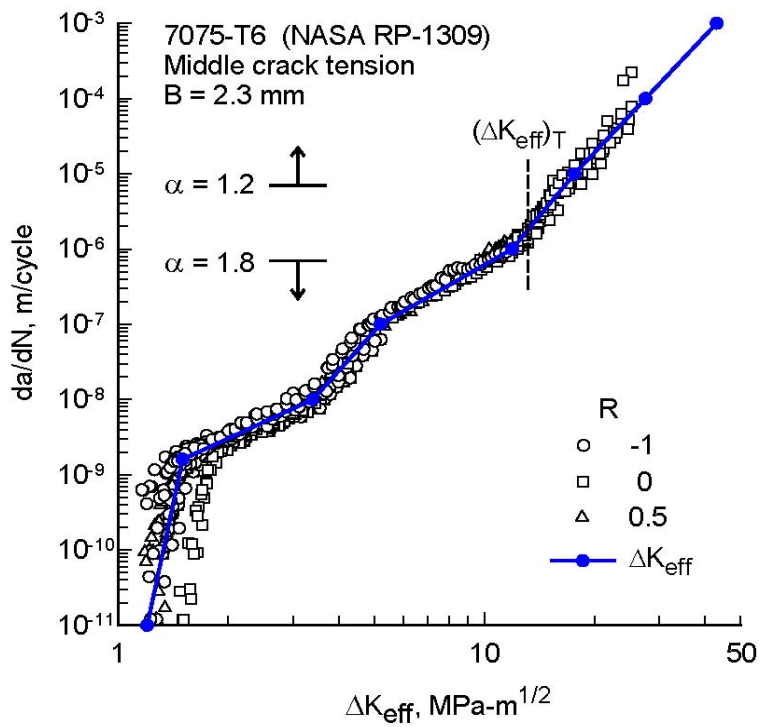

Figure B-7a. Effective Stress-Intensity Factor Range Against Rate for 7075-T6 Sheet for Various Stress Ratios on Small M(T) Specimens

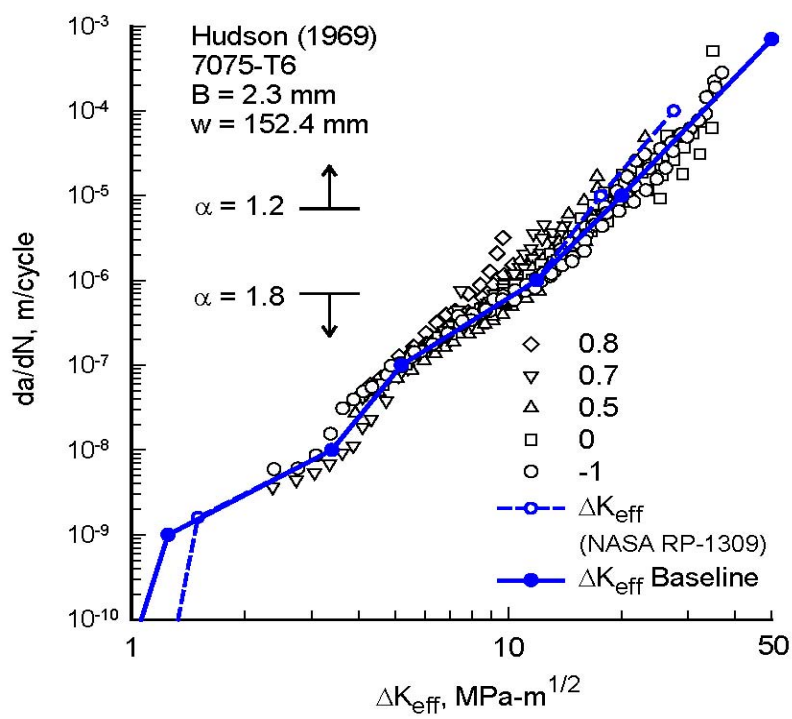

Figure B-7b. Effective Stress-Intensity Factor Range Against Rate for 7075-T6 Sheet for Various Stress Ratios on Large M(T) Specimens

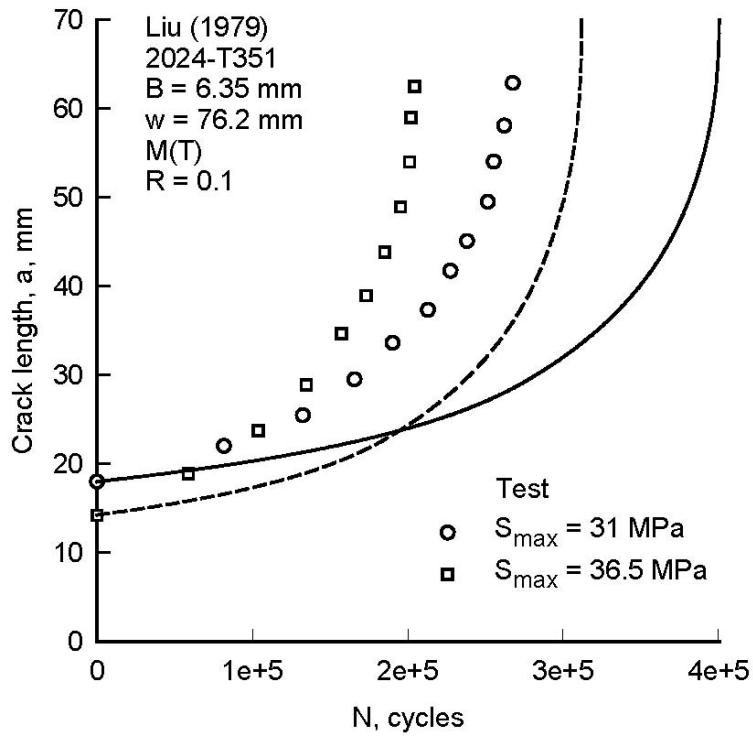

Figure B-8. Measured and Calculated Crack Length Against Cycles on M(T) Specimens Made of 2024-T251 Alloy Under Constant-Amplitude Loading

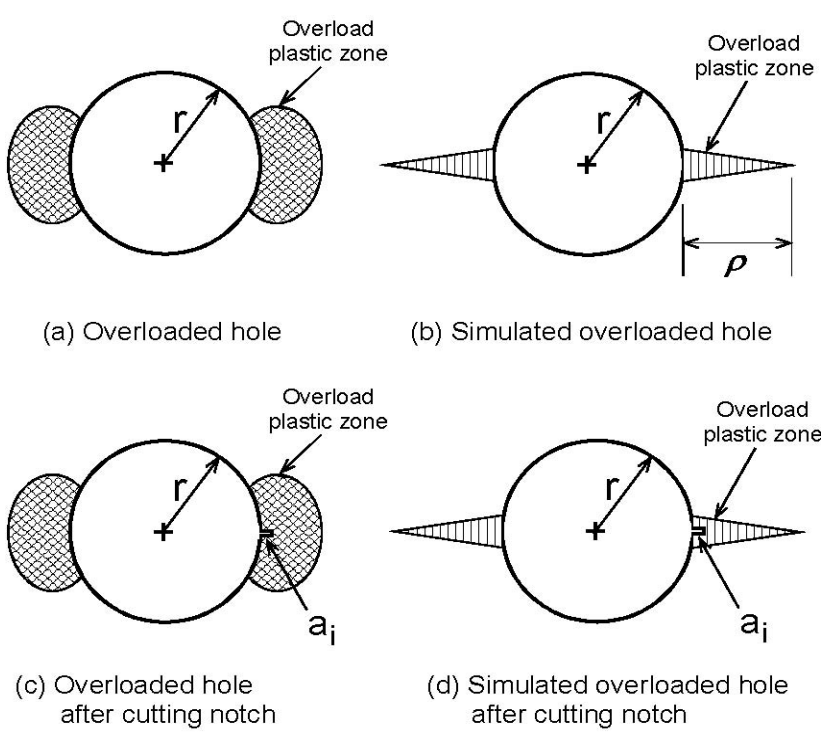

Figure B-9. Preyielded Hole With Overload and Simulated Behavior in FASTRAN

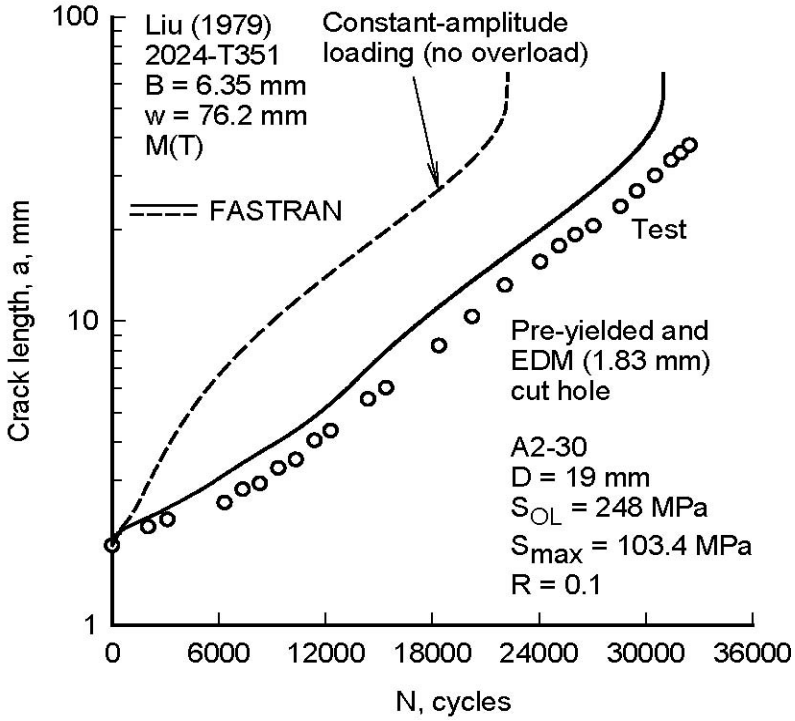

Figure B-10a. Measured and Predicted Crack Length Against Cycles Under Constant-Amplitude Loading After a Preyielded Hole was EDM Cut With 1.83-mm Notch

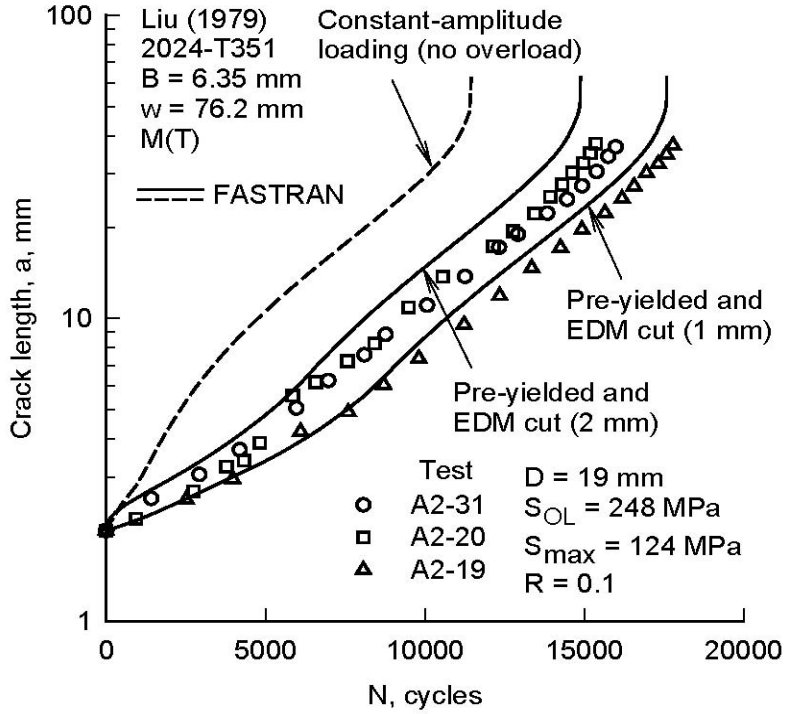

Figure B-10b. Measured and Predicted Crack Length Against Cycles Under Constant-Amplitude Loading After a Preyielded Hole was Cut With Various Size EDM Notches

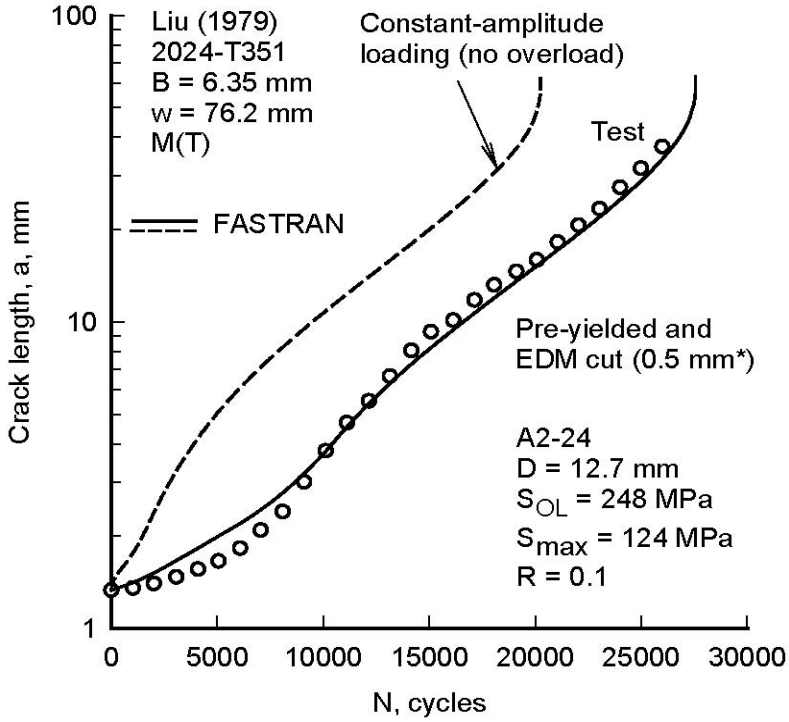

Figure B-10c. Measured and Predicted Crack Length Against Cycles Under Constant-Amplitude Loading After a Preyielded Hole With a Very Small EDM Cut

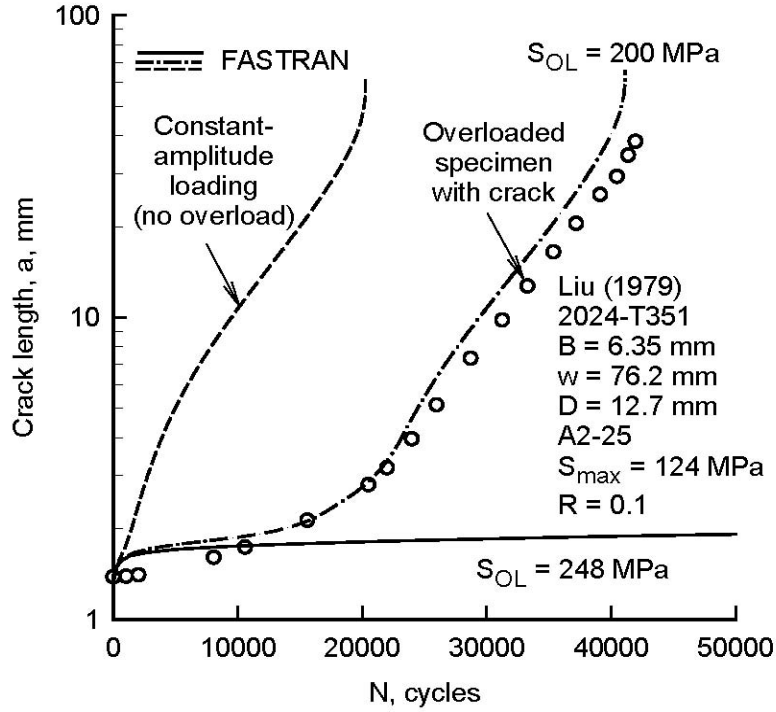

Figure B-11. Measured and Predicted Crack Length Against Cycles Under Constant-Amplitude Loading After an EDM Notch was Made at a Hole, Fatigue Precracked, and Then Overloaded

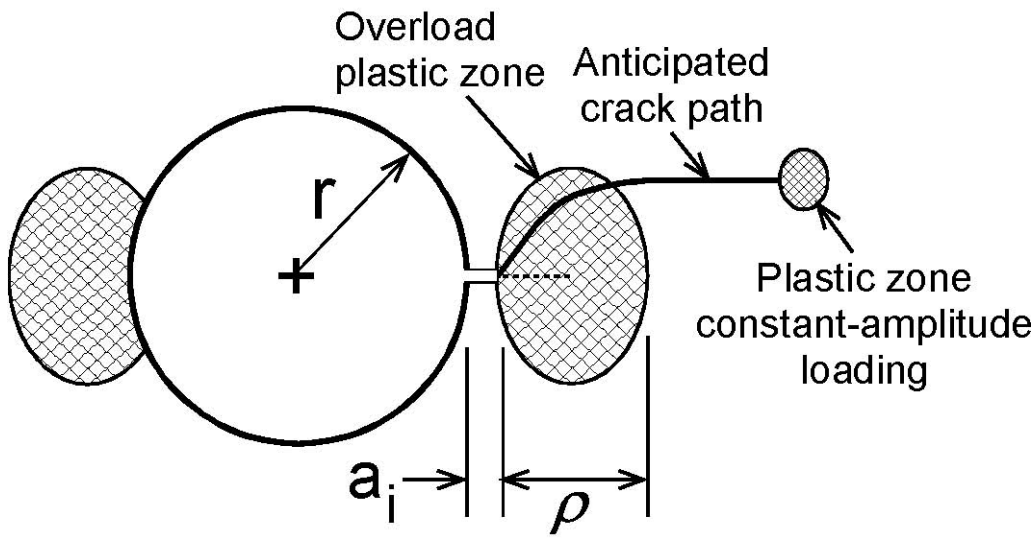

Figure B-12. Anticipated Crack Path in the Precracked Specimen During and After the Overload

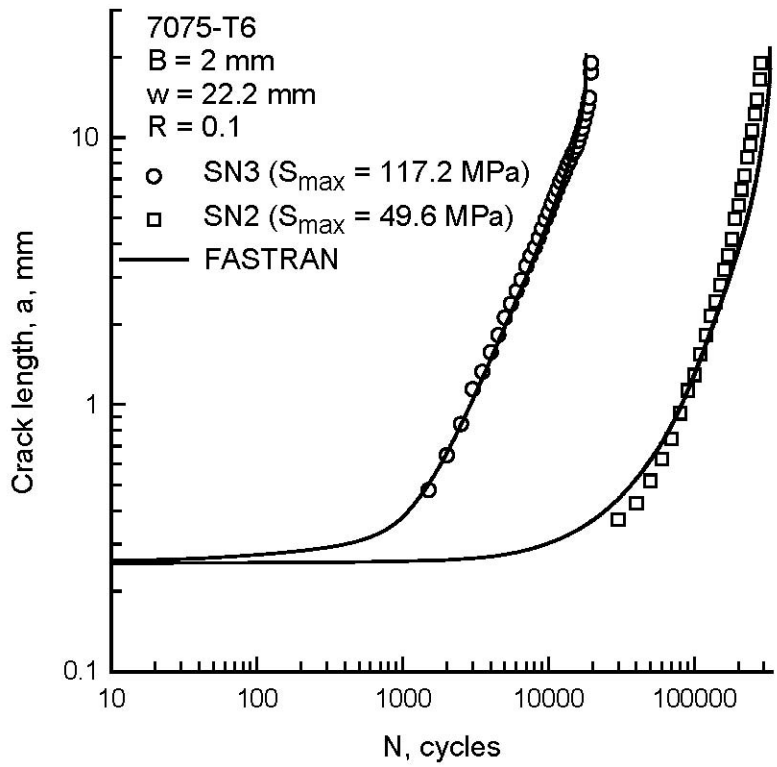

Figure B-13. Measured and Predicted Crack Length Against Cycles Under Constant-Amplitude Loading for Single Crack at a Hole Specimens Made of 7075-T6 Alloy at two Applied Stress Levels

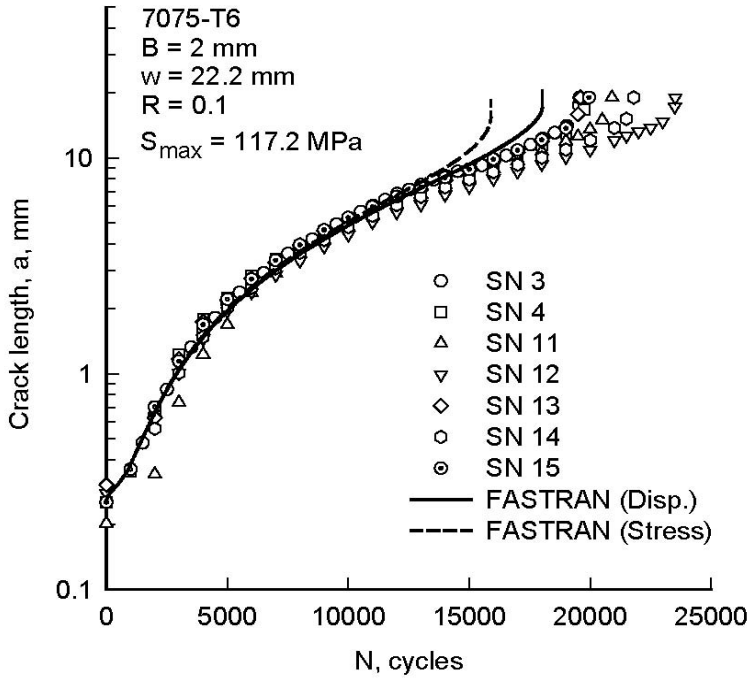

Figure B-14. Measured and Predicted Crack Length Against Cycles Under Constant-Amplitude Loading for Several Single Crack at a Hole Specimens Made of 7075-T6 Alloy

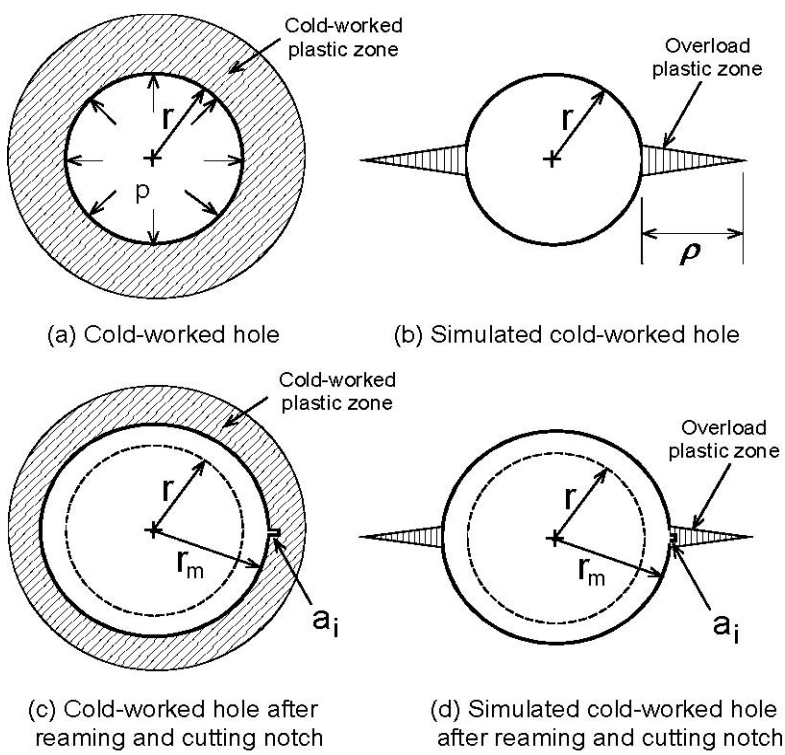

Figure B-15. Cold-Worked Hole and Simulated Behavior in FASTRAN

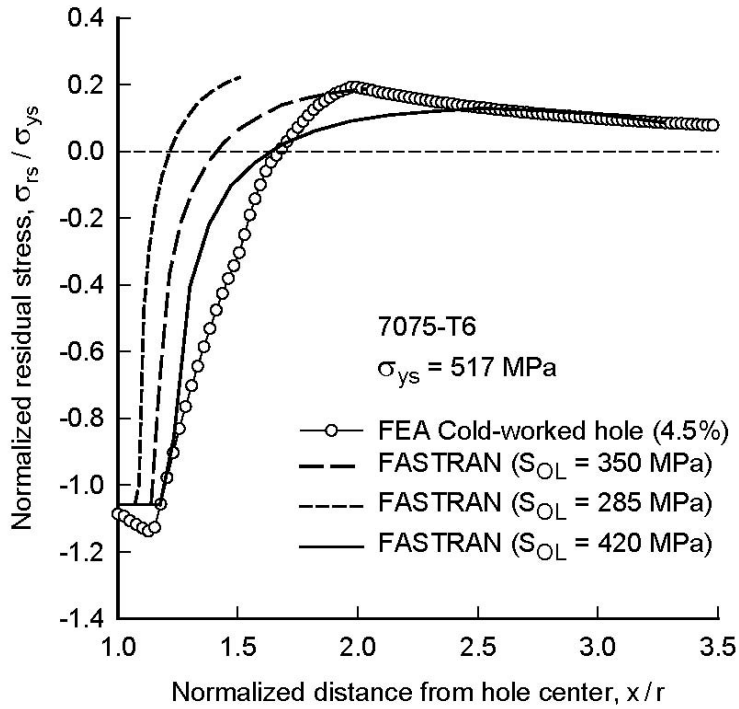

Figure B-16. Normalized Residual Stresses for Cold-Worked Hole From Finite Element Analyses and Simulated Behavior in FASTRAN

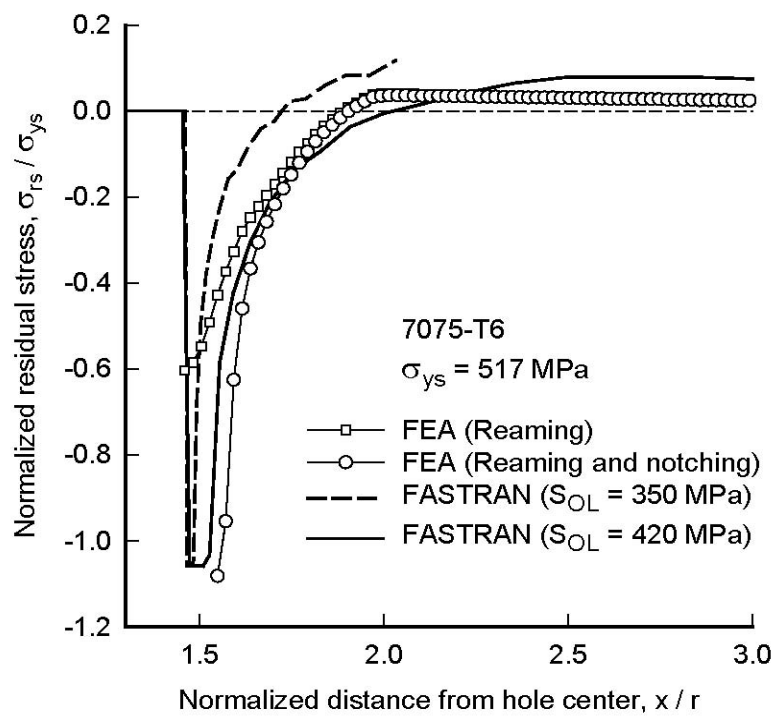

Figure B-17. Normalized Residual Stresses After Reaming and Notching Cold-Worked Hole From Finite Element Analyses and Simulated Behavior in FASTRAN

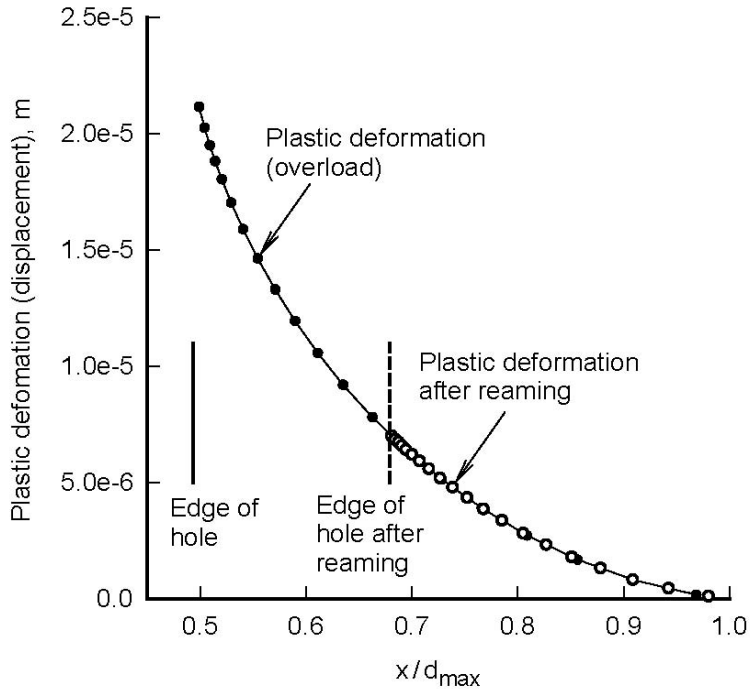

Figure B-18. Residual Plastic Deformations in FASTRAN During Simulated Cold Working and After Reaming

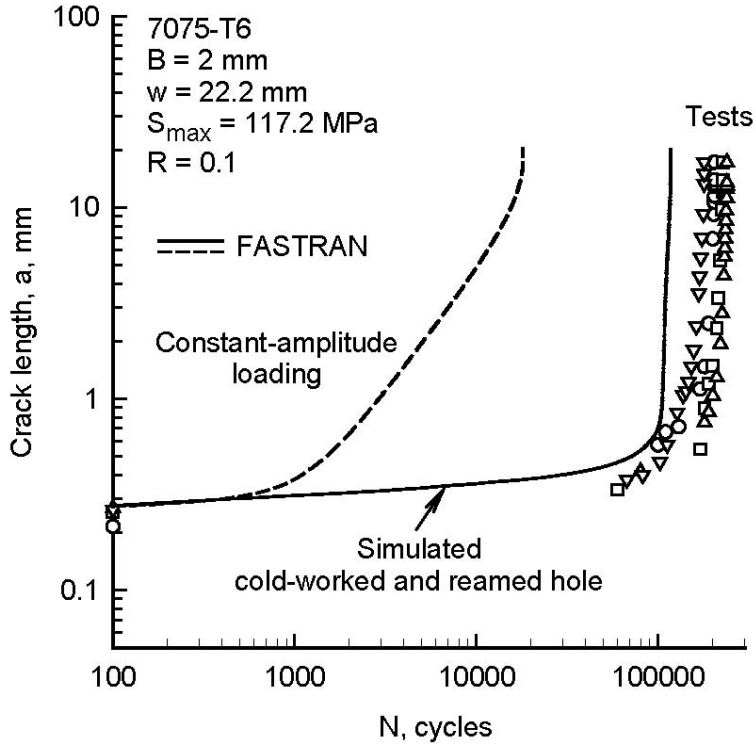

Figure B-19. Measured and Predicted Crack Length Against Cycles Under Constant-Amplitude Loading After Cold Working, Reaming, and Notching

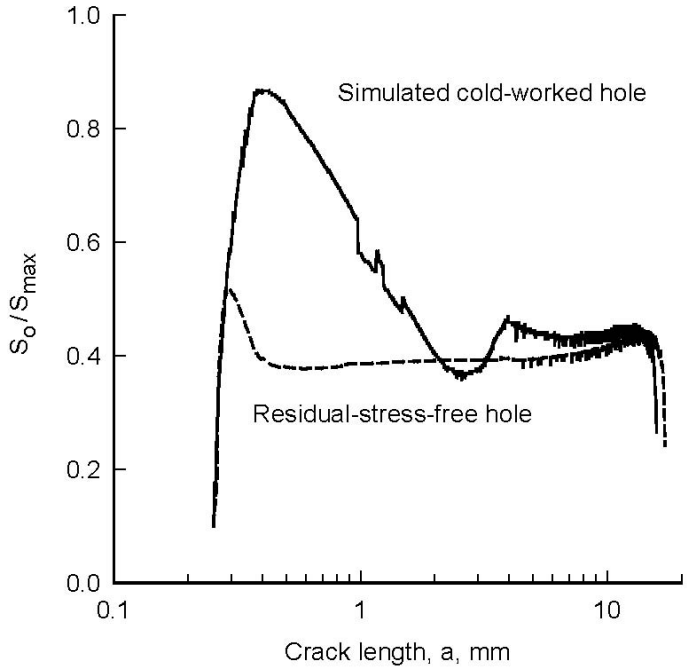

Figure B-20a. Calculated Crack-Opening Stress Levels as a Function of Crack Length During Constant-Amplitude Loading for a Residual-Stress-Free Hole and a Simulated Cold Worked Hole

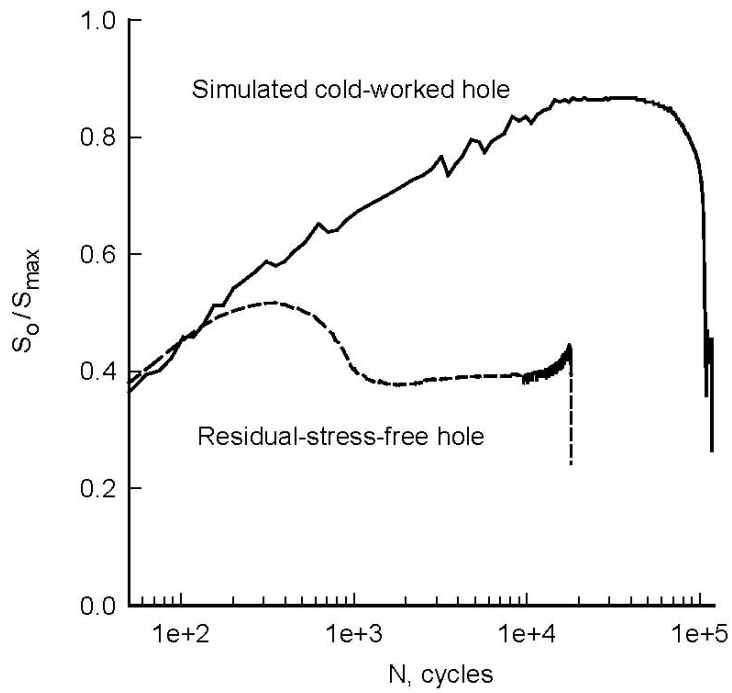

Figure B-20b. Calculated Crack-Opening Stress Levels as a Function of Cycles During Constant-Amplitude Loading for a Residual-Stress-Free Hole and a Simulated Cold Worked Hole